Thermal strain of concrete under low temperatures and durability and Processing techniques of concrete with CNTs

by

Xingang Wang

B.S., Southeast University, 2011

A thesis submitted to the

Faculty of the Graduate School of the

University of Colorado in partial fulfillment

of the requirement for the degree of

Master of Science

Department of Civil, Environmental, and Architectural Engineering

2013

This thesis entitled:

Thermal strain of concrete under low temperatures and

Durability and processing techniques of concrete with CNTs

Written by Xingang Wang

has been approved for the Department of Civil, Environmental and Architectural Engineering

_____

(Yunping Xi)

_____

(Frank Vernerey)

_____

(Keith Porter)

*Date*_____

The final copy of this thesis has been examined by the signatories, and we find that both the content and the form meet acceptable presentation standards of scholarly work in the above-mentioned discipline.

ABSTRACT

Xingang Wang (M.S. CEAE)

Thermal strain of concrete under low temperatures and durability and processing techniques of concrete with CNTs

Thesis directed by Professor Yunping Xi

This thesis consists of two topics: Thermal strain of concrete under low temperatures, and durability and processing techniques of concrete with CNTs. The low temperature test studies the anti-freezing action of concrete under cooling environment. Concrete mixes using different amounts of air-entraining agent and water/cement ratios were made and cured under different humidity environments. During the cooling process from 10 ℃ to -25 ℃, the strain of concrete was measured every 3~5 ℃. The strain-temperature curve of concrete under different mixing proportion was produced from these results. A numerical model was developed based on the theory of the self-consistent model. No knowledge of real pore shapes is needed to apply in the model. The only inputs for the model came from the (Brunauer-Emmett-Teller) BET test, which gave the pore size distribution of concrete sample. The validity of the numerical model was compared to the experimental results, and showed similarity in trend and peak strain.

CNT is one of the most popular topics in engineering. CNT has an extremely high strength and Young's modulus. CNT is a nano-scale material, however, and tends to clump together, which makes it difficult to apply. Other research has successfully incorporated CNT into cement paste and polymer materials. This has not yet been done into concrete. This research mainly focuses on the important factors that must be solved to adopt CNT in concrete area. An

ultrasonicator was used to aid the dispersion and distribution of CNT in water, while several chemicals were also adopted for this purpose. Both strength and durability were tested for CNT concrete of different mix designs. It is suggested that ultrasonicator can improve the strength of pure CNT concrete (without chemicals) by around 100%. In addition, the sodium polyacrylate treated CNT concrete has showed best durability result and good strength result.

ACKNOWLEDGEMENTS

This dissertation would not have been possible without the financial support of Yunping Xi, the assistance of the staff and manager in the structural lab, the students who participated and helped in the research, and the guidance of my academic advisor.

I wish to acknowledge and thank my advisor Yunping Xi for giving me this great opportunity in research, taking his precious time to get me on track. His academic intelligence, diligence, responsibility and patience established a fantastic model for me. His comprehensive knowledge about concrete also inspired me to broaden my perspective to come up with new ideas in this field. He challenged me to improve myself, and my writing skills.

I want to acknowledge and thank all the group members from Professor Xi's group: Inkyu Rhee, Musiket Kamtornkiat, Jun Fu, Yuxiang Jing, Tate Fairbanks, Brandon Buder, Young Sock Roh, Jin Xia and Ali Haraji, who all either gave me help in the structural lab or advice during meetings. I am particularly thankful to Yao Wang who helped me with mixing CNT concrete, Benjamin Gallaher who provided guidance of equipment and Yu-Chang Liang who helped me to prepare for all of these activities in my first semester. Thanks also to Sarah Welsh-Huggins, who helped to review and edit the final draft of these thesis.

I also wish to thank the lab stuff and management group, including Ken, Nent and Scott, for providing and setting up experimental devices, energy resources and for cleaning. I also express my thanks to Kimberly Zimmer from the chemical department for conducting the BET test for me.

Lastly, I would like to thank my family for supporting me while studying abroad. I also thank my girlfriend Linyi Sun, who accompanied me and gave me emotional support all along this wonderful journey.

TABLE OF CONTENTS

CHAPTER 1

INTRODUCTION

OVERVIEW

Concrete, of course, after being discovered, has been and will still be one of the most important construction materials. Concrete, has been studied extensively about how to increase its strength and durability. Because of its heavy weight, it is not economically wise to increase the size of concrete beam or column for enhancing loading carrying capacity of structural members. Fibers of different types have been used in concrete to improve its strength and stiffness. Carbon nanotube is a new high performance material and it can be considered as a very small fiber. One of the research topics in this thesis is to incorporate CNT into concrete and study the mechanical property and durability properties of the CNT reinforced concrete.

Concrete used in cold regions becomes cold and wet from the exposure to rain and/or snow. During the cooling period, the concrete is susceptible to frost damage. The other topic of this thesis is to study the deformation behaviors of conventional concrete with different mix designs at different humid environments and under continuous cooling.

FORMAT OF THESIS

There are two main chapters in the thesis for the two research topics. It is intended that the results of the thesis will be submitted as two journal papers. As for this reason, each of the main chapters will have its own abstract, introduction, literature review, research plan, test results, conclusion and bibliography (references). The concluding chapter will discuss about the real world implication and future prospect. Besides the references included in each chapter, there will be an integrated list of reference at the end of the thesis.

CHAPTER 2

THERMAL STRAIN OF CONCRETE UNDER LOW TEMPERATURE

ABSTRACT

This paper aims at studying the strain behavior of concrete under continuous cooling. Water/cement ratio, saturation degree of concrete and air entraining agent (AEA) all have an influence on the anti-freezing property of concrete. The goals are to find an optimal water/cement ratio that will cause the minimum dilation of concrete under cooling, and also to find an optimal dosage of AEA in different saturation conditions that will cause minimum dilation. During the cooling process from 10 ℃ to -25 ℃, the strain of concrete was measured every 3~5 ℃. The strain-temperature curves of concrete under different mixing proportions were produced from these test results. A dosage of 50ml/kg of AEA was found to be very good for controlling the expansion of highly saturated concrete, while a higher dosage of AEA can help to control the concrete of low degree of saturation. A low water/cement ratio (in our case 0.4) will help control the thermal deformation of concrete specimen. Based on the self-consistent model, a theoretical model was developed to calculate the strain at various temperatures. The only input for the model is the (Brunauer-Emmett-Teller) BET test result, which gives the pore size distribution of concrete sample. Combining the pore size distribution and the relationship between pore size and freezing point the present model can predict the effective strain of concrete under various temperatures. The comparison with our test data showed that the theoretical model can predict the basic trend of strain-temperature relations quite well.

Introduction and Literature Review

This part of thesis aims to study the thermal property of concrete under continuous cooling. In cold regions, concrete becomes cold and wet from the rain and/or snow. During the cooling period, the behavior of concrete is different from that under freeze/thaw cycles (Chatterji 2013). Freezing of water in pores is considered as a potential reason that concrete suffers from frost damage. The results of this study will provide some fundamental and detailed information on the damage of concrete due to ice formation.

Generally, there are two ways for water to freeze inside pores in concrete: nucleation and ice front penetration. For the larger pores, nucleation of ice crystals in the pores is the main freezing mechanism. For the smaller pores, ice front penetration will possibly be the cause, this is because that, the freezing point can be as low as -55 ℃ in small pores, the water with a high free energy (higher than that of ice) will move to the location of ice (with low free energy). As soon as the water reaches ice particles, it turns into ice. In this way, more ice accumulates on the existing ice particles and the expansion of ice in the concrete generates the damage. (Fagerlund et al. 1997)

Helmuth et al. (1961) found that the ice front has an average rate of penetration of 10mm/s. It is thus not possible that all the pore water will freeze at the same temperature. He recommends conducting the freezing test further down to -50 or -60 ℃ to obtain a thorough study of the freezing properties of concrete under extremely low temperatures.

The contribution of ice to frozen concrete was also studied by Chatterji (1999). He discussed how the freezing of water inside pores of concrete is different from the freezing of bulk water. At 0 ℃, only the water in the air bubbles will freeze. Water in smaller pore such as in the capillary and gel pores will freeze under temperatures much lower than 0 ℃. This system

was modeled by Chatterji (1999). Since the air bubbles are not usually saturated in the concrete under service condition, the space in air bubbles provides an escape space for the water in smaller pores. So, the water in smaller pores can diffuse into the air bubbles, turn into ice, and do not generate any damage. Air-entraining agents can help introduce uniformly distributed air bubbles in the concrete mixture, thus decreasing the potential expansion due to the ice formation.

Along this line of consideration, there may be a critical degree of saturation, at which the free space in the pore structure is not sufficient to accommodate the extra volume generated due to the formation of ice. So, for the concrete with a degree of moisture saturation near or higher than the critical degree of saturation, there will be freezing damage or freeze/thaw damage in the cold region. Lars-Erik Larsson et al. (1980) did a test to study the critical degree of saturation for lightweight cellular concrete. He used a model WIT2 HBM inductive-motion transducer to measure longitudinal deformation of concrete under low temperature for the single cycle instead of hundreds of freeze thaw cycles. The critical saturation degree he found was 50% ~ 60%. For the low degrees of saturation, 5.4%, 21.6%, 28.1% 33.6%, 36.6%, and 38.7%, respectively, the concrete samples contracted until around -10 ℃, having an instant small dilation and then continues to contract under cooling. For higher degrees of saturation, 42.3%, 49.2%, 56.3%, and 54.3%, respectively, the concrete samples contracted first under cooling, then they dilated until around -10 ℃, and the concrete contracted again until around -25 ℃, then it dilated again, and continued to contract afterwards. The third phenomenon observed was that the concrete contractd to -10 ℃, but after a small dilation, the concrete continued to expand. At around -35 ℃, the concrete began to contract again. Under high degrees of saturation, 59.1%, 54.3%, 60.7%, and 66.9%, respectively, the dilation of concrete was significant, and the strain of concrete went above zero (i.e. expansion), up to +0.15%.

Zhou et.al (2008) did a continuous cooling test for concrete. They found that when the water/cement ratio was 0.65, the concrete expanded linearly up to -5 ℃, but when the water/cement ratio was 0.45, the expansion of concrete started after -15 ℃. Zhou et.al (2008) also proposed a mechanics model which considered the freezing induced strain is composed of four parts: thermal strain, expansion caused by pore pressure, freezing shrinkage, and incremental strain caused by the micro cracks. The reduction of water/cement ratio will also result in different amount of freezable water in the 0 to -20 ℃ ranges, thus affecting the ice forming process (Zhou et.al 2011).

Sun et al. (2010) found that air-entrained mortar contracted under cooling, while none air-entrained mortar expanded. Therefore, the effect of air-entraining agent is very significant. Considering concrete is a more complicated composite material than mortar is, the effect of AEA on concrete is worth of studying.

As mentioned briefly in previous section, there are three classes of pores: gel pores, capillary pores, and entrained air bubbles. The diameter of gel pores varies in the range of nanometer; the diameter of capillary pores varies in the range of micrometer. The air entrained bubbles are much larger than the other two kinds of pores; their diameters are in the range of millimeter. While the AEA dosage is an important issue, the average space between air bubbles also has a huge influence on the thermal behavior of concrete. A model accounting for local thermodynamics equilibrium between different phases was built by Zuber and Marchand (2004), which indicates that concrete with a large air void space has a tendency to dilate and vice versa.

RESEARCH PLAN

Objectives

A testing method based on ASTM C671 will be used to study and understand the effect of ice formation on coefficient of thermal expansion (CTE) of the concrete under subzero condition. Concrete cylinders will be used as specimens.

As indicated in the literature review, concrete may expand (instead of contract) during a cooling period. The possible expansion is due to ice formation in the concrete. The phase transformation of water to ice is associated with a large volume expansion of 9%. CTE of concrete depends on temperature. The reason is that the state of moisture inside of concrete depends on temperature. Under low temperatures, liquid water or vapor turns into ice which is associated with a 9% volume expansion. After all moisture freezes, the effective CTE of concrete is a mixture of CTE of concrete and CTE of ice. The CTE of ice is about 5 times of the CTE of concrete without ice. Therefore, at very low temperatures, the CTE of concrete is not the same as the CTE of concrete at room temperature. The effective CTE of concrete depends both on temperature and on the ice content (how much water turned into ice), and thus on the moisture content and internal pore structure of concrete.

Literature review shows that the ice formation starts at 0 ℃ and completes at about -15 ℃ or lower depending on the microstructure of concrete. This freezing process is due to the fact that the freezing point of water depends on pore size in concrete. The freezing point of water in large air voids is close to 0 ℃, and thus the water in large air voids freezes first; the freezing point in small pores could be well below 0 ℃. For a continuous cooling process, the length change of a concrete specimen is shown in Fig. 1, contracts first, expands due to ice formation, and then

contracts again after the completion of ice formation. In Fig. 1, the slope of the curve is the CTE, and it is apparent that the slope, i.e. the CTE is not a constant.

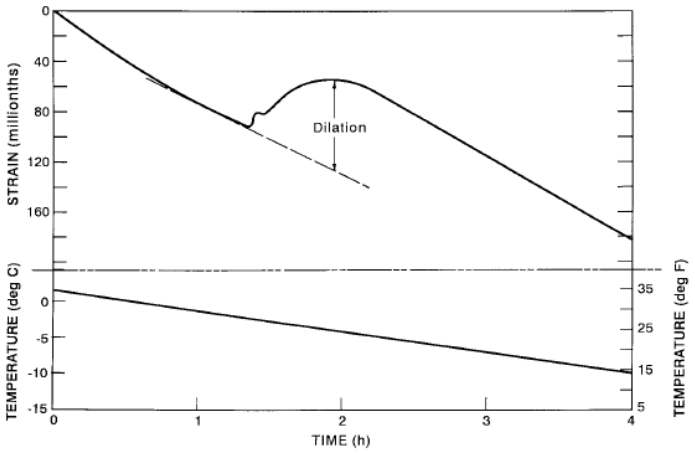

Fig. 1. Typical length change and temperature curve (ASTM C671)

Depending on the concrete mix design, the dosage of additives (e.g. air-entraining agent), and the degree of saturation, the strain-temperature relationship could be significantly different. The ideal curve is that the concrete contracts monotonically without expansion under continuous cooling. In this study, the CTE of concrete will be measured continuously under a cooling process, and the CTE as a function of temperature will be obtained for each concrete mix design. The concrete mix design and dosage of additives will be adjusted such that the expansion (dilation) part of the strain-temperature curve does not appear. So, the damage of concrete structure in cold climate region can be avoided.

Test Parameters

There are two sets of concrete samples. The first set did not consider the dosage of air-entraining agent, while the second set took into account the effects of air-entraining agent and the degree of saturation (Table1 & 2).

The parameters for them are shown separately as follows.

Test parameters of the first set

Water/cement ratio: 0.45, 0.5, and 0.6.

Saturation degree: 20%, 40%, 60%, 100%.

Air-entraining agent: no.

Test parameters of the second set

Saturation degree: 20%, 40%, 60%, 100%.

Air-entraining agent amount: 0 ml/kg, 50 ml/kg, 100 ml/kg, 150 ml/kg

Experimental Procedures

Four different environmental conditions were created in the lab to obtain four different degrees of saturation. In order to have uniform distribution of the moisture in the concrete, the concrete samples were kept in the specific environments for a long time (from 30-60 days). The first group of concrete was submerged completely in the water for 30 days until fully saturated (see Fig. 2a), which is the group of specimens with 100% degree of saturation. The second group of concrete was kept in an environmental chamber, in which the relative humidity was kept to be 60% (see Fig. 2b), which is the group of specimens with 60% degree of saturation. The third group of concrete was placed in the lab, where the average humidity is around 40%. (See Fig. 3)

The last group was dried out in a small oven, which is the group of specimens with 20% degree of saturation (Fig. 4).

Fig. 2a. Concrete samples kept in water, with100% saturation

Fig. 2b. Concrete samples kept in an environmental chamber, at around 60% saturation

Fig. 3. Concrete samples kept in the lab at around 40% saturated

Fig. 4. Concrete samples kept in a small oven at 20% saturation

Concrete samples were tested in the freeze thaw machine (Fig. 5). Concrete samples were placed put in dry chambers in the machine first (Fig. 6). A smart control model was used for the machine to run a single continuous cooling curve (Fig. 7&8). The green number on the panel shows the target temperature, while the red number shows the real-time temperature of the air inside the cabin. Temperature saddle points for every 5 ℃ were set for the freeze thaw machine. The temperature dropped from 5~10 ℃ to -25~-30 ℃ at a step of 3 ℃/hour, but the temperature was kept constant at the saddle point for half an hour to make the heat transfer thoroughly inside the concrete. Several sensors were buried in a sample at different depth to track the temperature of concrete. Finally, we took the average of all these numbers to represent the actual temperature of specimen at that time point (Fig. 9). A transition box was used to transfer data from the sensors to the computer, so that all the data can be recorded. A pair of bolts was attached to the

concrete specimen using epoxy (Fig. 10). A dial gauge was used to measure the length change between the bolts. This gauge has a precision of 0.0001 in.

We also considered using a strain gauge to test the longitudinal strain in the concrete. It can only measure strain at a certain point on the surface of concrete. Since the strain gauge is not precise under low temperatures, so, the dial gauge was used for this test. We measured the bolts' distance three times to reduce the error. The distance change of bolts was measured every 5 ℃.

The technique of Brunauer–Emmett–Teller (BET) test was used to determine the pore structure of the concrete, because it offers the prospect of both pore volumes and size of pores over the widest possible range. (Barrett et al. 1951)

The air-entraining agent was obtained from Sika Inc. All dosages are according to feasible range in the instruction book. The dosage of air entraining agent was based on the mass of cement.

Fig.5 Freeze Thaw machine

Fig. 6. Specimen in dry chambers

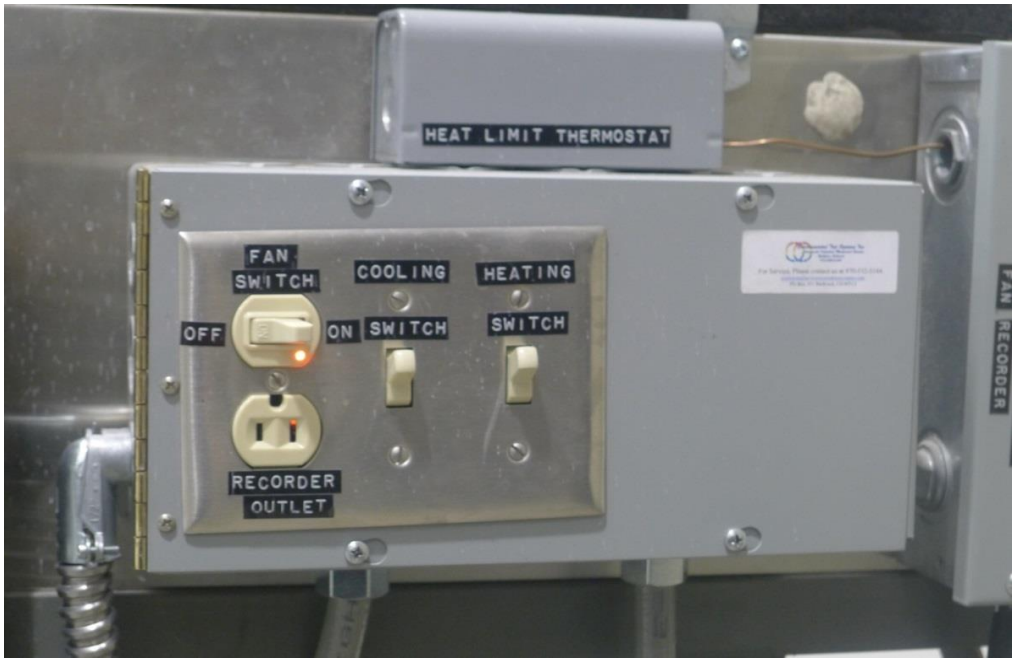

Fig. 7. Heating, Cooling and Fan Controller

Fig. 8. NH1100 Controller

Fig. 9. Sensor buried in different depth of sample specimen

Fig. 10. Bolts Attaching to Specimen for convenient use of Dial Gauge

Table.1 Mixing Proportion for first test

Mix ID	w/c	Cement (Kg/m 3)	water (Kg/m 3)	Fine agg (Kg/m3)	Coarse agg type	Coarse agg (Kg/m3)	Sat (%)	AEA (%)	HWRA (%)
I-1	0.45	400	180	750~800	limestone	1050~1100	100%	0.02	1
I-2	0.45	400	180	750~800	limestone	1050~1100	100%	0.02	
I-3	0.45	400	180	750~800	limestone	1050~1100	100%		1
I-4	0.45	400	180	750~800	limestone	1050~1100	100%		
I-5	0.45	400	180	750~800	limestone	1050~1100	60%	0.02	1
I-6	0.45	400	180	750~800	limestone	1050~1100	60%	0.02	
I-7	0.45	400	180	750~800	limestone	1050~1100	60%		1
I-8	0.45	400	180	750~800	limestone	1050~1100	60%		
I-9	0.45	400	180	750~800	limestone	1050~1100	40%	0.02	1
I-10	0.45	400	180	750~800	limestone	1050~1100	40%	0.02	
I-11	0.45	400	180	750~800	limestone	1050~1100	40%		1
I-12	0.45	400	180	750~800	limestone	1050~1100	40%		
I-13	0.45	400	180	750~800	limestone	1050~1100	20%	0.02	1
I-14	0.45	400	180	750~800	limestone	1050~1100	20%	0.02	
I-15	0.45	400	180	750~800	limestone	1050~1100	20%		1
I-16	0.45	400	180	750~800	limestone	1050~1100	20%		
II-1	0.5	400	200	750~800	limestone	1050~1100	100%	0.02	1
II-2	0.5	400	200	750~800	limestone	1050~1100	100%	0.02	
II-3	0.5	400	200	750~800	limestone	1050~1100	100%		1
II-4	0.5	400	200	750~800	limestone	1050~1100	100%		
II-5	0.5	400	200	750~800	limestone	1050~1100	60%	0.02	1
II-6	0.5	400	200	750~800	limestone	1050~1100	60%	0.02	
II-7	0.5	400	200	750~800	limestone	1050~1100	60%		1
II-8	0.5	400	200	750~800	limestone	1050~1100	60%		

Table.1 Mixing Proportion for first test (Cont.)

Mix ID	water/cement	Cement (Kg/m3)	Water (Kg/m3)	Fine agg(Kg/m3)	Coarse agg type	Coarse agg(Kg/m3)	Saturation (%)	AEA(%)	HWRA (%)
II-9	0.5	400	200	750~800	limestone	1050~1100	40%	0.02	1
II-10	0.5	400	200	750~800	limestone	1050~1100	40%	0.02	
II-11	0.5	400	200	750~800	limestone	1050~1100	40%		1
II-12	0.5	400	200	750~800	limestone	1050~1100	40%		
II-13	0.5	400	200	750~800	limestone	1050~1100	20%	0.02	1
II-14	0.5	400	200	750~800	limestone	1050~1100	20%	0.02	
II-15	0.5	400	200	750~800	limestone	1050~1100	20%		1
II-16	0.5	400	200	750~800	limestone	1050~1100	20%		
III-1	0.6	400	240	750~800	limestone	1050~1100	100%	0.02	1
III-2	0.6	400	240	750~800	limestone	1050~1100	100%	0.02	
III-3	0.6	400	240	750~800	limestone	1050~1100	100%		1
III-4	0.6	400	240	750~800	limestone	1050~1100	100%		
III-5	0.6	400	240	750~800	limestone	1050~1100	60%	0.02	1
III-6	0.6	400	240	750~800	limestone	1050~1100	60%	0.02	
III-7	0.6	400	240	750~800	limestone	1050~1100	60%		1
III-8	0.6	400	240	750~800	limestone	1050~1100	60%		
III-9	0.6	400	240	750~800	limestone	1050~1100	40%	0.02	1
III-10	0.6	400	240	750~800	limestone	1050~1100	40%	0.02	
III-11	0.6	400	240	750~800	limestone	1050~1100	40%		1
III-12	0.6	400	240	750~800	limestone	1050~1100	40%		
III-13	0.6	400	240	750~800	limestone	1050~1100	20%	0.02	1
III-14	0.6	400	240	750~800	limestone	1050~1100	20%	0.02	
III-15	0.6	400	240	750~800	limestone	1050~1100	20%		1
III-16	0.6	400	240	750~800	limestone	1050~1100	20%		

Table 2. Mixing Proportion for second test

Mix ID	water/cement	Cement(Kg/m3)	Water(Kg/m3)	Fine Agg(Kg/m3)	Coarse agg(kg/m3)	Saturaion(%)	AEA
I-1	0.5	356	178	848	1032	100%	0
I-2	0.5	356	178	848	1032	60%	0
I-3	0.5	356	178	848	1032	40%	0
I-4	0.5	356	178	848	1032	20%	0
II-1	0.5	356	178	848	1032	100%	50ML/KG
II-2	0.5	356	178	848	1032	60%	50ML/KG
II-3	0.5	356	178	848	1032	40%	50ML/KG
II-4	0.5	356	178	848	1032	20%	50ML/KG
III-1	0.5	356	178	848	1032	100%	100ML/KG
III-2	0.5	356	178	848	1032	60%	100ML/KG
III-3	0.5	356	178	848	1032	40%	100ML/KG
III-4	0.5	356	178	848	1032	20%	100ML/KG
IV-1	0.5	356	178	848	1032	100%	150ML/KG
IV-2	0.5	356	178	848	1032	60%	150ML/KG
IV-3	0.5	356	178	848	1032	40%	150ML/KG
IV-3	0.5	356	178	848	1032	20%	150ML/KG

TEST RESULTS OF STRAIN

Since there are at least three parameters, fixing two of them and analyzing the influence of the third parameter was a good way to analyze the problem. The test data can be analyzed from two aspects: strain of concrete under low temperature, and the CTE (coefficient of thermal expansion) under low temperature. This section presents only the strain results, because CTE is the slope in the strain curve and can be read and analyzed from the same chart.

Result of The First Test

Effect of AEA

Blue----Air-entraining agent Red----None Air-entraining agent

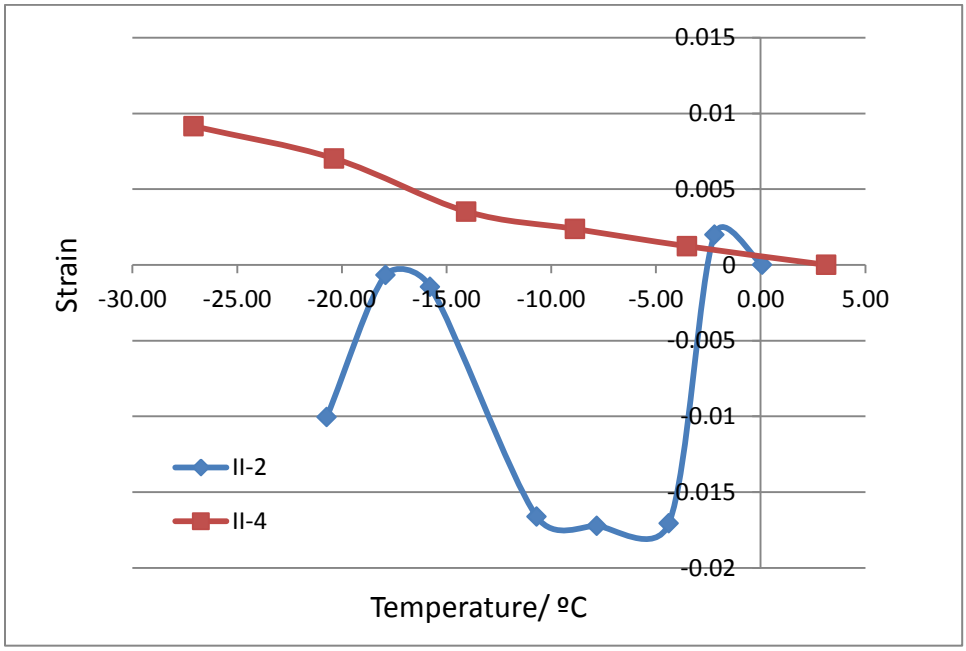

Fig. 11. water/cement=0.5, saturation degree=100%

Blue----Air-entraining agent Red----None Air-entraining agent

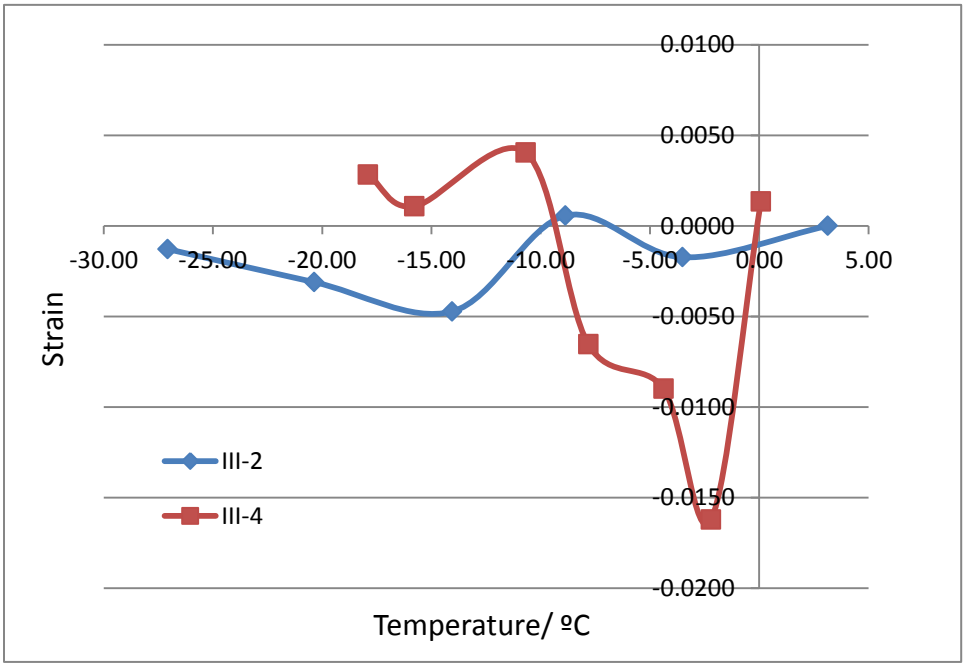

Fig. 12. water/cement=0.6, saturation degree =100%

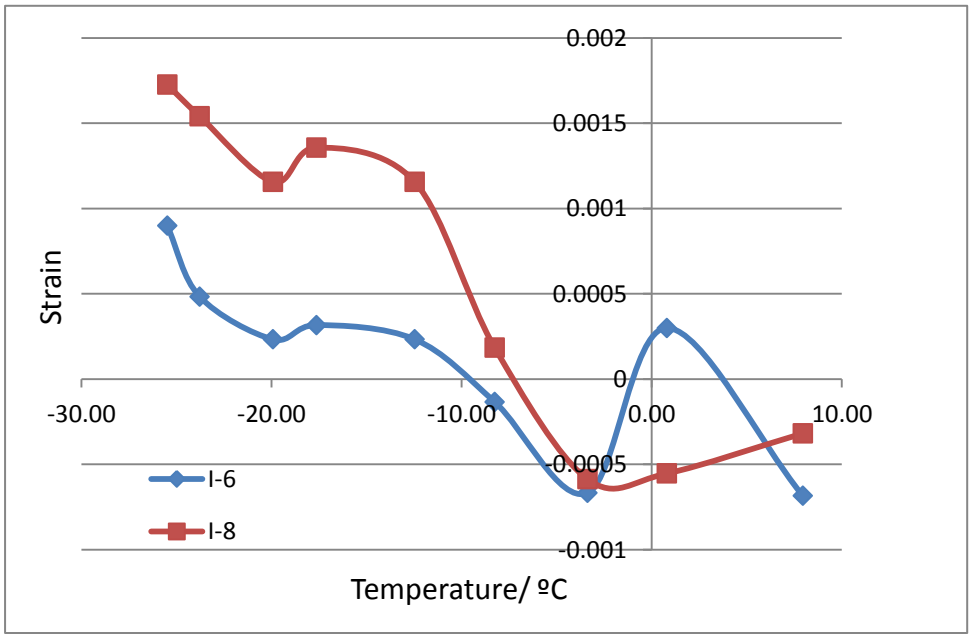

Fig. 13. water/cement=0.45, saturation degree =60%

Blue----Air-entraining agent Red----None Air-entraining agent

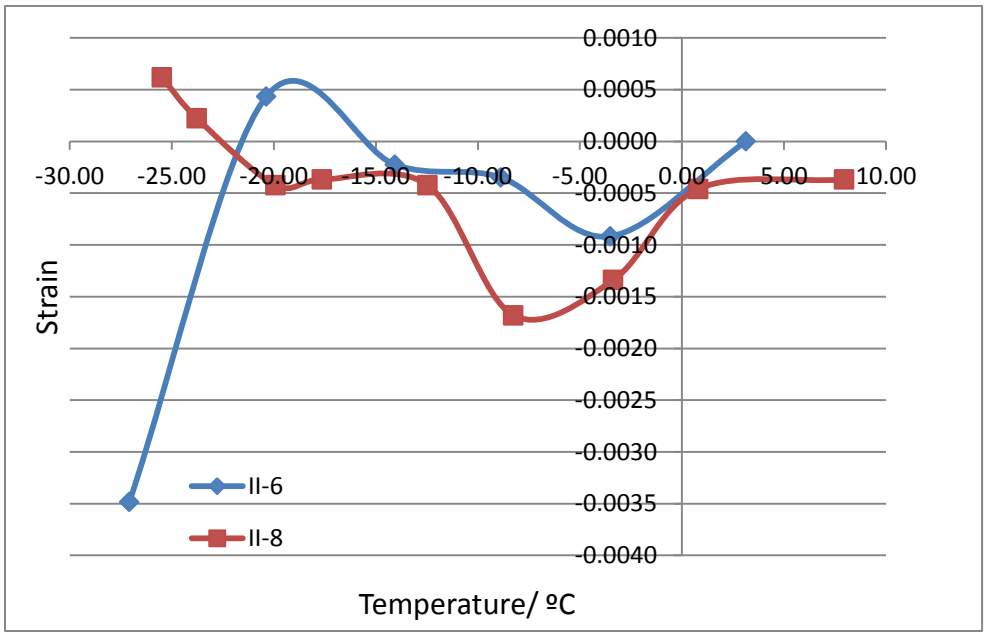

Fig. 14. water/cement=0.5, saturation degree =60%

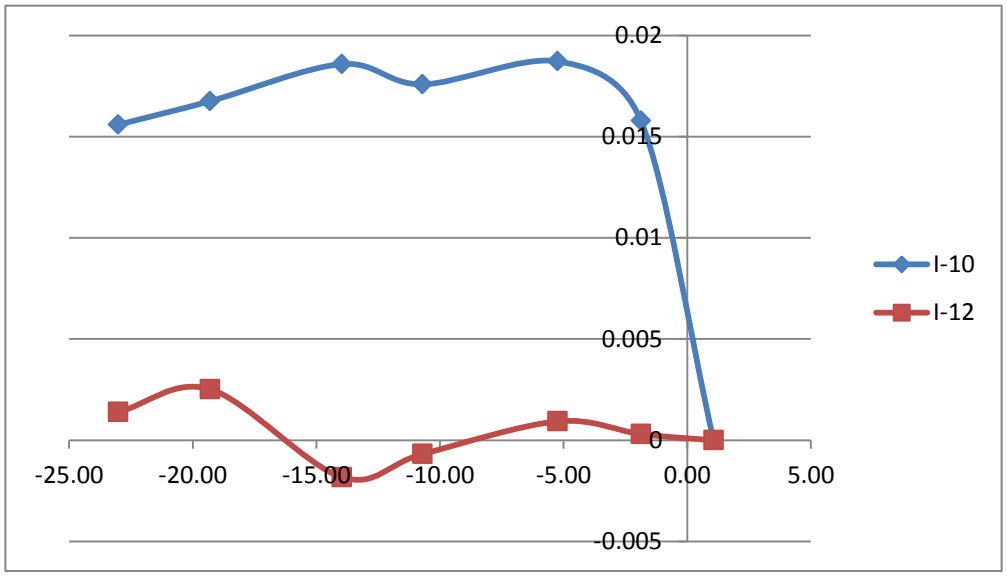

Fig. 15. water/cement=0.45, saturation degree =40%

Blue----Air-entraining agent Red----None Air-entraining agent

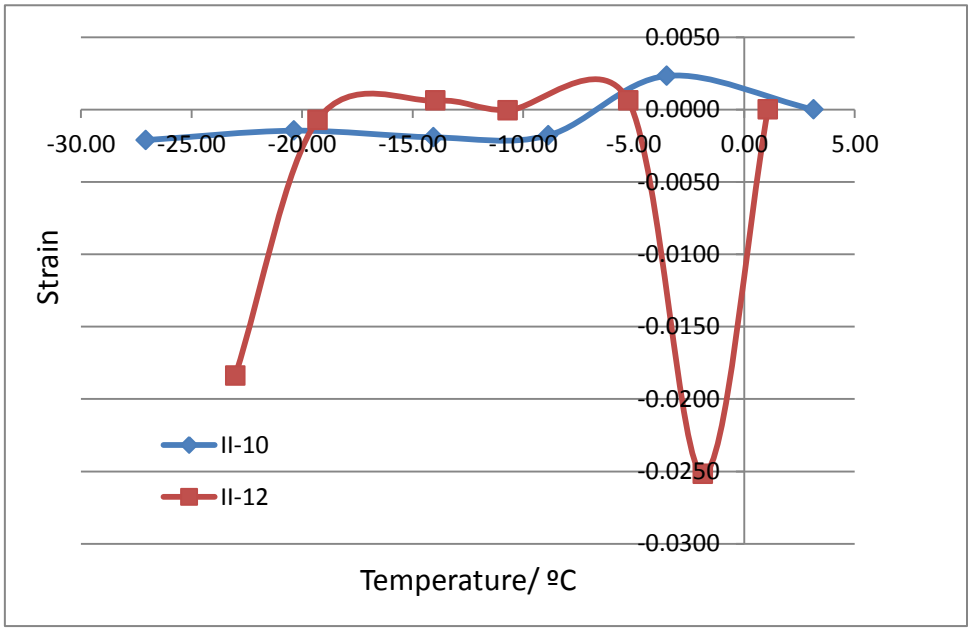

Fig. 16. water/cement=0.5, saturation degree =40%

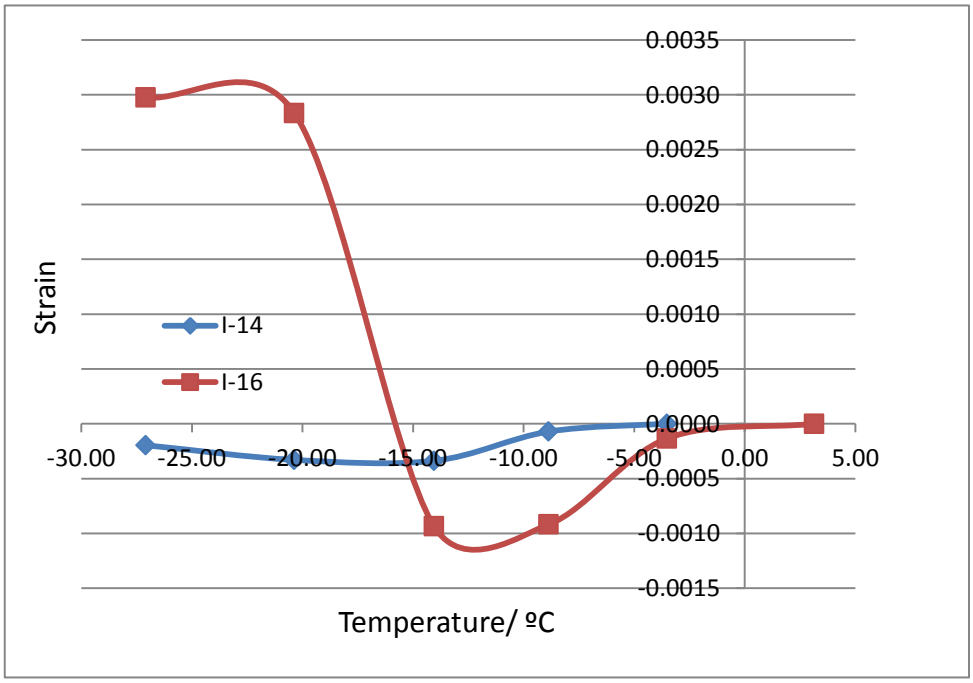

Fig. 17. water/cement=0.45, saturation degree =20%

Blue----Air-entraining agent Red----None Air-entraining agent

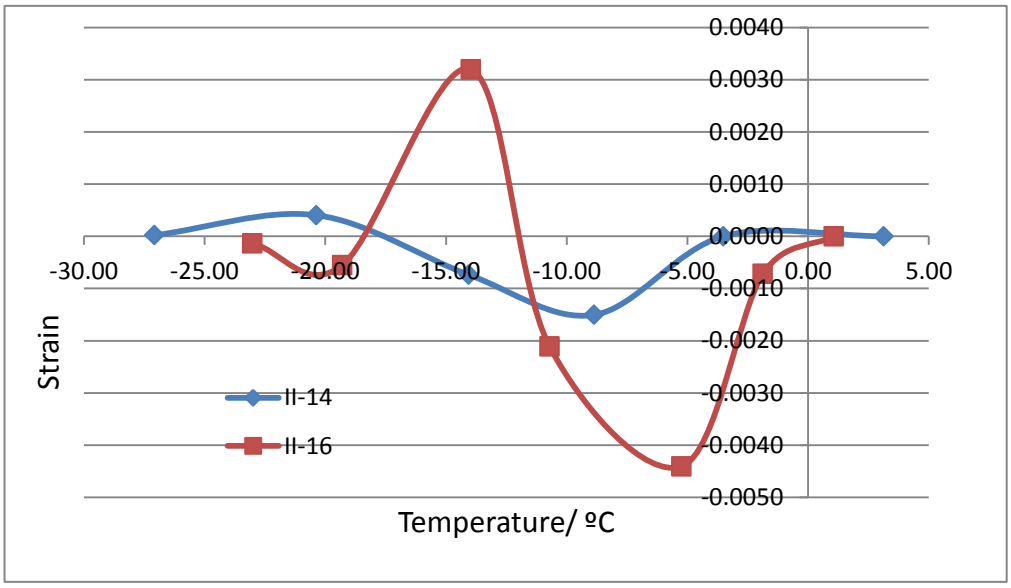

Fig. 18. water/cement=0.5, saturation degree =20%

As regarding the general trend of strain curves shown in the charts above, the concrete samples tended to contract first till a certain temperature (around -5 ℃~-10 ℃). This is because little or no ice was formed inside pores of concrete at higher temperatures than this temperature point. A significant expansion period can be observed after the temperature point, because the water in majority of pores will turn into ice when the temperature decreases to the freezing point of pores with a certain size. The temperature at the peak expansion is generally -15 ℃ to -20 ℃. Most of the specimens will have a second contraction period after -20 ℃, as seen in the charts. Some of the specimens will continue to expand after -20 ℃.

In these figures, we can compare the thermal strains of concrete samples with and without air-entraining agent (AEA). AEA can introduce a system of air bubbles into concrete, which can help releasing the hydraulic pressure associated with ice formation. For the highly saturated specimens, AEA reduced the expansion of concrete samples more effectively than those without

AEA. For those concrete specimens with a low degree of saturation, AEA can reduce the expansion of concrete significantly, as evidenced in Fig. 17 and Fig. 18.

Furthermore, with the addition of AEA the temperature corresponding to the peak contractive strain sometimes can also be shifted. For example, in Fig. 18, the temperature of the maximum contractive strain shifted from -7.5 ℃ to -10 ℃, and the temperature of the maximum dilative strain shifted from -15 ℃ to -20 ℃. However, AEA does not always work effectively, because the addition of AEA may cause random changes in the pore structure, and this can be seen in the figures.

Effect of Saturation Degree

Blue ---- 100% saturation, Red ----60% saturation,

Green ---- 40 % saturation, Violet---- 20 % saturation

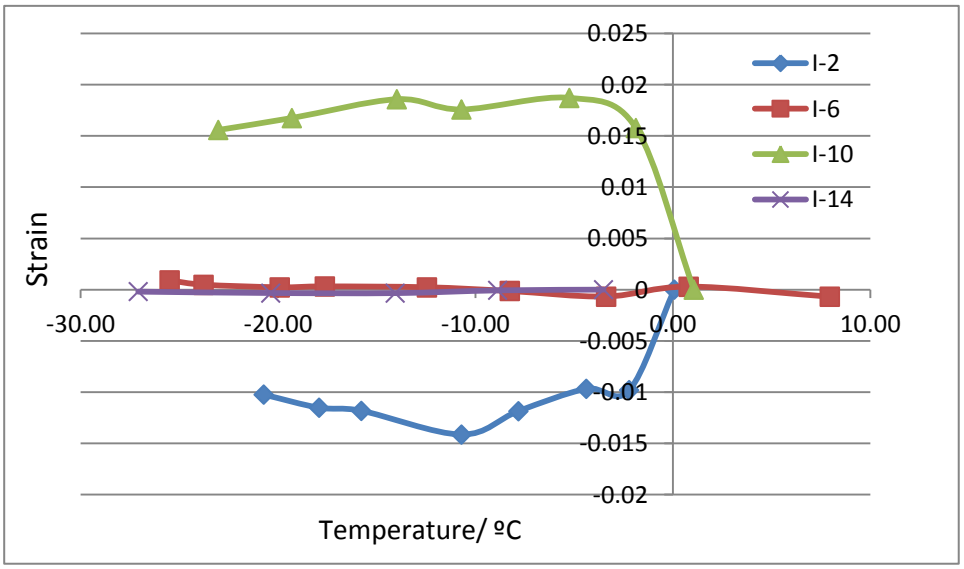

Fig. 19. water/cement=0.45, AEA

Blue ---- 100% saturation, Red ----60% saturation,

Green ---- 40 % saturation, Violet---- 20 % saturation

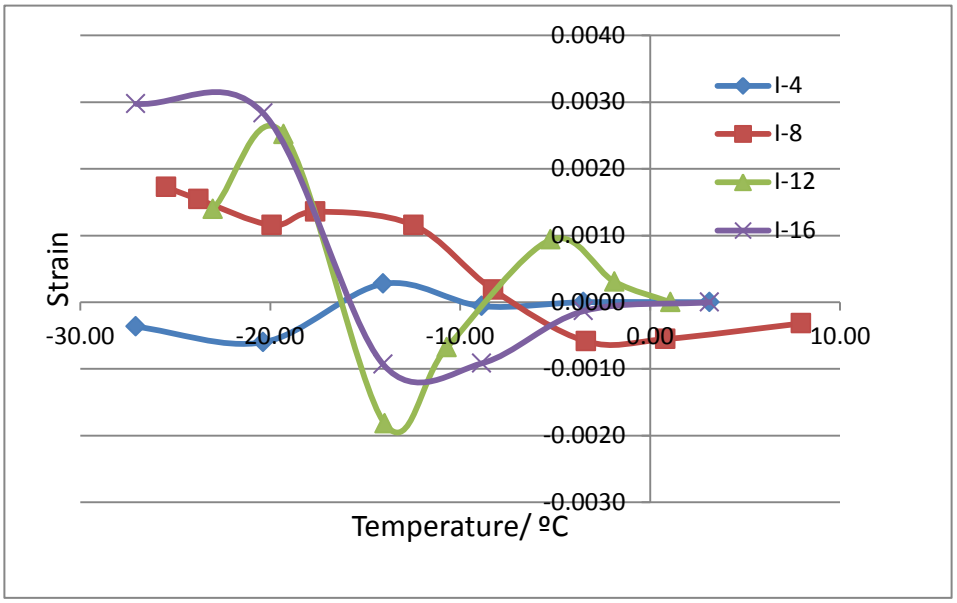

Fig. 20. water/cement=0.45, No AEA

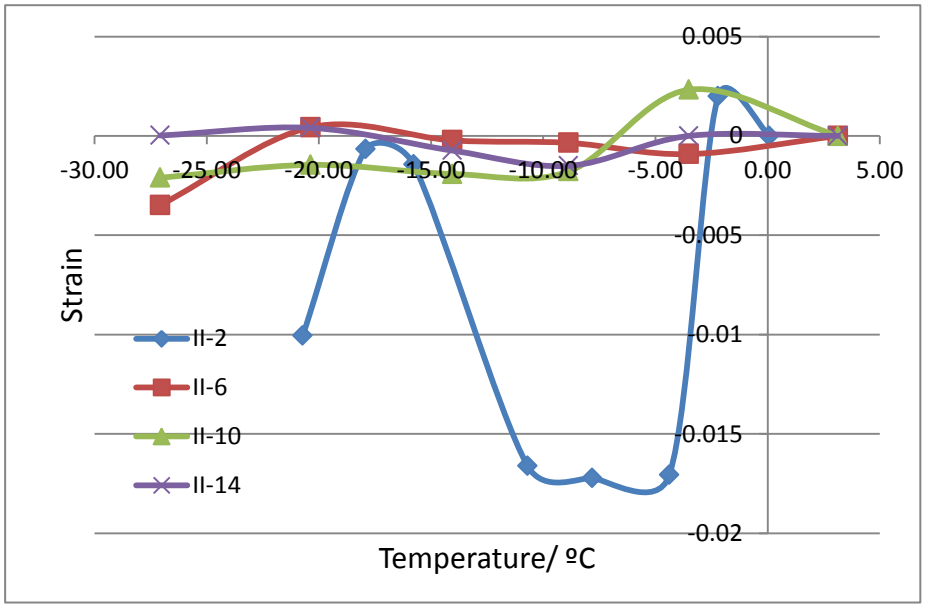

Fig. 21. water/cement=0. 5, AEA

Blue ---- 100% saturation, Red ----60% saturation,

Green ---- 40 % saturation, Violet---- 20 % saturation

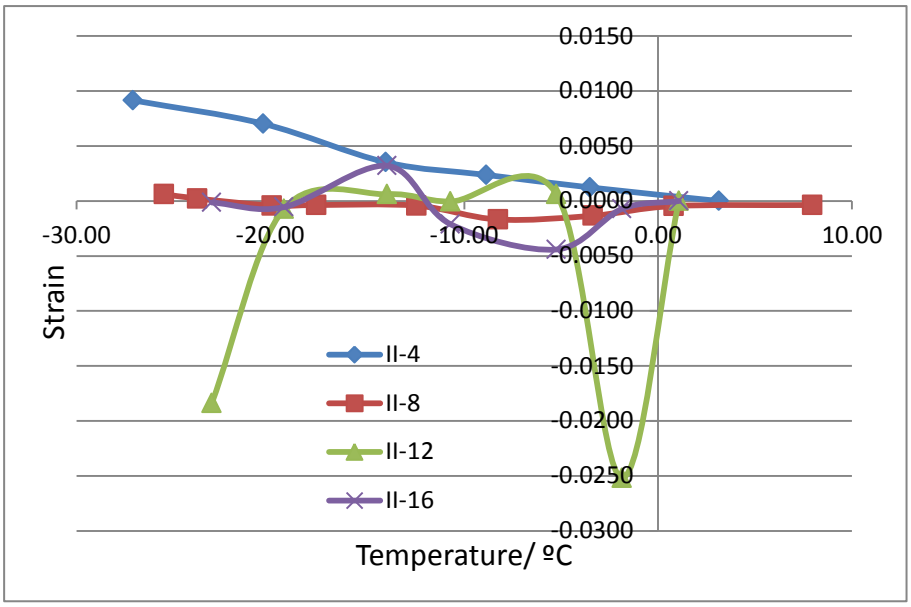

Fig. 22. water/cement=0.5, No AEA

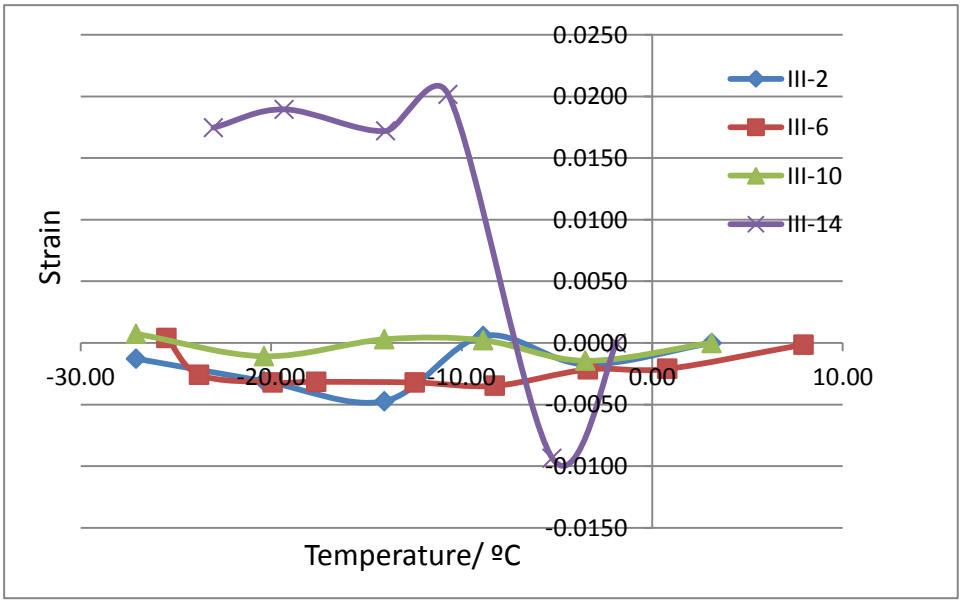

Fig. 23. water/cement=0.6, AEA

Blue ---- 100% saturation, Red ----60% saturation,

Green ---- 40 % saturation, Violet---- 20 % saturation

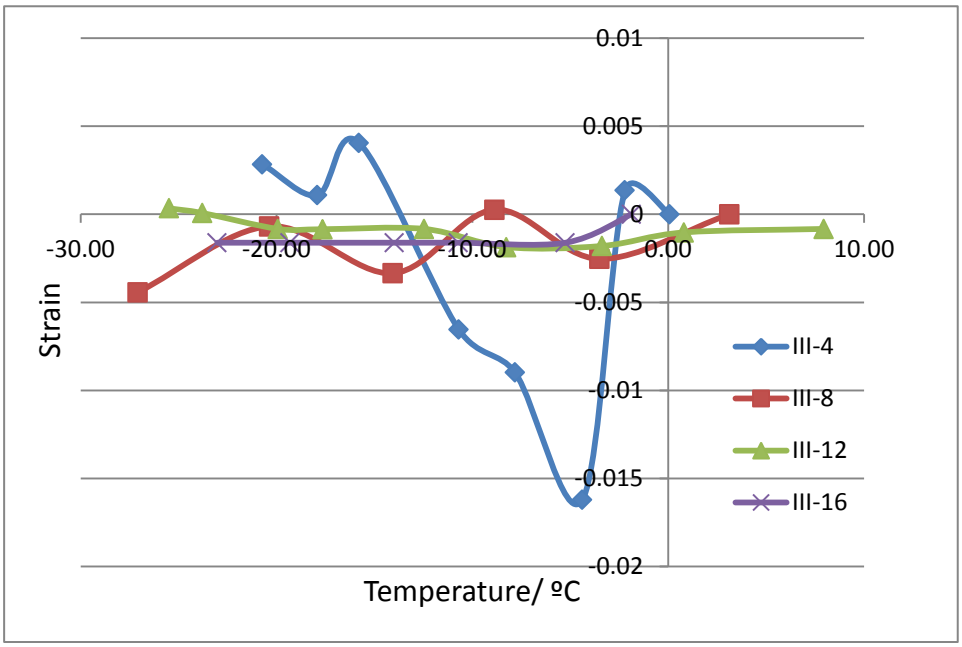

Fig. 24. water/cement=0.6, No AEA

In general, we can see from the graphs that the dilation of concrete under fully saturation condition is higher than those under the other conditions. That is because the total water content under this condition is higher than those of the other conditions. When the water turns into ice, the associated volume expansion of ice causes the dilation of concrete. With all three water/cement ratios (0.45, 0.5 and 0.6) used in the study; the 100% saturated specimens with AEA contracted the most. This is expected, because AEA generates air bubbles in the concrete and thus increases the porosity. The higher the porosity, the higher the coefficient of thermal expansion (contraction) for the samples without AEA, the basic trend is not so clear. With

water/cement ratios of 0.45 and 0.6, the 100 % saturated concrete will still contract the most. For a water/cement ratio equal to 0.5, the 100 % saturated concrete will dilate the most.

Comparing the specimens under 20% saturation and 40% saturation, (the purple curve and the green curve), the 20% saturated concrete has the largest dilation under the condition that water/cement ratio equal to 0.45 without AEA. When the water/cement ratio equals 0.6 and AEA is added, the largest dilation also occurs. The 40% saturated concrete dilates the most at a water/cement ratio of 0.45, with added AEA. The 40% saturated concrete contracts the most when the water/cement ratio equals 0.5 and no AEA is added. The table below (Table 3) summarized these results.

Table 3. Critical saturation data under different w/c and w/o AEA

Saturation Degree	0.45		0.5		0.6	
	Contracts most	Dilates most	Contracts most	Dilates most	Contracts most	Dilates most
AEA added	100 % saturated	40% saturated	100 % saturated	100 % saturated	100 % saturated	20% saturated
None AEA	100 % saturated	20% saturated	40% saturated	40% saturated	100 % saturated	Not obvious

Compared with the research of Lars-Erik et al. (1980), which used cement-bound concrete samples and lime-bound cellular concrete, our specimens made of regular concrete under the saturation of 60% have the same shape of deformation curve as the Lars-Erik study. The values of strain are also quite close. The air-entrained concrete at saturation 20% has the same trend of deformation curve. In the case of 40% saturation, this study reached different results.

It is worthwhile to point out that Lars-Erik's paper is the only previous study that had a similar scope of research, that is why the paper was used here for comparison.

Effect of water/cement ratio

Blue --- water/cement=0.45, Red ---water/cement= 0.5, Green --- water/cement= 0.6.

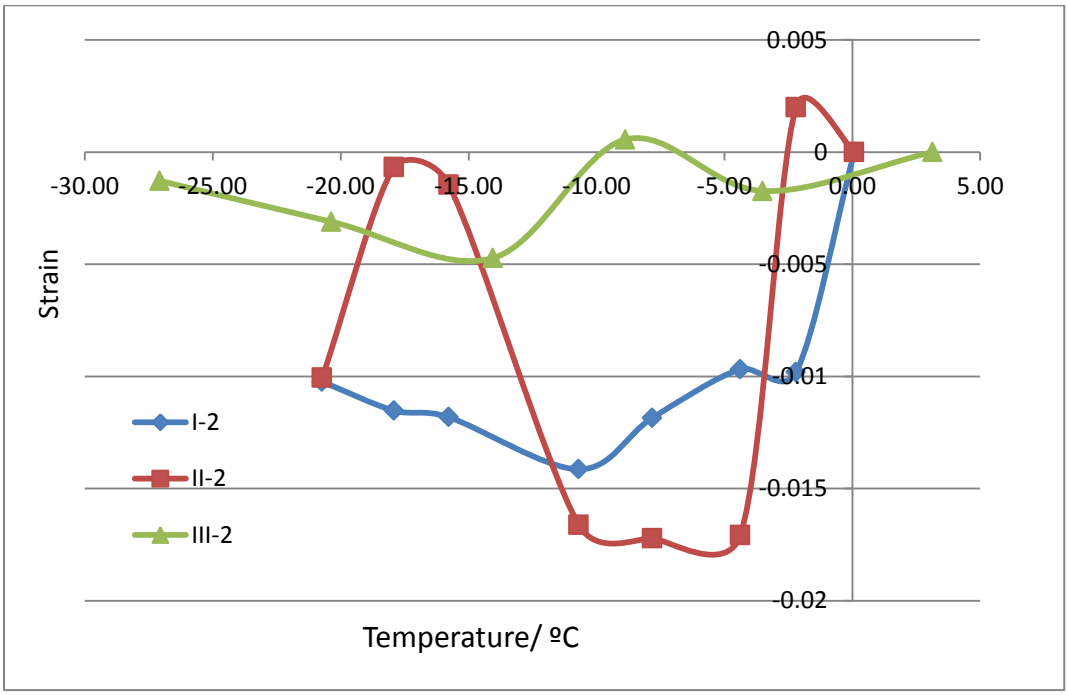

Fig. 25. Saturation degree =100%, AEA

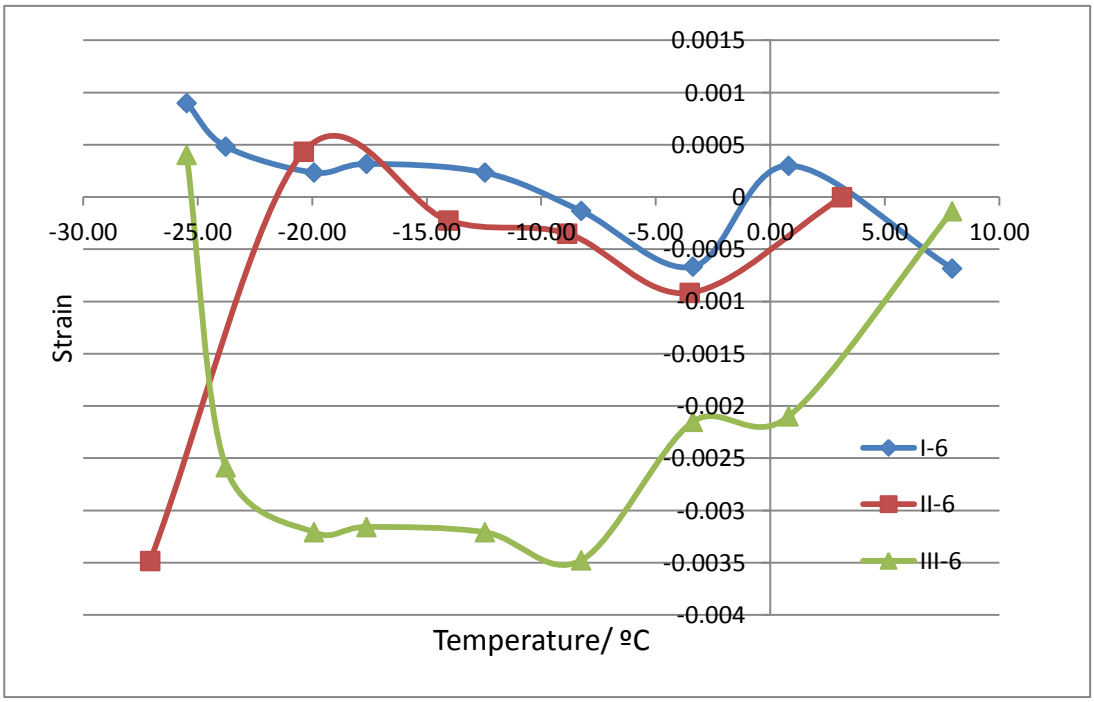

Fig. 26. Saturation degree =60%,AEA

Blue --- water/cement=0.45, Red ---water/cement= 0.5, Green --- water/cement= 0.6.

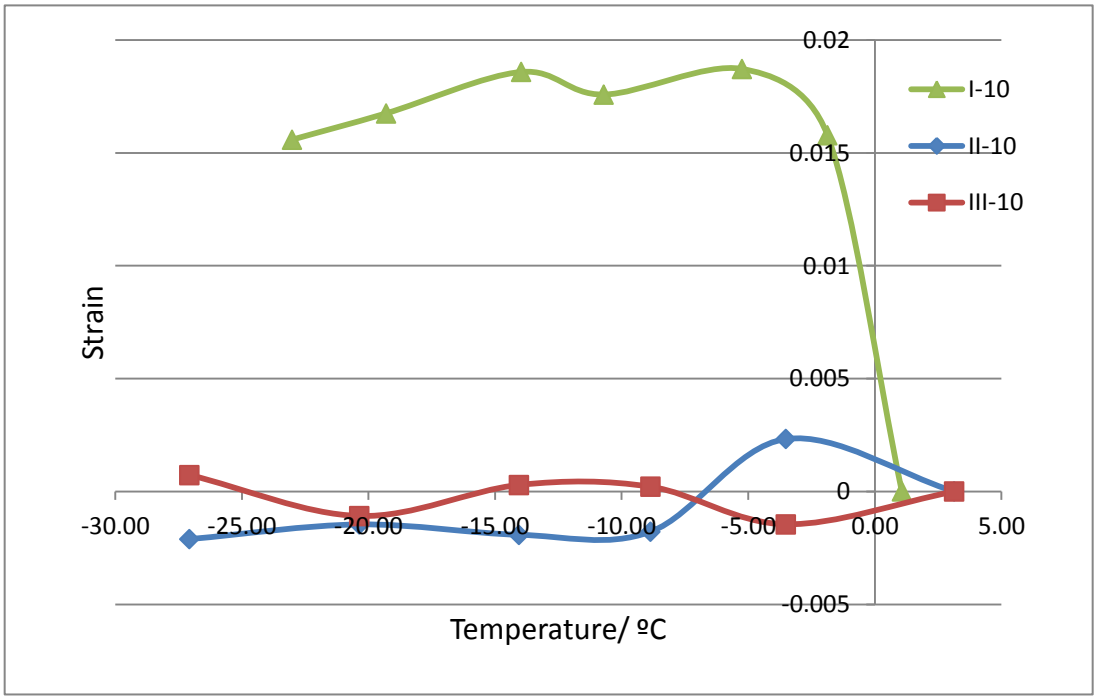

Fig. 27. Saturation degree =40%,AEA

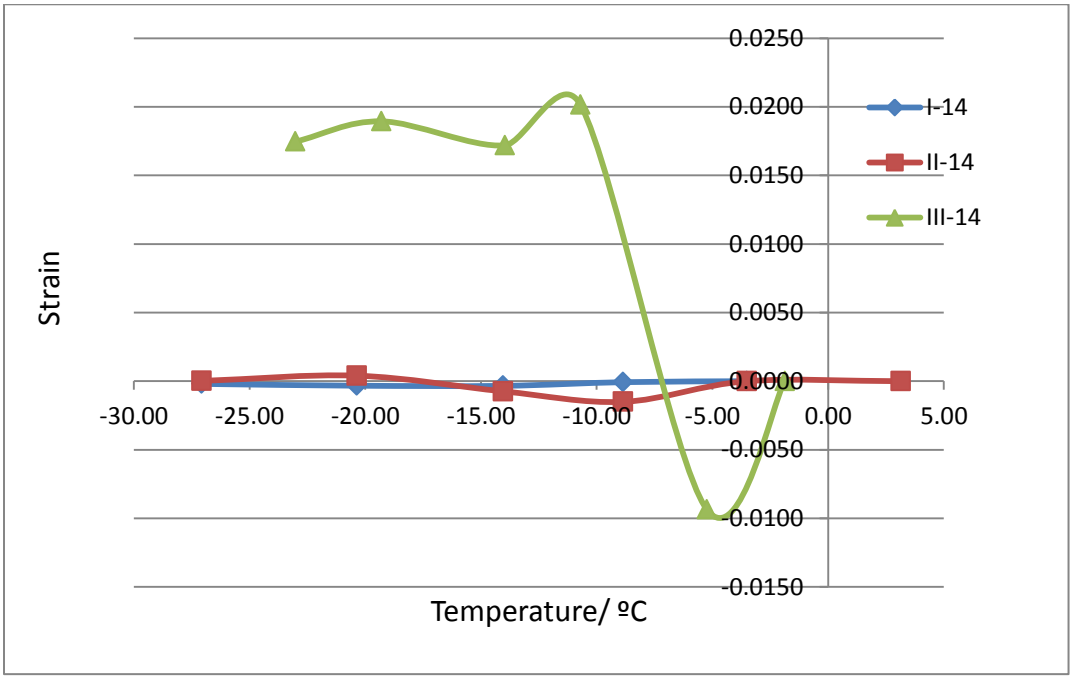

Fig. 28. Saturation degree =20%,AEA

Blue --- water/cement=0.45, Red ---water/cement= 0.5, Green --- water/cement= 0.6

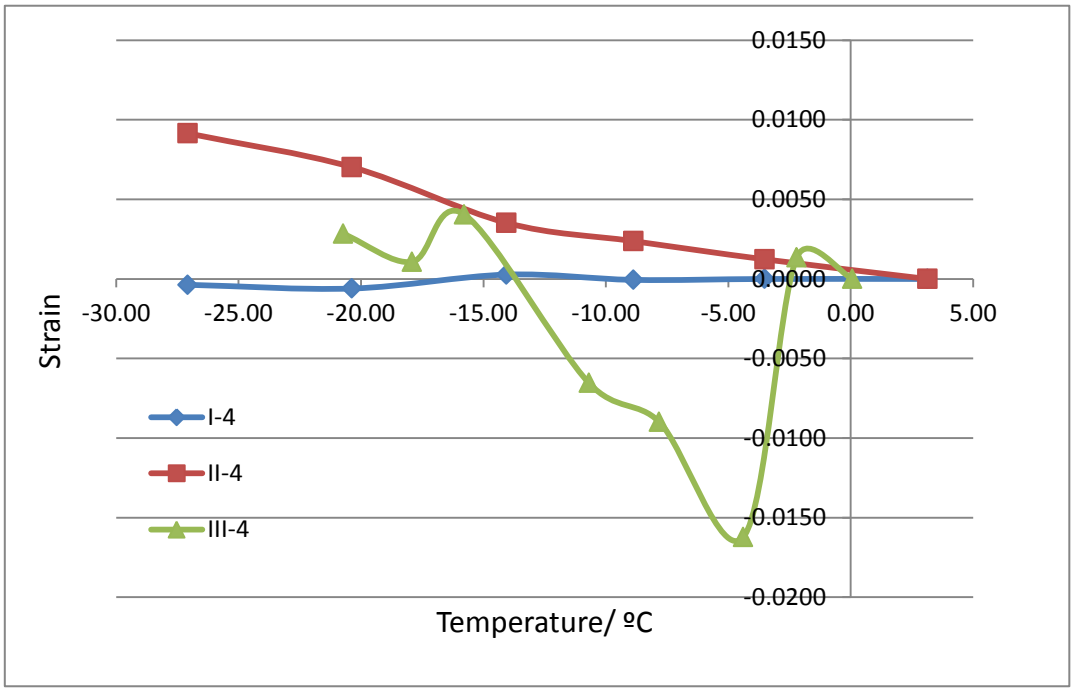

Fig. 29. Saturation degree =100%, No AEA

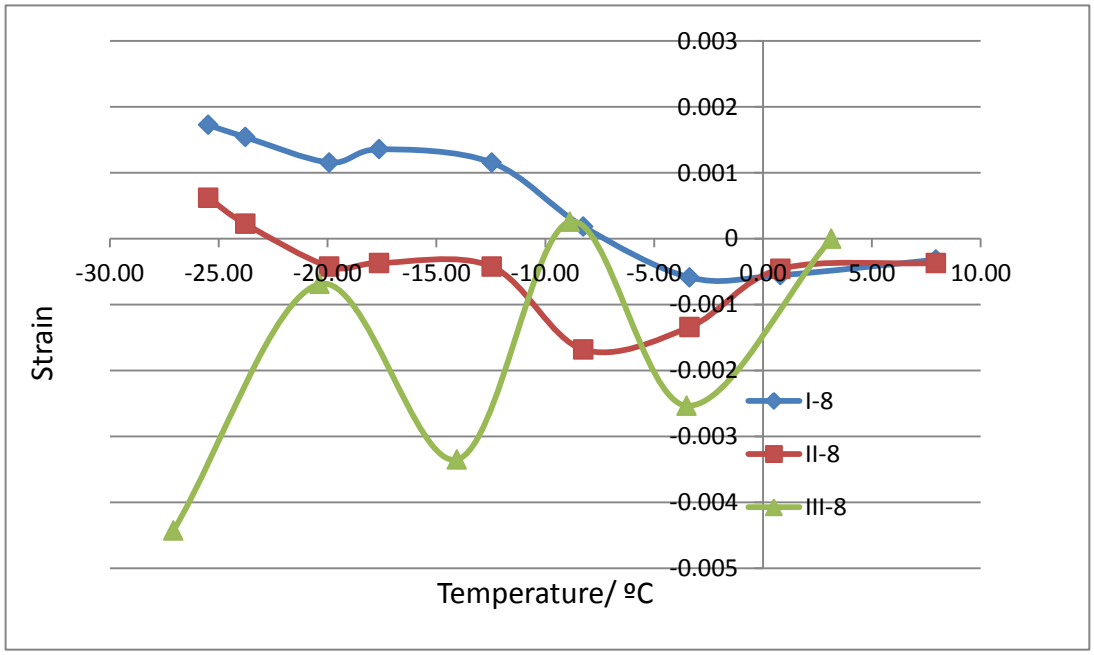

Fig. 30. Saturation degree =60%, No AEA

Blue --- water/cement=0.45, Red ---water/cement= 0.5, Green --- water/cement= 0.6

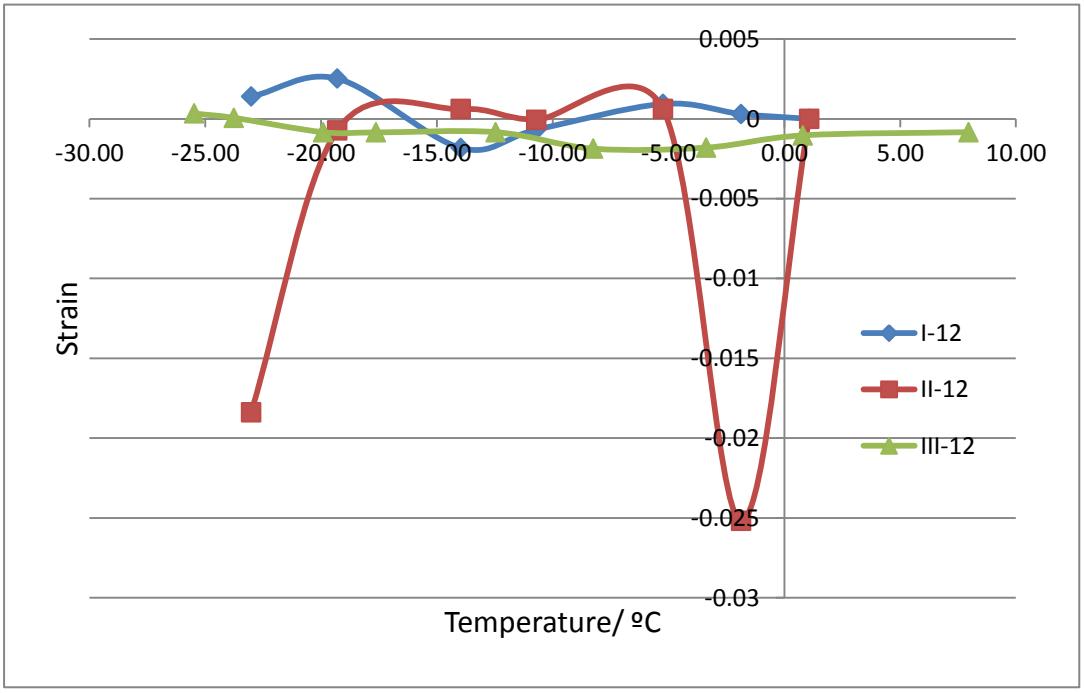

Fig. 31. Saturation degree =40%, No AEA

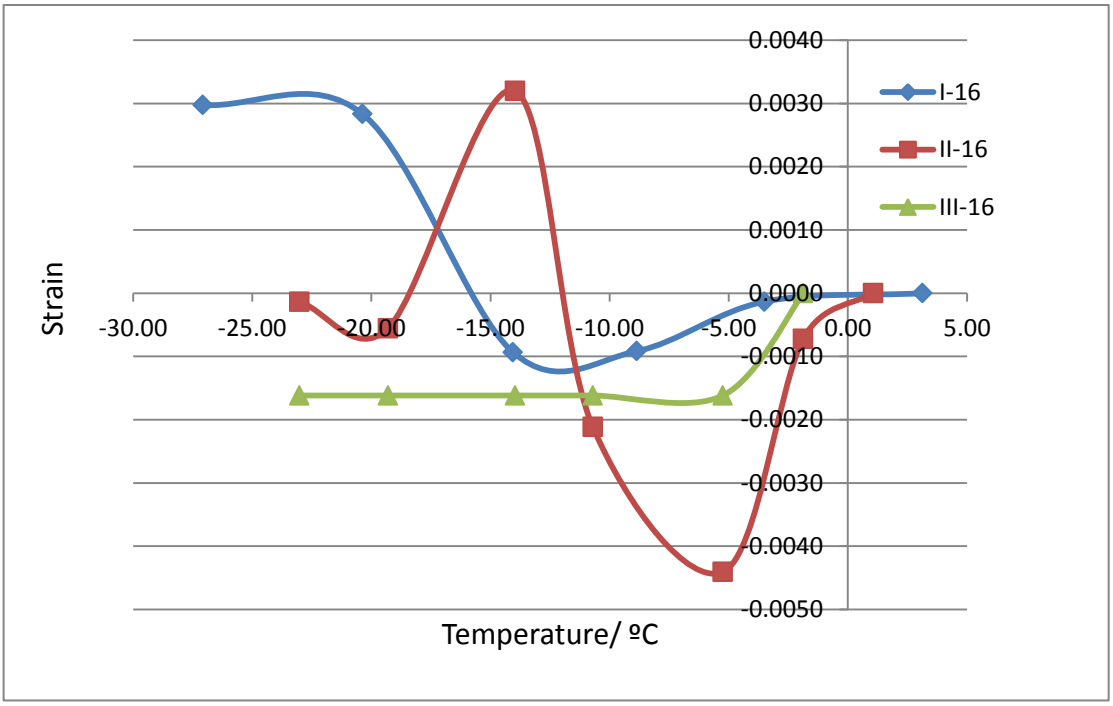

Fig. 32. Saturation degree =20%, No AEA

The total porosity will increase with the increase of the water/cement ratio, which helps to release the hydraulic pressure. Increases in the water/cement ratio will also result in an increase in the amount of evaporable water, which means a larger amount of ice formed during cooling. Increased water/cement ratio therefore has both positive and negative effects on the strain of fully saturated concrete. For conditions with the same saturation degree and added AEA, changes in the water/cement ratio results in large changes in the pore structure of the concrete. Variations in the water/cement ratio in this condition will also produce randomness in how the AEA introduces air bubbles to the concrete. These varying effects make it difficult to discuss the effect of water/cement ratio. But, some general trend can be observed from the present test data. For example, in the none-AEA and 100% saturated case (Fig. 29), the only influential factor is the water/cement ratio. When the water/cement ratio is 0.45, the deformation of I-4 is the smallest; when the water/cement ratio is 0.6, the deformation of III-4 appears to be the largest.

Compared with 0.5 and 0.6, water/cement ratio 0.45 will lead to small expansion. The concrete samples with low water/cement ratio outperformed those with higher water/cement ratio. Therefore, a low water/cement ratio is suggested to be used for concrete in freezing environment.

Result of the second test

Below is the mixing design for the second test. The first test studied the effect of air entraining agent, saturation degree, and water/cement ratio. The second test evaluated the effect of AEA's amount and saturation degree, with a fixed water/cement ratio 0.5.

Table 3. Mixing design for the second test

Mix ID	water/cement	Cement(Kg/m3)	Water(Kg/m3)	Fine Agg(Kg/m3)	Coarse agg(kg/m3)	Saturaion(%)	AEA
I'-1	0.5	356	178	848	1032	100%	0
I'-2	0.5	356	178	848	1032	60%	0
I'-3	0.5	356	178	848	1032	40%	0
I'-4	0.5	356	178	848	1032	20%	0
II'-1	0.5	356	178	848	1032	100%	50 ml/kg
II'-2	0.5	356	178	848	1032	60%	50 ml/kg
II'-3	0.5	356	178	848	1032	40%	50 ml/kg
II'-4	0.5	356	178	848	1032	20%	50 ml/kg
III'-1	0.5	356	178	848	1032	100%	100 ml/kg
III'-2	0.5	356	178	848	1032	60%	100 ml/kg
III'-3	0.5	356	178	848	1032	40%	100 ml/kg
III'-4	0.5	356	178	848	1032	20%	100 ml/kg
IV'-1	0.5	356	178	848	1032	100%	150 ml/kg
IV'-2	0.5	356	178	848	1032	60%	150 ml/kg
IV'-3	0.5	356	178	848	1032	40%	150 ml/kg
IV'-4	0.5	356	178	848	1032	20%	150 ml/kg

Effect of saturation

This study fixed the air entraining amount, but changed the saturation degree.

Blue ---- 100% saturation, Red ----60% saturation,

Green ---- 40 % saturation, Violet---- 20 % saturation

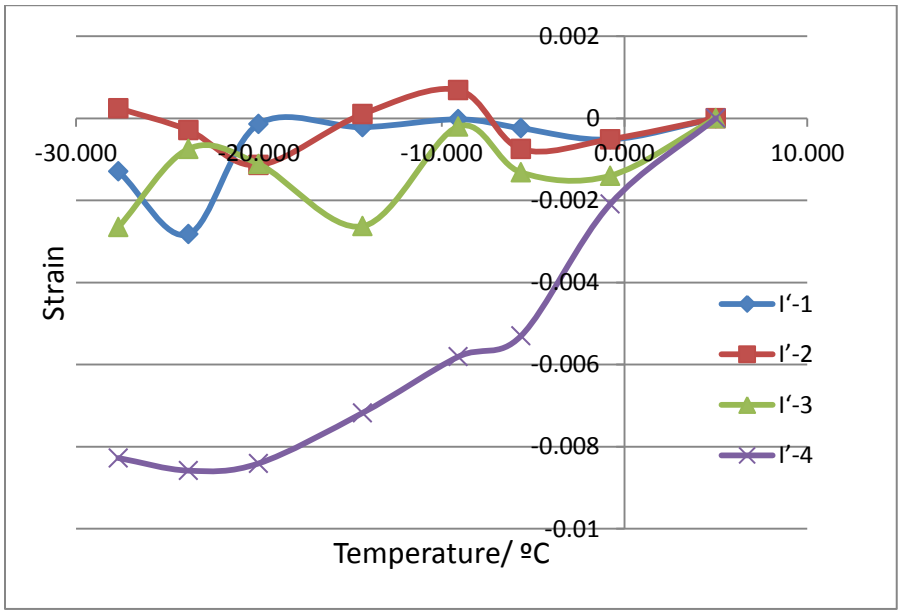

Fig. 33. AEA=0

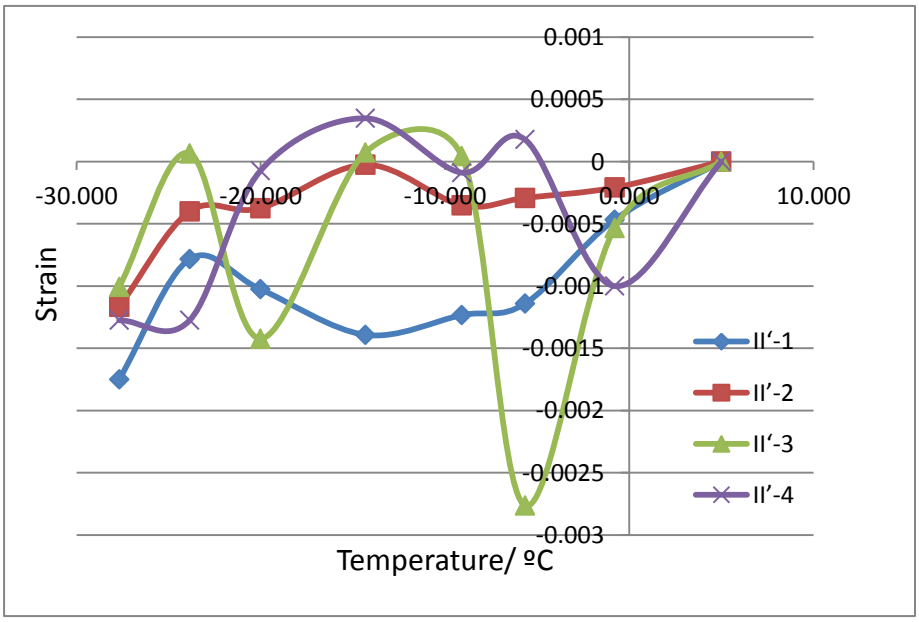

Fig. 34. AEA=50ml/100kg

Blue ---- 100% saturation, Red ----60% saturation,

Green ---- 40 % saturation, Violet---- 20 % saturation

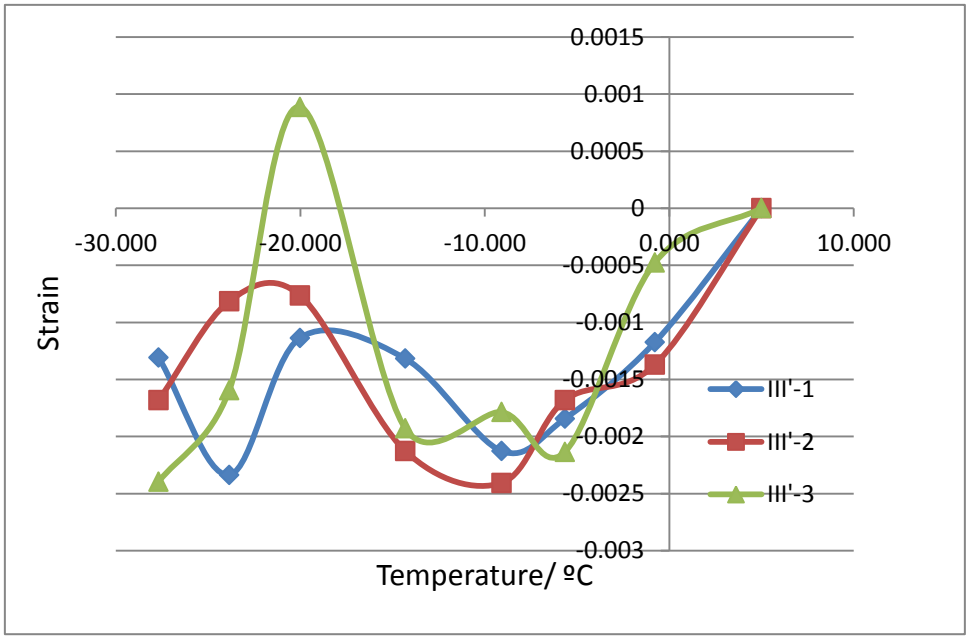

Fig. 35. AEA=100ml/100kg

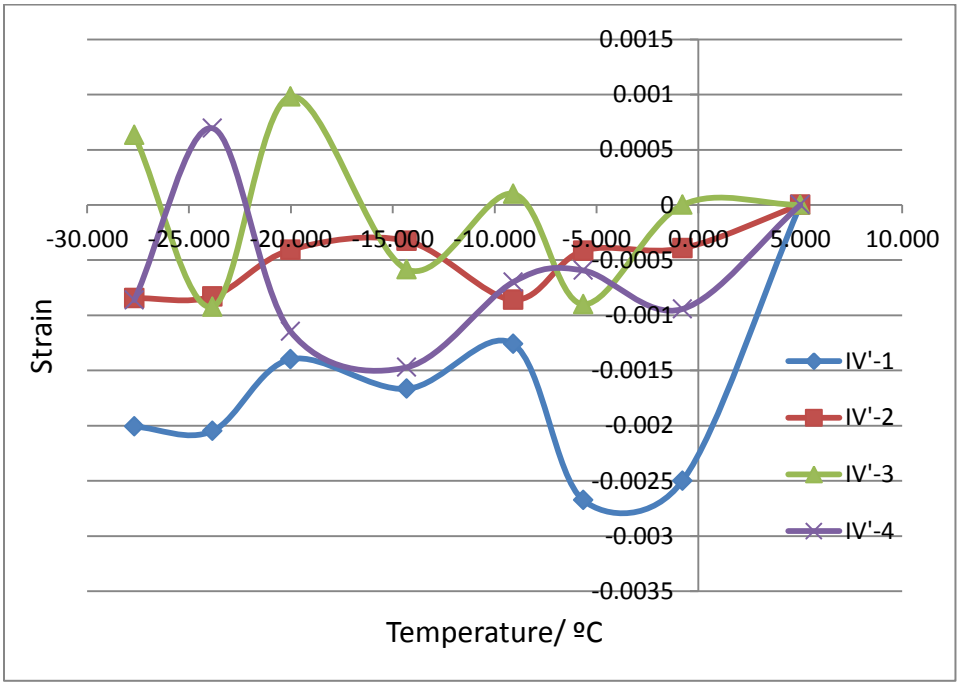

Fig. 36. AEA=150ml/100kg

The blue, red, green and purple curves present, respectively, 100%, 60%, 40%, and 20% degree of saturation When there is no air-entraining agent added (Fig. 33), specimen I'-4 (20% saturation) has a significant amount of contract since it has the lowest degree of saturation: 20%. This occurs because the hydraulic pressure can be released early enough to avoid a large expansion. By comparison, when the AEA dosage approaches the upper limit of the suggested dosage of 180ml/kg (Fig. 36), the 100% saturated specimen had the most contraction at the first period. At this saturation degree, the CTE of dilation is also larger than others afterwards. Additionally, looking at Fig. 35, when the dosage of AEA is 100ml/kg, the CTE of specimens (the slope in the graph) is so close to each other. Only the strain of III'-3 exceeds 0 to be positive (tensile), other remain below 0. As seen in Fig.34, a dosage of 50 ml/kg made the CTE of II'-1 and II'-2 small, with a flat strain curve. From one perspective, the 50 ml/kg dosage is good for controlling deformation of high saturated specimens. Conversely, a high dosage of AEA is better for controlling specimens of low saturation. A higher dosage of AEA has bigger risk to let the strain go above zero to be tensile, however, which is undesirable for concrete.

Effect of Air-entraining agent dosage

Blue ---- 0, Red ----50 ml/kg, Green ---- 100 ml/kg, Violet ---- 150 ml/kg

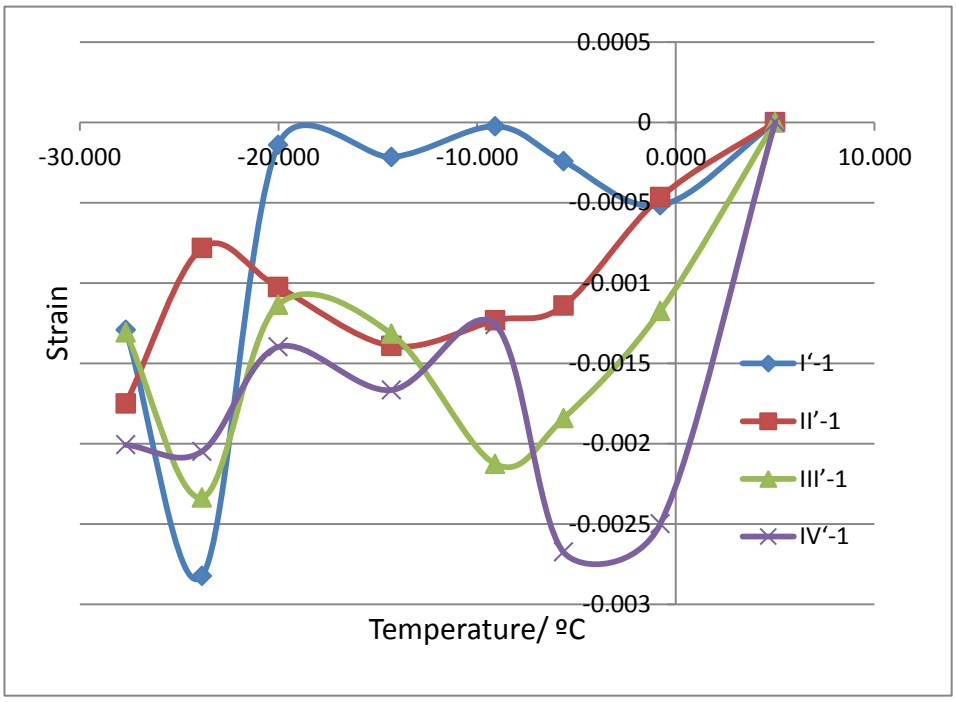

Fig. 37. Saturation degree =100%

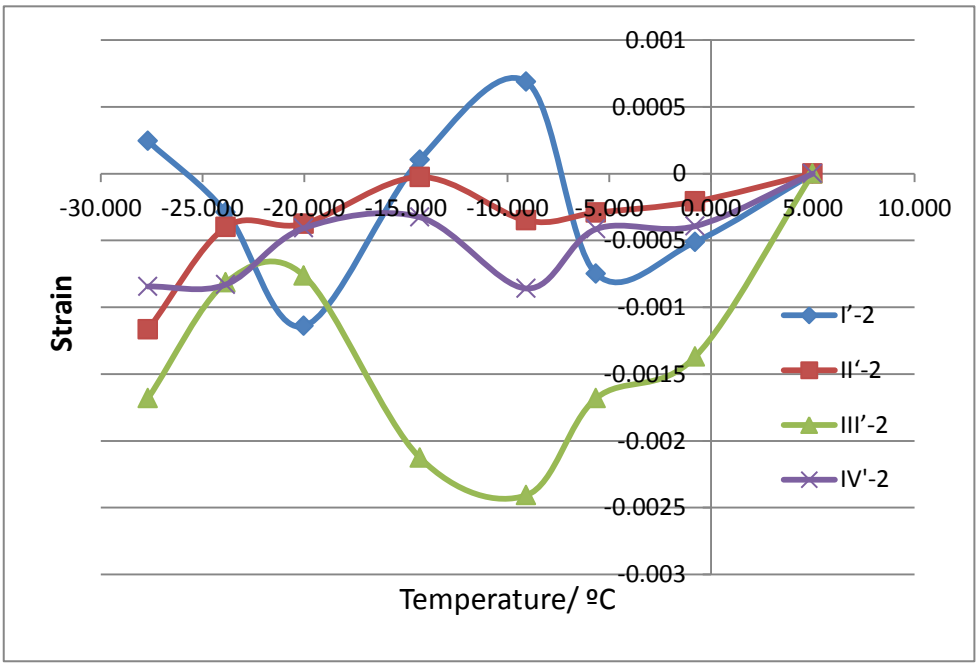

Fig. 38. Saturation degree =60%

Blue ---- 0, Red ----50 ml/kg, Green ---- 100 ml/kg, Violet ---- 150 ml/kg

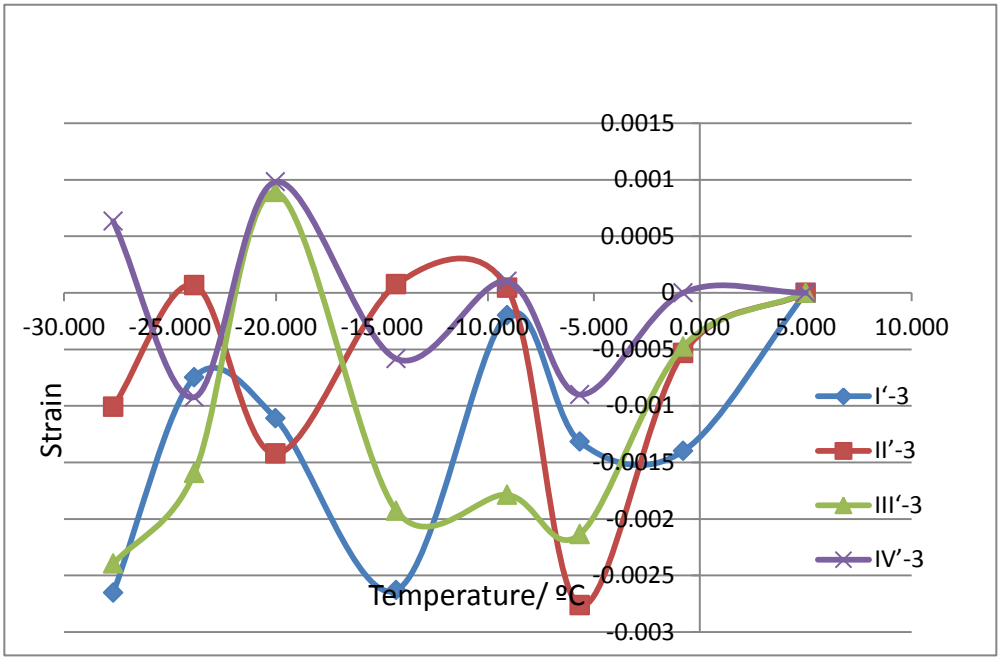

Fig. 39. Saturation degree =40%

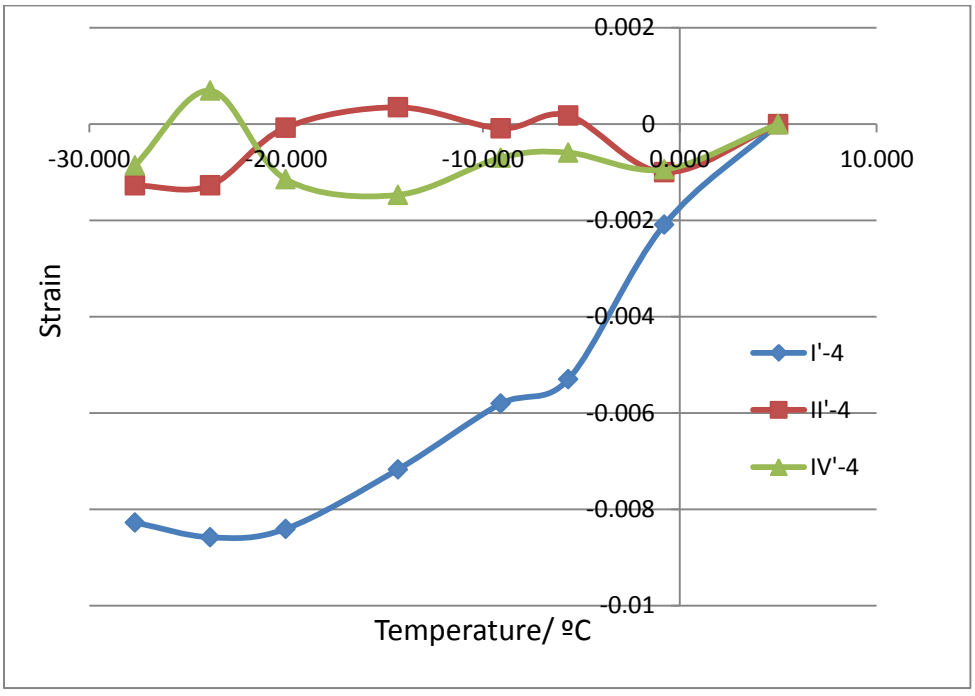

Fig. 40. Saturation degree =20%

The blue, red, green and purple curves respectively stand for specimens without AEA, 50ml/kg, 100ml/kg and 150ml/kg of AEA (on a basis of cement's mass). Despite the randomness of air bubbles AEA has introduced into concrete, more AEA is suggested for use with high saturation degrees. By comparison, it is not suggested to add large amounts of AEA for specimens with low degree of saturation, because more evaporable water due to new pores will cause a lot of expansion. Summarizing the best effect of AEA, a dosage of 50ml/kg based on cement's mass shows good result at saturation of 100%, 60%, and 20%. Alternatively, a dosage of 150 ml/kg has a good effect to control the dilation when saturation is 60% and 20%, and a dosage of 100ml/kg shows two peaks on the strain curve.

The reasonable dosage of air-entraining agent should be based on the saturation degree of concrete. A dosage of 50ml/kg is good to control the expansion of highly saturated concrete, while a higher dosage of AEA helps to control the concrete of low saturation. An optimal dosage of air-entraining agent for minimizing the dilation of concrete under different saturation is shown in the table below.

Table.4a Optimal AEA Dosage verse Saturation degree

Saturation	Possible Environments	Optimal AEA Dosage	Maximum Dilation Strain
20%	Arid above-ground	0	0
40%	Semi-arid above-ground	150ml/kg	0.002
60%	Humid above-ground	50ml/kg	0.003
100%	Marine	50ml/kg	0.008

These results suggest that the amount of AEA and the saturation degree are related closely. This study, however did not establish an exact correlation of the relationship between these two parameters.

Brunauer-Emmett-Teller RESULT

With the experimental results discussed above, we found out that pore size distribution in concrete is important for analyzing the behavior of concrete under low temperatures. Desorption data at different saturated pressure provides the pore volume of different sizes (Barrett et al. 1951). Thus, the BET test was conducted on some of the concrete samples, which yielded information of incremental and cumulative pore volume at different diameters.

Two of our fully saturated samples with different amounts of AEA content were used for the BET test. e BET test results are attached in the Appendix.

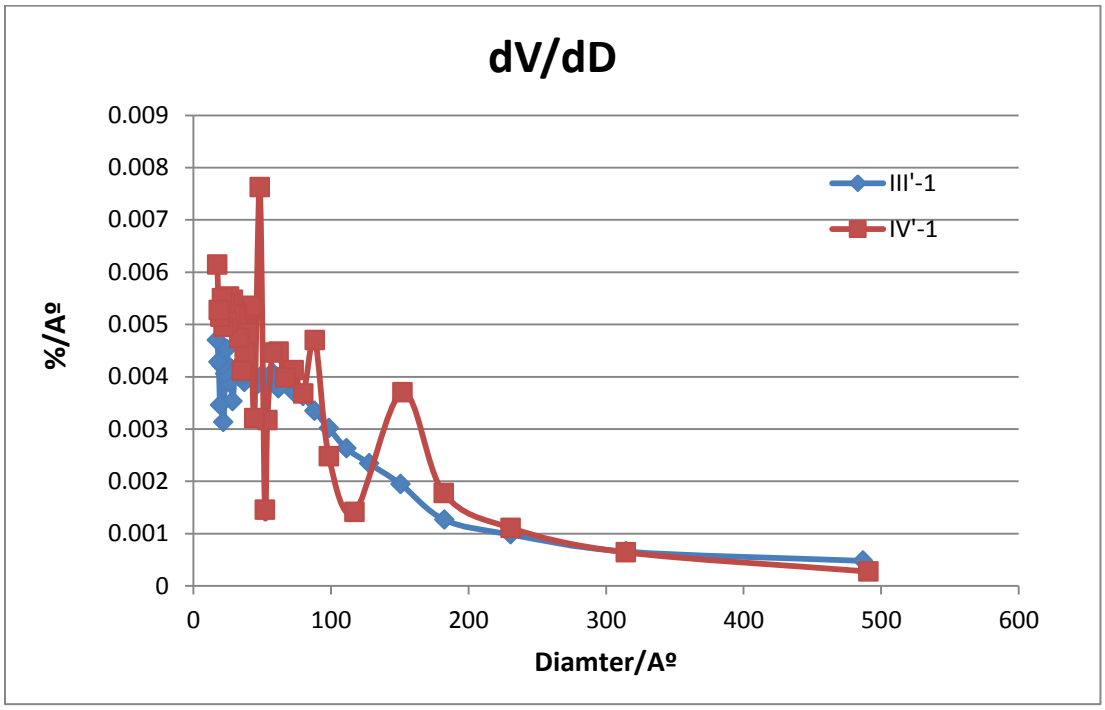

Fig. 41. dV/dD (percentage)

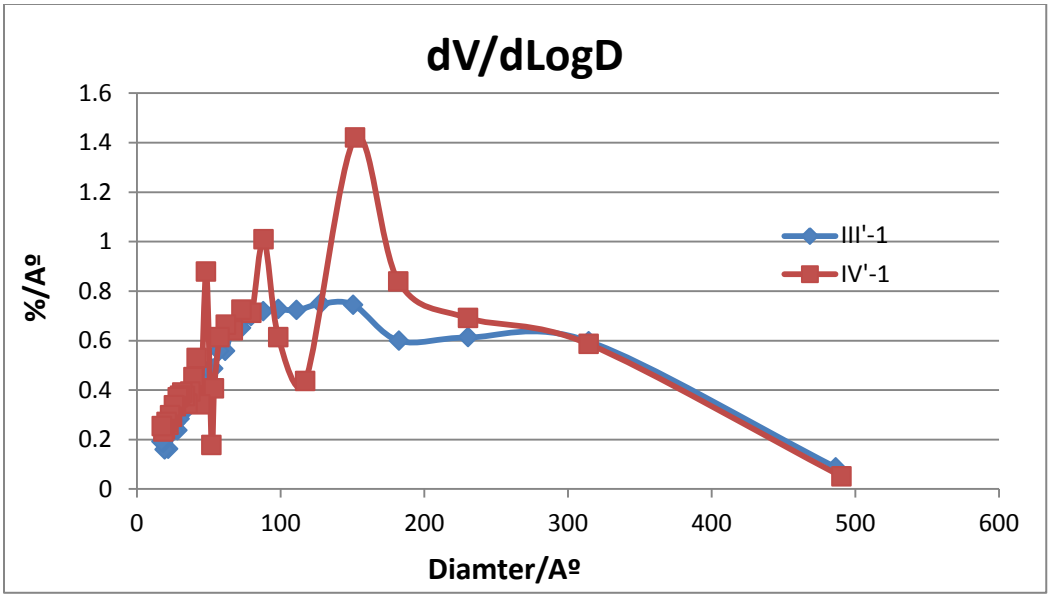

Fig. 42. dV/dLogD (percentage)

Figures 41 and 42 show the pore size distribution for specimens III'-1 and IV'-1, in two different scale systems. Worth mentioning, these two specimens are 100 % saturated, which makes it convenient to build a theoretical model for prediction of the thermal deformation. Meanwhile, studying these two specimens shows the effect of air entraining agent on a microscopic level. In Fig.42, the change of volume is plotted against the change of diameter. In Fig.43, the change of volume is against the change of log function of diameter. The advantage of a log function makes the pore size distribution more like a normal distribution. For both specimen III'-1 and IV'-1, there are several local peaks on the pore size distribution curves. There are also several peaks on the strain-temperature curves. Theoretically, these peaks should correspond to each other. It is known that the freezing point of concrete varies with the size of pores . If the temperature reaches a point where a lot of pore water will freeze at the same time, significant dilation will occur. This explains why the peaks on the strain curve and pore size

distribution should match. At the same time, the contraction of concrete and nucleated ice is not negligible. The total strain of concrete is a combination of these two behaviors..

Figures 41 and 42 are expressed by percentage. The absolute data was also plotted below in Figures 43 and 44. It should be noticed that the IV'-1 has a higher dosage of AEA than III'-1. Additionally, the absolute pore volumes of IV'-1 in both Fig. 41 and Fig. 42 are much higher than that of III'-1 at certain diameter. However, at some diameters, the pore volumes of IV'-1 are below those of III'-1. This phenomenon is also demonstrated well in Fig. 37, where the green curve and purple curve overlap significantly. The green curve and purple curve have different local peak temperatures, because their peaks in the pore size distribution happened at different diameters. This makes the dilation occur at different temperatures. In Fig. 37, strain curves of III'-1 and IV'-1went up and down at different temperatures. For example, the IV'-1 curve begins to dilate around -5 ℃, while the purple curve begins to go down around -10 ℃ and the green curve begins to go up. The diameter corresponding to IV-1's peak is higher than that of III-1's (seen in Fig. 41). As a result, the dilation of IV'-1 will occur at a higher temperature. That is in agreement with the strain curve.

All detailed BET results for III'-1 and IV'-1 are listed in Appendix A and Appendix B.

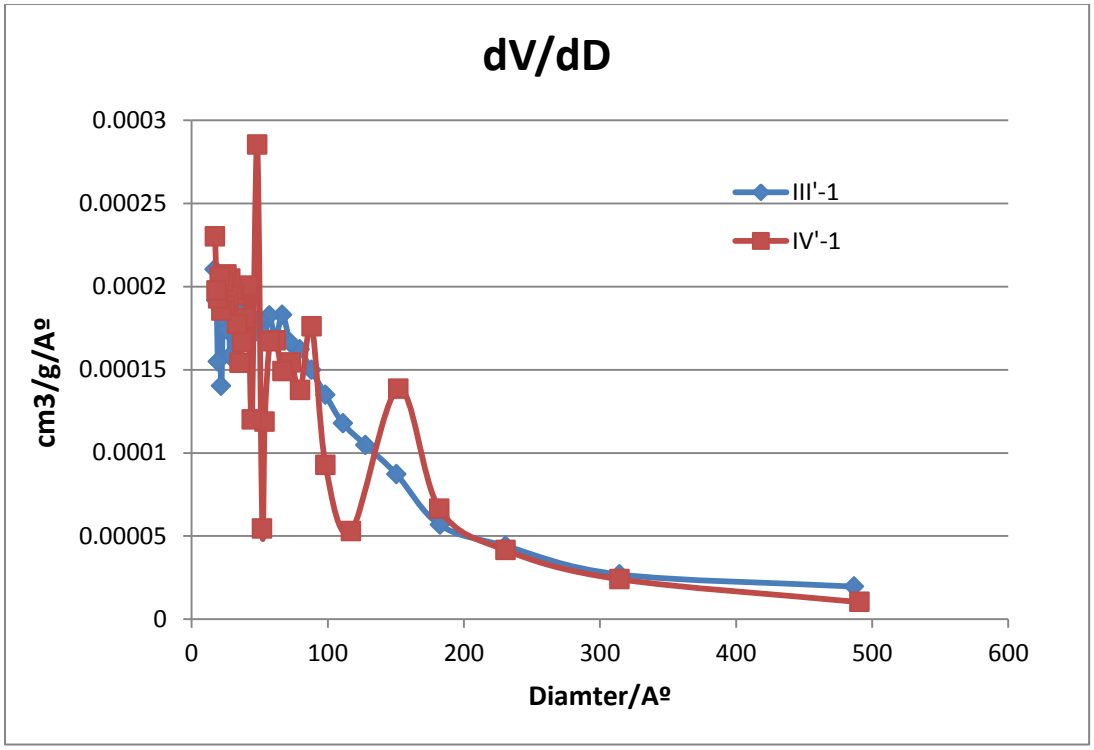

Fig. 43. dV/dD (absolute value)

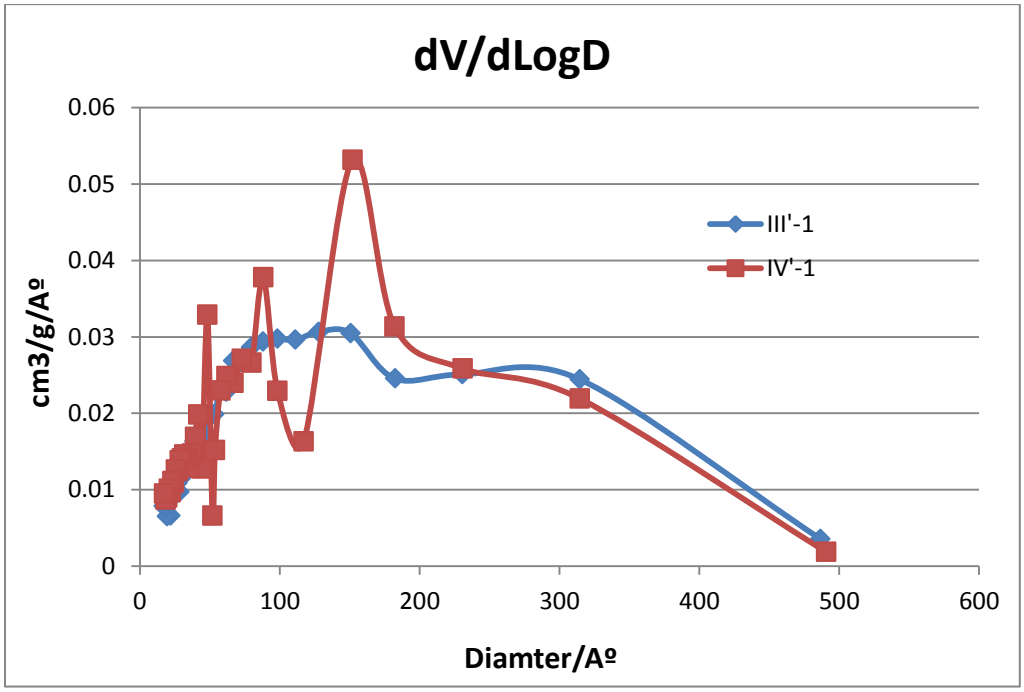

Fig. 44. dV/dLogD (absolute value)

DESCRIPTION OF MODELING PROCESS

The main purpose of establishing a theoretical model is to simulate the freezing process of concrete and to calculate the strain of concrete under different temperatures. The theoretical model is based on the study on modeling the drying shrinkage of concrete by a multiscale effective homogeneous theory (Xi et al. 1997). Xi et al. introduced a method to model the effective bulk modulus and effective shrinkage strain of concrete material constructed of two or more phases. Fig. 45 is the flow chart describing how this model works. From the BET test, the pore size distribution and cumulative pore volume percentage can be obtained and a relationship between cumulative pore volume and pore diameter can be established. The temperature will be lowed until all the pore water turned into ice. The last group of pores which will freeze is the pores of the smallest diameter. Therefore the 100% cumulative pore percentage will be set at the smallest pore diameter. At Step 5, the freezing point of different sizes of pores can be obtained from Bazant et al. (1988), see Fig. 46a Combining Step 4 and Step 5, a relationship between cumulative frozen pore volume and cooling temperature can be established. The theoretical model was coded by Excel to find a formula for cumulative frozen pore volume in terms of cooling temperature. As it can be seen in Fig. 46b, the curve fitting result precise to 30 digits after the point almost had no error. This formula can tell how much of total pore water will freeze at a certain temperature.

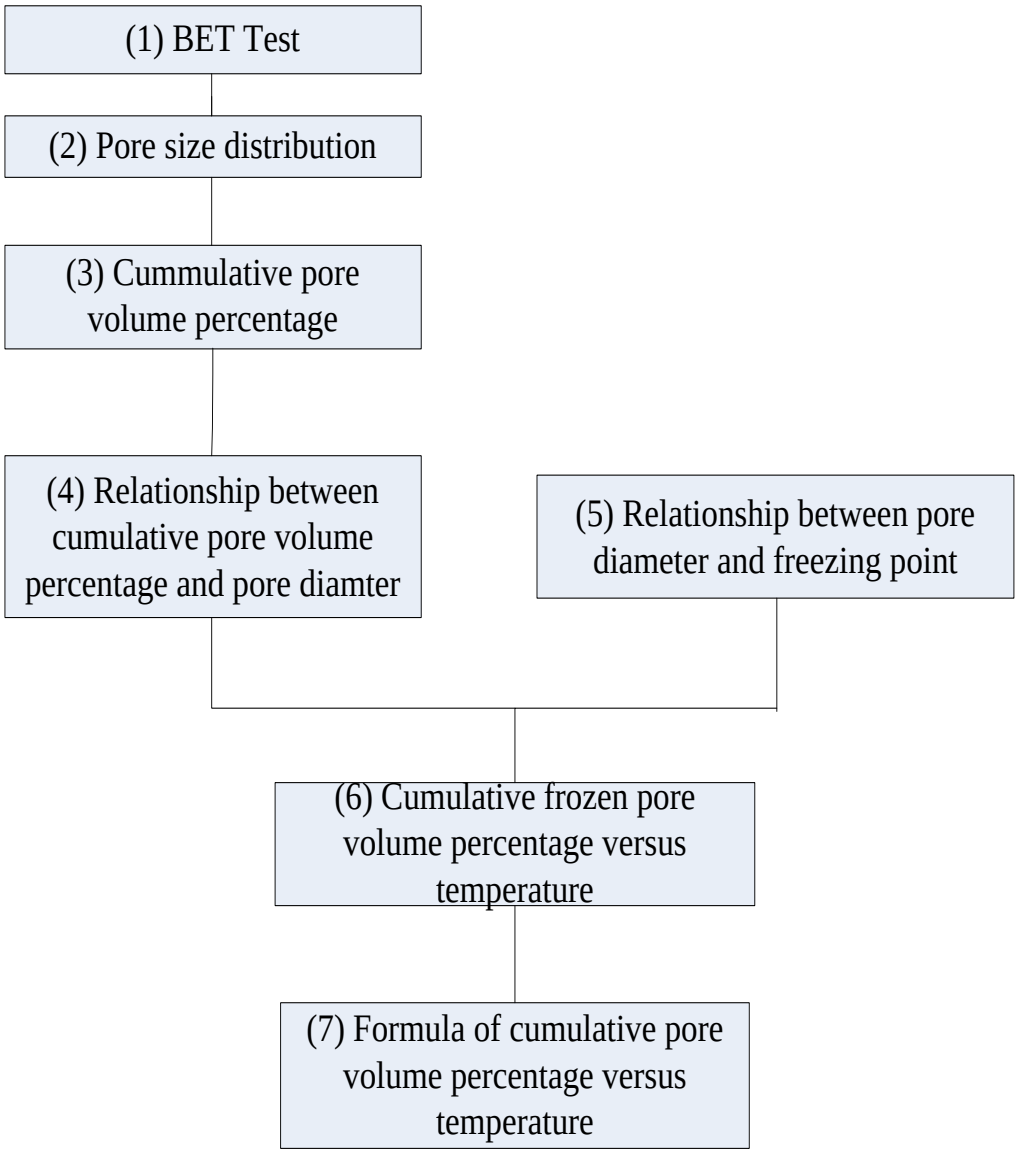

Fig. 45. Process of numerical model

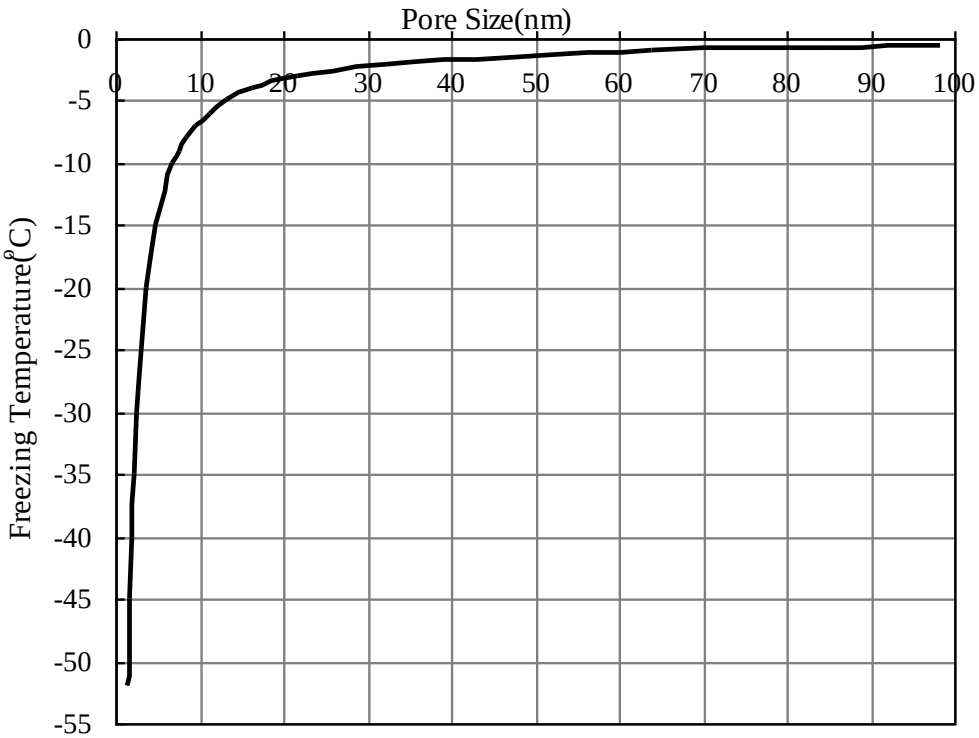

Fig. 46a. Variation of freezing temperature in terms of pore size at constant pressure for water [Bazant et. al. 1988]

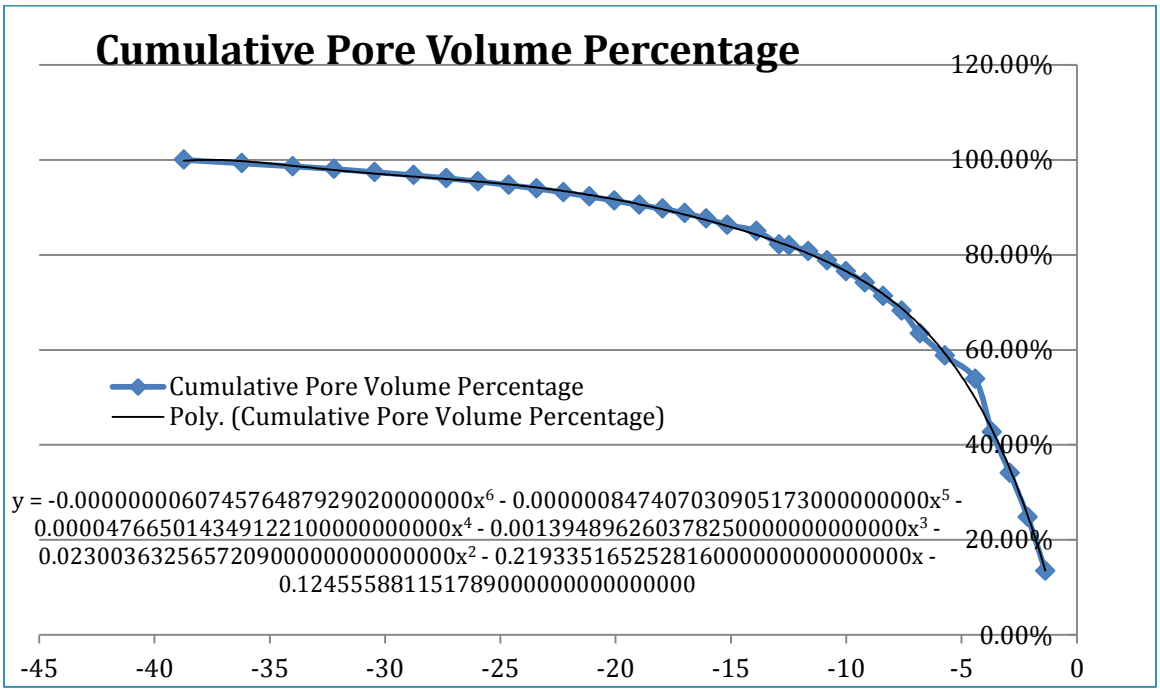

Fig. 46b. Cumulative pore volume percentage at different temperature

Based on the model developed by Xi et al. (1997), we modified the multiscale model by considering ice as phase 1, the concrete without ice as phase 2, and the concrete + ice as the homogeneous effective medium (Fig. 47).

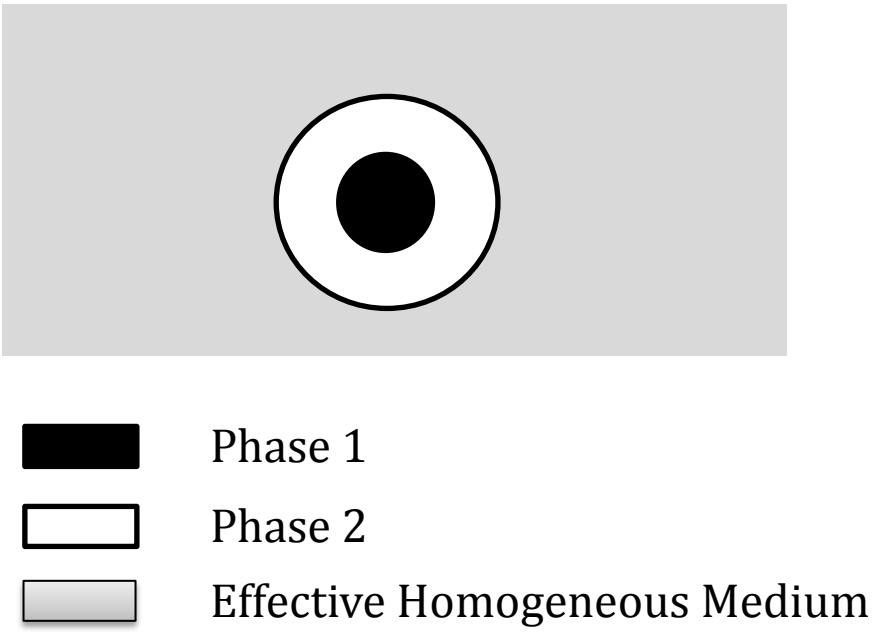

Fig. 47. The composite model for concrete with ice

There are several assumptions or simplification with this numerical model. First, the model neglected the movement of the water under freezing. Second, there is only one phase of water for each pore: frozen or unfrozen. Third, only the water from the humid environment is counted for the freezable water. Fourth, the water is considered as the same CTE as the concrete in the beginning. Last, we just considered thermal strain in the model, neglecting the incremental strain cause by micro cracks.

Until the water in the first pore freezes, the concrete's behavior is considered as a homogeneous contraction. After the pore water freezes, the two-phase self-consistent model is used to obtain effective strain and bulk modulus at every temperature step. The formulas are as follows:

$$K_{eff} = \frac{K_2(3K_1 + 4G_2) - 4c_{12}G_2(K_2 - K_1)}{(3K_1 + 4G_2) + (3K_2 - 3K_1)c_{12}}$$

$$\varepsilon_{eff} = \frac{K_1 c_{12}\varepsilon_1(3K_2 + 4G_2) + K_2\varepsilon_2(1 - c_{12})(3K_1 + 4G_2)}{K_2(3K_1 + 4G_2) - 4c_{12}G_2(K_2 - K_1)}$$

In this case, ε_1 is the strain caused by the dilation of ice. ε_2 is the strain caused by the contraction of the concrete. K_1 and K_2 are the bulk modulus for phase 1 and phase 2 (ice and concrete). G_1 and G_2 are the bulk modulus for the phase 1 and phase 2. c_{12} is the volume ratio of phase 1 terms of total volume, that is, the ice content.

As described above, the temperature step is an important parameter in the model. The expansion of newly formed ice will depend greatly on this step. The density of ice is 0.917 g/cm ^{3}; the density of water is 1 g/cm ^{3}; therefore the expansion will be around 9%. In a pore of certain size, when the freezing point is reached, the water in the pore turns into ice, creating the 9% volume expansion; then the phase 1 (ice) contracts with the value of its CTE at all temperatures. .

For ice, the typical value of Young's modulus is 9.0 GPa and Poisson's ratio is 0.33 at -5 ℃. The coefficient of thermal expansion of ice equals 50x10-6/C. For concrete, the typical value of Young's modulus is 4,000 ksi and Poisson's ratio is 0.2. The coefficient of thermal expansion of concrete is 6x10-6/C (this value varies depending on the aggregate).

$$\mathrm{K}_1 = \frac{E_1}{3(1 - 2v_1)} = 9.091GPa \qquad \mathrm{G}_1 = \frac{E_1}{2(1 + v_1)} = 3.383GPa$$

$$\mathrm{K}_2 = \frac{E_2}{3(1 - 2v_2)} = 15.316GPa \qquad \mathrm{G}_2 = \frac{E_2}{2(1 + v_2)} = 11.489GPa$$

MODELING RESULTS

This section presents some of the simulation results. BET test was performed for III'-1 and IV'-1. The pore size distributions were then incorporated into the model. III'-1 and IV'-1 were chosen because there are several peaks on the experimental strain curves, and the AEA dosages were different for the two specimens. It is worth comparing them by the model to see if the same trend can be obtained.

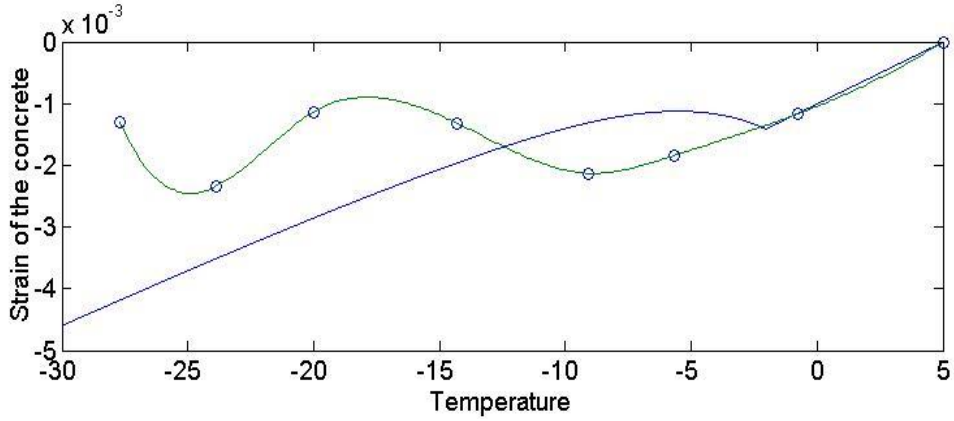

Fig. 48. III'-1 Modeling result and experimental result

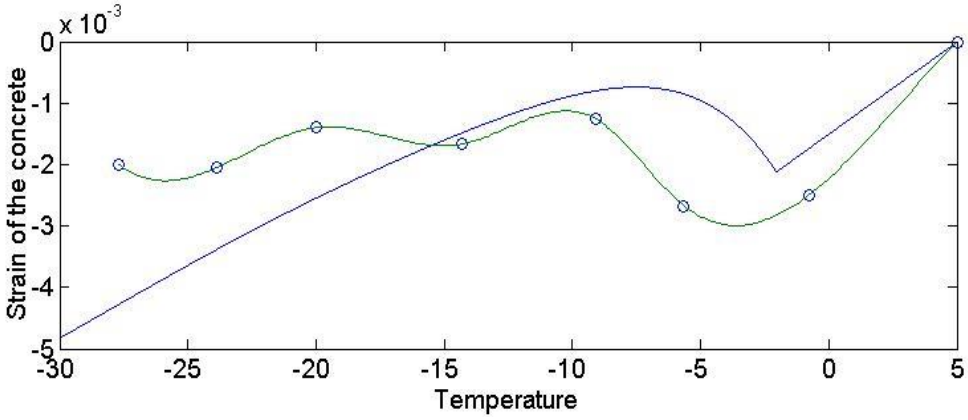

Fig. 49. IV'-1 Modeling result and experimental result

The graphs above compared the modeling results and experimental results. We can see that the values of the negative strain of experimental and modeling ones are close. For III'-1, the strain at -25 ℃ is around -0.025 and model shows the strain is -0.0038. For IV'-1, the strain at -25 ℃ is around -0.0023, and the model indicates the strain is -0.0037. This is an acceptable difference for strain at low temperatures. We next considered the transition zone; the transition point describes where the concrete went from dilation to contraction or from contraction to dilation. There are three transition points: -10 ℃, -17 ℃ and -25 ℃ for specimen III'-1, but the model can just simulate two transition points, around -2 ℃ and -7 ℃. For IV'-1, the model simulated the transition points around -5 ℃ and -12 ℃, while in the model they are -2.5 and -8 ℃. Therefore, the model matches better for specimen IV'-1 than III'-1. Even just comparing the two modeling results of two specimens it can be seen that, the transition point has shifted, and IV'-1 has a bigger contraction. This is reasonable since IV'-1 has 50ml/kg more (on a basis of cement's mass) AEA than III'-1. The contraction should be larger at a lower temperature.

The volume fraction of ice on a basis of volume of concrete has been plotted, as well. It shows that theoretically the volume faction of ice grows smoothly. To analyze the behavior of transition points, the concrete's instant strain of contraction and the ice's instant strain of dilation at each temperature were plotted in the Fig. 48. Instantly, the strain caused by dilation is more significant than the contraction of concrete after the first pore reaches the freezing point. The instant strain of ice, however, will go down while the instant strain of concrete will stay almost the same. From Fig. 48, the absolute values of green curve were first greater, and then grew smaller than the blue curve. Additionally, the value of red curve was first positive, then negative. This explains why the transition point will happen.

Overall, the model explains the phenomenon well, but may not be precise enough to detect every actual change.

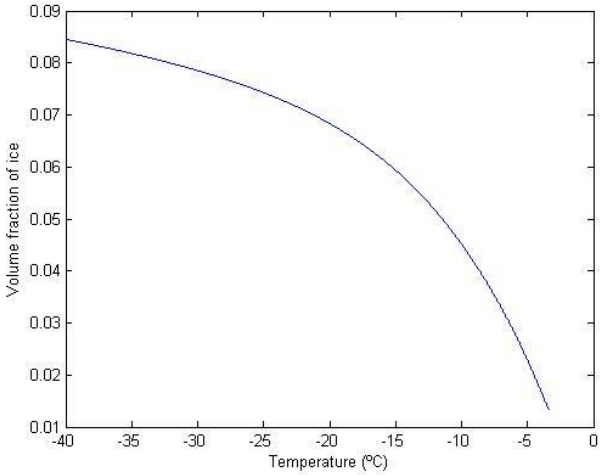

Fig. 50. Volume fraction of ice

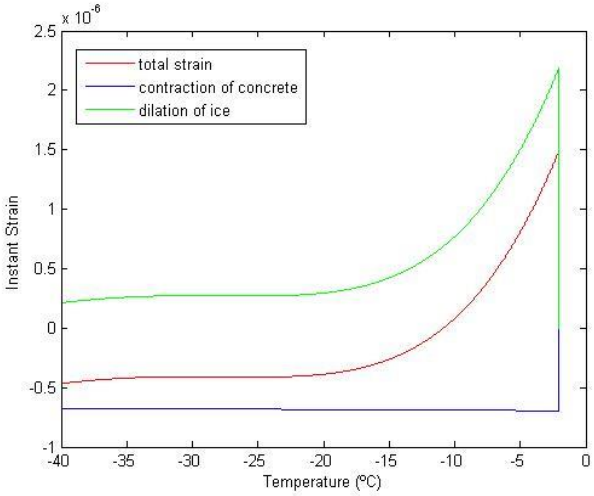

Fig. 51. Comparison of instant strain

CONCLUSION AND FUTURE PROSPECT

- The water/cement ratio, air-entraining agent dosage and saturation degree all have an influence on the freezing property of concrete. Their combined effect will determine the pore size distribution. This will govern the anti-freezing property of concrete, which controls how concrete dilates and contracts when temperature decreases.
- A critical saturation degree exists for concrete. The critical saturation degree depends on the pore size distribution of the concrete. In this study, the critical saturation degree is believed to be 40%, because all concrete specimens have a dilation of at least 0.002..
- The reasonable dosage of air-entraining agent should be based on the saturation degree of concrete. A dosage of 50ml/kg is good to control the expansion of highly saturated concrete, while a higher dosage of AEA helps to control the concrete of low saturation. Optimal dosages of air-entraining agent for minimizing the dilation of concrete under different saturations are shown below.

Table.4b Optimal AEA Dosages verse Saturation degrees

Saturation	Possible Environments	Optimal AEA Dosage	Maximum Dilation Strain
20%	Arid above-ground	0	0
40%	Semi-arid above-ground	150ml/kg	0.002
60%	Humid above-ground	50ml/kg	0.003
100%	Marine	50ml/kg	0.008

- A low water/cement ratio will help control the deformation of concrete specimen as it lowers the total volume of pores inside concrete. A water/cement ratio of 0.4 is a good option for concrete used under low temperatures.
- A machine that can control precisely the degree of saturation will improve test results.

- The optimal dosage of air-entraining agent for different saturation conditions can be determined after more systematic tests.
- The plot dV/dLogD versus diameter can better reflect the pore size distribution than the plot dV/dD.
- The pore size distribution of concrete and cumulative pore volume will determine how the concrete will act against freezing temperature. BET test is an advantageous way to know the characteristics of pores inside concrete.
- Considering the pore size distribution in the two phase self-consistent model, a theoretical model was developed to predict the thermal strain of concrete under low temperatures. This model can simulate the basic trend of concrete deformation under low temperature very well.
- A difference of 5 ℃ exists between the transition points of numerical model and experiment result. The difference of peak strain between model and experiment is around 0.001.
- More sophisticated theoretical model about the anti-freezing action of partially saturated concrete can also be built. That could verify the actual strain of concrete under low temperature in different environments.

REFERENCES

Atahanm, H.N., Oktar, O.N. and Tasdemir, M.A. (2009). "Effects of water–cement ratio and curing time on the critical pore width of hardened cement paste." *Construction and Building Materials*, (23), 1196–1200.

Barrett, E.P., Joyner L.G., and Halenda, P.P. (1951). "The Determination of Pore Volume and Area Distributions in Porous Substances. I. Computations from Nitrogen Isotherms." *J. Am. Chem. Soc.*, 73(1), 373-380.

Bazant, Z.P., Chern, J.C., Rosenberg, A.M., and Gaidis, J.M. (1988). "Mathematical Model for Freeze-Thaw Durability of Concrete." *J AMER CERAM SOC* , 71(9), 776-783.

Chen X., & Wu, S. (2013). "Influence of water-to-cement ratio and curing period on pore structure of cement mortar," *Construction and Building Materials*, (38), 804–812.

Chatterji, S. (2003). "Freezing of air-entrained cement-based materials and specific actions of air-entraining agents." *Cement & Concrete Composites*, (25), 759-765.

Chatterji, S. (1999). "Aspects of the freezing process in a porous material – water system: Part 2. Freezing and the properties of water and ice." *Cement and Concrete Research*, (29), 781–784,

Fagerlund, G. (1997). "On the Service Life of Concrete Exposed to Frost Action." *Freeze thaw Resistance of Concrete*, 23-41.

Helmuth, R.A. (1961). "Dimensional changes of hardened Portland cement pastes caused by temperature changes." *Highway Research Board Proceedings*, (40), 315–336.

Larsson, L-E., & Purins, E. (1980). "Determination of the critical degree of saturation autoclaved lightweight aerated concrete by studying deformations in single-cycle freezing tests." *The International Journal of Lightweight Concrete, cement and concrete research*, 2(1), 33-41.

Setzer, M., Augberg, R., and Keck, H-J. (2002). "Frost Resistance of Concrete." Essen, Germany: RILEM Publications,

Sun, Z.H. & Scherer, G.W. (2010). "Effect of air voids on salt scaling and internal freezing." cement and concrete research, (40), 260-270.

Xi, Y., & Jenning, H.M. (1997). "Shrinkage of cement paste and concrete modeled by a multiscale effective homogeneous theory," Materials and Structures, (30), 329-339.

Zuber, B., Marchand, J., Delagrave, A., and Bournazel, J.P. (2000). "Ice formation mechanisms in normal and high-performance concrete mixtures," *Journal of Materials in Civil Engineering*, 12(1), 16-23,

Zhou, Z. & Mihashi, H. (2008). ”Micromechanics Model to Describe Strain Behavior of Concrete in Freezing Process.” *J. Mater. Civ. Eng.* 20, SPECIAL ISSUE: Durability and Service Life of Concrete Structures: Recent Advances, 46–53.

Zuber, B. & Marchand, J. (2004).“Predicting the volume instability of hydrated cement systems upon freezing using poro-mechanics and local phase equilibria.” Materials and structures/Concrete science and engineering, (37), 257-270.

CHAPTER 3

DURABILITY AND PROCESSING TECHNIQUES OF CONCRETE WITH CNTs

ABSTRACT

Having an extraordinary mechanical property, also having a good thermal and chemical resistance, CNT has promising future to be applied into concrete. However, the high Van Der Walls force between CNTs due to the high aspect ratio make the CNT tend to agglomerate and less effective in use. Several mechanical methods were tried, but didn't succeed to distribute CNT well in water. In order to solve the dispersion issue, an ultrasonicator was then used and was capable of dispersing CNT well in water. Several chemicals were also utilized in order to get a more stable CNT aqueous solution. CNT concrete were made following the general procedure. Compressive strength, chloride resistance and freeze thaw durability were the three big concerns in this research. Results showed that CNT can increase the compressive strength of concrete a lot. However, without the help of chemicals, CNT concrete tend to have a terrible durability. Among the chemical treated CNT concrete, Sodium Polyacrylate treated concrete shows good result in compressive strength, chloride resistance and freeze thaw durability, which was a discovery for this CNT concrete research. Besides this, the optimal CNT mass content, the optimal ultrasonication time were all found in this research. Even showing good result in small samples, CNT still has a long way to go if needed to put into utilization in industry.

BACKGROUND AND OBJECTIVES

Introduction

The discovery of the carbon nanotubes (CNTs) in 1991 has been considered as one of the most important discoveries in materials. Carbon nanotubes yield quite high Young's modulus and tensile strength values which make them excellent candidates for application in cementitious materials such as Portland cement concrete (Raki 2010; Hunashyal 2011). Specifically, carbon nanotubes have moduli of elasticity on the order of TPa, tensile strength on the order of GPa, and unique electronic and chemical properties (Mukhophyay 2011). Carbon nanotubes are found in two forms, Single-Wall Carbon Nanotubes (SWCNTs) or Multi-Wall Carbon Nanotubes (MWCNTs). Both of them are well structured graphene cylinders with aspect ratios (the ratio among length and perimeter of section) of ~1000 or higher (Xie 2005). The diameters of CNT are usually bigger than 1 nm. SWCNTs are single graphene tubes, while MWCNT's are multiple concentric graphene cylinders coaxially arranged around a hollow core (Shanchez 2009). In addition to high stiffness and high strength, high aspect ratio, small size, low density, and unique chemical and physical properties are important properties of CNTs (Metaxa 2010; Tyson 2011).

Giving the superior properties of CNTs, there has been a high expectation that adding CNTs in cementitious materials will improve significantly the strength and stiffness of the material. The application of CNTs in cementitious materials, however, has proven not to be easy. The main problem with using CNTs in a cementitious material is that CNTs are hydrophobic, which minimizes the interfacial interactions between the matrix and the CNT's. CNTs also are prone to agglomerating, or clumping, due to strong Van der Waals forces (Makar 2005). In order to make the utilization of CNT's in cementitious materials more effective, there are two main concerns to be addressed: uniform dispersion of the nanoparticles and sufficient bonding to the matrix

(Cwirzen 2008). The majority of literature focuses on these two concerns in a variety of different approaches.

Dispersion methods

There are two types of dispersion methods that have been used so far: physical methods and chemical methods. Physical methods use different levels of power in processing of CNTs to reduce the agglomeration, like ball mixing, magnetic mixing, and hand stirring. Chemical methods meanwhile use different chemicals to change the surface properties of CNTs. With different surface properties of CNTs, the degree of dispersion of CNTs in water can be improved.

A.Cwirzen et al. (2008) found that MWCNTs treated with polyacrlic acid are added in concrete, they can improve the compressive strength of concrete up to 50%. Luo et al. (2009) used five chemicals SDBC, NaDC, AG (Arabic Gum), TX10, and CTAB to aid the dispersion of CNT in aqueous solution. Among the five chemicals, the combined use of SDBS and TX reached a uniform distribution of MWCNT in cement paste. Rajdip et al. (2001) found that Arabic Gum can aid the dispersion of CNT in water up to 15 wt% (by weight of water). Collins et al. (2011) reported that although some chemicals can improve the dispersion of MWCNT in water, this does not mean necessarily that the strength of CNT reinforced mortar will increase, because chemicals might change the consistency of concrete. That study also reported that the surplus amount of CNT acts like the crack initiator in the cement paste. Chung (2005) found that the degree of dispersion can be improved by the use of conventional admixtures (or polymers) such silica fume, acrylic particle dispersion, methylcellulose solution, and silane. Yu et al. (2009) used SDS as a surfactant and achieved a good dispersion of CNT solution. Maria et al. (2010) studied the optimizing ratio of surfactant to CNT and found that the optimum ratio equals to 4 by weight of cement. Improvements in dispersion were also achieved when MWCNTs were treated

with a solution of H2SO4 and HNO3 and uniformly dispersed into a cement paste vie ultrasonic energy.

In other studies, CNTs were treated with polyacrylic acid and polymers, and SEM analysis showed highly improved dispersion within the cement matrix, although some clusters of CNT's were still present (Cwizen 2008). Better results were seen when MWCNTs were treated with a solution of H2SO4 and HNO3 and uniformly dispersed into a cement paste vie ultra-sonic energy. Both the untreated and treated were dispersed homogenously, but SEM analysis confirmed that the treated CNTs were covered with the calcium-silicate-hydrate. Bridging across crack and voids were also seen by the SEM, thus ensuring load transfer (Li 2006). The experiment was also done earlier in 2004 (Li 2004) with similar results and again in 2009 (Shanchez 2009).

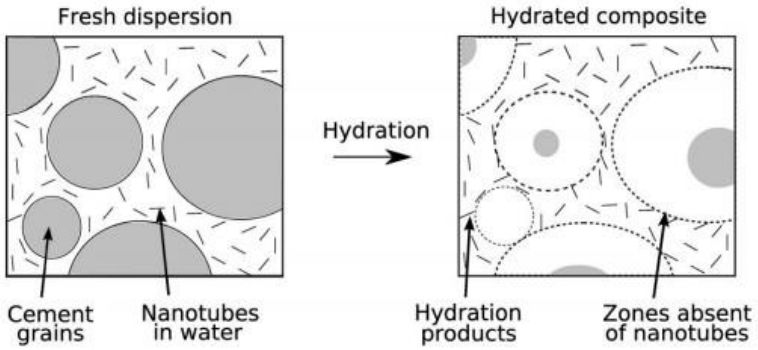

Fig. 52. CNT concrete bonding mechanism

The results of previous research indicate that a combination of physical and chemical dispersion methods is better than only physical or chemical method (Konsta-Gdoutos 2010). Specifically, ultrasonic power stirring and chemical surfactants are the most efficient ways to disperse CNTs in water and in cement paste.

The functions of CNTs in cementitious materials

Both Single Wall CNTs (SWCNTs) and Multiple Wall CNTs (MWCNTs) were used in previous studies. MWCNTs were mainly used for the application in cementitious materials,. Since cementitious materials are highly porous with a wide spectrum of pore size distribution, the functions of CNTs in the materials have not been clearly understood. The question arises where play a role to bridge the cracks, thereby improving the mechanical properties of the cementitious materials, or whether they are simply fillers to reduce the porosity of the materials. To this end, the dispersion of CNTs in the cement paste matrix is important because poorly dispersed CNTs can only serve as fillers, but well dispersed CNTs may possibly perform as a bridging agent.

In almost every study, a Scanning Electron Microscope (SEM) analysis was conducted to observe how well dispersed the CNTs were in the matrix, what the interfacial interactions were, and if there was any bridging observed between cement particles with CNTs. An earlier study employed sonication in isoproponal to 0.02 by weight CNT/cement ratio and mixed at varying water to cement ratios. SEM analysis showed that the CNT composite was very porous and that CNT's were clustered together (Makar 2005). CNTs that were mixed in aqueous solutions, found grains of cement that had completely hydrated without any CNT's present, disallowing any bridging and uneven dispersal at an early age (Tyson 2011).

The majority of investigations in the literature to date tested the compressive strength and rupture strength of cement paste, mortar and composite materials. Studies where dispersion and bridging were observed, more often also observed increases in strength. There were, however, some experiments that yielded higher compressive strengths than ordinary Portland cementitious materials regardless of the quality of dispersion. Different types of MWCNTs—as-grown,

annealed and carboxyle functionalized--were mixed in plain cement paste and compared. As-grown and annealed MWCNTs saw improvements of 10-20%, while the functionalized MWCNT saw a massive reduction in strength, due the hydrophilic nature of the f-MWCNT (Musso 2009). Pure CNTs in the cement showed weaker strengths at 7 and 14 day test, but superior strength at 28 day when compared to ordinary Portland cement (Tyson 2009). Contrary to the previous study, when pure CNT's were added to an ultra-high performance concrete, the MWCNTs had poor interfacial interaction with the cement paste. SEM analysis indicated that the CNTs were becoming disconnected after loading (pull-out). The CNTs showed no significant influence on the compressive or tensile strength (Kay 2010).

When treatments were applied to the CNT mixes, the results became more consistent, but some variations were still observed. When CNTs at 0.06%-0.42% by weight were introduced as a water suspension with added surfactant, admixtures negatively affected the compressive strength even though good dispersion was achieved (Cwirzen 2008). Later in 2008, Cwirzen treated MWCNTs with polyacylic acid polymers and found dispersion had been improved. He observed that workability had also improved. More importantly, the compressive strength was roughly 50% higher than Portland cement under loadings between 0.045 and 0.15 wt.% (Cwirzen 2008). Recently, surfactants were mixed using ultra-sonic energy to 0.048% to 0.08 wt% CNTs, and the results improved dispersion (Shah 2009). In mortar, H2SO4 and HNO3 solutions were ultrasonically mixed with 0.5% wt MWCNTs and saw up to a 19% compressive strength increase (Li 2004).

Objectives of the project

Most of previous studies have focused on the properties of CNT reinforced cement pastes and mortars. Since cement pastes and mortars are not commonly used in the construction

industry, the purpose of this research aims to study the property of CNT reinforced concrete. This is a composite material made of cement paste, CNTs, and fine and coarse aggregate. Significantly, this project studies not only the compressive strength of CNT reinforced concrete, but also the durability of the concrete. The two objectives for this study are as follows:

- Develop an optimum processing method or methods for CNT reinforced concrete. The processing method will be developed based on different types and dosages of dispersion agents and dispersion methods. The evaluation criterion will be mechanical properties of the CNT reinforced concrete such as compressive strength.
- Develop an experimental program to test durability properties of CNT reinforced concrete. Freeze/thaw resistance and chloride permeability will be the two main focus of the experimental program. These are important for the application of the CNT reinforced concrete in bride decks and overlays on bridges.

RESEARCH PLAN

Information of CNTs

In this study, a CNT from the Cheaptubes Inc. was used. The CNT fiber length ranges from 10 μm~20μm and the outside diameter ranges from 50nm~80nm. Therefore, the aspect ratio ranges from 125~400.

Processing methods

All concrete samples were prepared using a regular concrete mix design as shown in Table 1. The grading curve of aggregate is shown in Fig. 53.

Table 5.Concrete mixing designs (in lb/yd^3)

C	W	S	G	w/c	Wtotal	a = s + g	a/ Wtotal	s/g
600	300	1430	1740	0.5	4070	3170	0.78	0.82

C = cement; W = water; S = sand; G = gravel; Wtotal = the weight/yd^3; a = aggregates

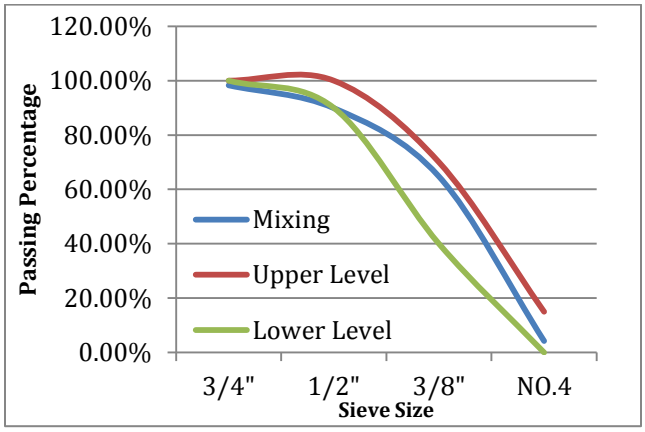

Fig. 53. Grading curves of the aggregate used in the study

The distribution of CNTs in fresh concrete mixtures may be different from the dispersion of CNTs in cement paste, because there are coarse aggregates in the mixture. The fabrication procedure of CNT concrete can be divided into two steps: the dispersion of CNTs in water or an aqueous solution (with different chemicals) and the dispersion of CNTs' suspension in the concrete mix.

Based on the literature review, we selected and studied four different processing methods in the present study: magnetic mixing, ball mixing, ultrasonic dispersion, and different chemical combinations. The dosage of chemicals is usually calculated as 0.1% of the weight of cement. The chemicals used were purchased from the Carolina Biology Supply Company (see the following list):

1. Nitric Acid
2. Sulfuric Acid
3. Gum Arabic
4. Propanol
5. Ethanol
6. Sodium Polyacrylate Snow
7. Methyl Cellulose
8. Silica Fume
9. Dedycel Sod Sulf
10. Superplasticizer (high range water reducer, HRWR)

The ball mixing and magnetic mixer were used first with different chemicals, the agglomeration of CNTs can be observed by unaided eyes, indicating that the two mixing methods are not effective. The resistance readings are in Appendix C. Therefore, these two mixing methods were dropped for the next phase of the study.

Next, an ultrasonicator was used in the project, as shown in Fig 54. The machine has a frequency of 20 KHz, possessing volume ranging from 300 μl – 300ml, and an output power 450W. These characteristics can handle making small concrete specimens. CNT aqueous solution processed by the ultrasonicator is a mesh-like solution with very litter agglomeration. Better CNT dispersion, with almost no agglomeration of CNTs, was reached when appropriate chemicals were incorporated in the solution.

Fig. 54. The ultrasonicator (450W)

When using the ultrasonicator, 300g water and 3g CNT were mixed with different combinations of chemicals in a glass container. A highly precise multimeter (Fig. 55) was used to test the resistance of the solution. Because CNT is more conductive (or less resistive) than water, the electric resistance of the solution was used as an indication of the degree of CNT dispersion. If the chemically treated CNT solution is purely black, meaning no agglomeration of CNTs at all, then the resistance of the chemically treated CNT solution usually becomes much

lower than that of the pure CNT solution (without chemicals) or pure chemical solution (without CNTs). In this case, we considered the corresponding chemical and dispersion method as a promising combination that can produce a desirable CNT dispersion.

The ultrasonicator was set to a mode of two seconds that ran with one second interval. The resistance of the solutions was tested every three minutes. The test continues until the variation of the resistance of solution reduced to a minimum (for more details see Section 2.4). The color change of the CNT solutions, which indicates the improvement in the degree of dispersion using the ultrasonic dispersion method, can be seen in Fig 4.

Fig. 55. The high precision multimeter

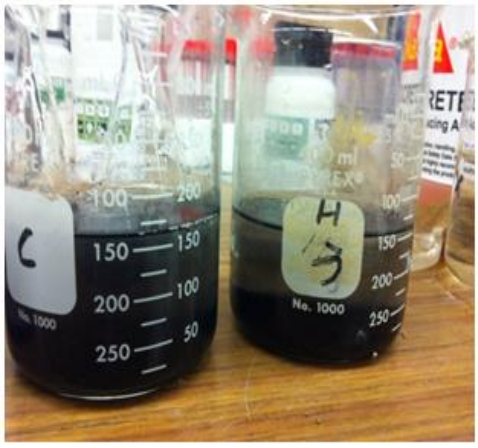

Fig. 56. Color change of CNT solutions

Based on the results of the chemicals studied (all listed above), seven types of dispersion agents were selected for further investigation:

1. Gum Arabic
2. Propanol
3. Ethanol
4. Sodium polyacrylate
5. MethylCellylulose
6. DEDYCEL SOD SULF
7. Silane

Experimental parameters for strength of CNT reinforced concrete

The compressive strength (ASTM C39) was used as the primary index to examine the effectiveness of the processing techniques. The mixing and curing method of CNT concrete follows the general requirement and standard. The processing methods that resulted in good compressive strength were selected for further study on the durability of CNT reinforced concrete. The following five parameters were used to prepare the concrete samples:

1. CNT contents. The mass of CNT was increased every 0.25% by weight of cement. For example: 0, 0.25%, 0.5%, 0.75%, 1.00 %.
2. Water/cement ratios, w/c. Three different water/cement ratios were used: 0.75, 0.5, and 0.4.
3. Ultrasonic dispersion periods
4. Chemical agents. The seven types listed above.
5. Mixing sequences
    - CNT dispersed in the fixed amount of water (300 ml)
    - CNT dispersed with cement and water at the same time
    - CNT dispersed in the total amount water (could be more than 300 ml)

    All the data of mixing of concrete can be found in the Appendix.

COMPRESSIVE STRENGTH RESULT OF CNT CONCRETE

The effects of CNT content and w/c

Five CNT contents and three w/c ratios were used in the study as listed above. Since CNT has a significant effect on the workability of CNT concrete, the effects of CNT content and w/c must be studied together. Superplasticizer (HRWR) was added in the concrete with the w/c = 0.4 due to its low workability. CNT concrete with and without HRWR were prepared and compared.

For w/c = 0.5, the workability of concrete is adequate when CNT content is not greater than 1.25%. When the CNT content is higher than 1.25%, however, the workability of the concrete becomes low. Based on this, the highest CNT content for this set of specimens was 1.25%. The test results indicated that the CNT has a significant effect on workability of fresh concrete mixtures. The test data of average compressive strength of CNT reinforced concretes are shown in Fig. 57. The average strengths were obtained as the average of three concrete samples (or two if the first two results were close). The deviation of compressive strength test results was around 10% from the average value. The basic trend is that the compressive strength of concrete increases with increasing CNT content. Comparing with the control specimen (CNT content = 0%), the compressive strength is increased by 59.5%.

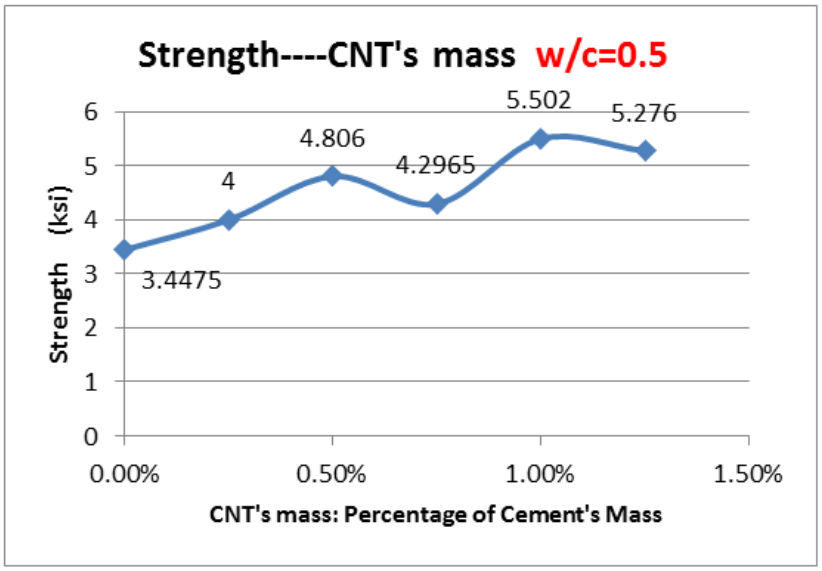

Fig. 57. Test data with w/c = 0.5 and different CNT contents

For w/c = 0.75, the strength of control specimen (CNT content = 0%) is low because of the high w/c. Test data in Fig. 58 suggested the average compressive strength showed almost no improvement up to CNT content of 1%. With the increasing CNT content above 1%, the compressive strength increases first and then decreases. The maximum value of compressive

strength occurred at around CNT content of 1.25%. Comparing with the control specimen (CNT content = 0%), the compressive strength increased by 71.7% (although it then dropped to almost the same value as the control specimen).

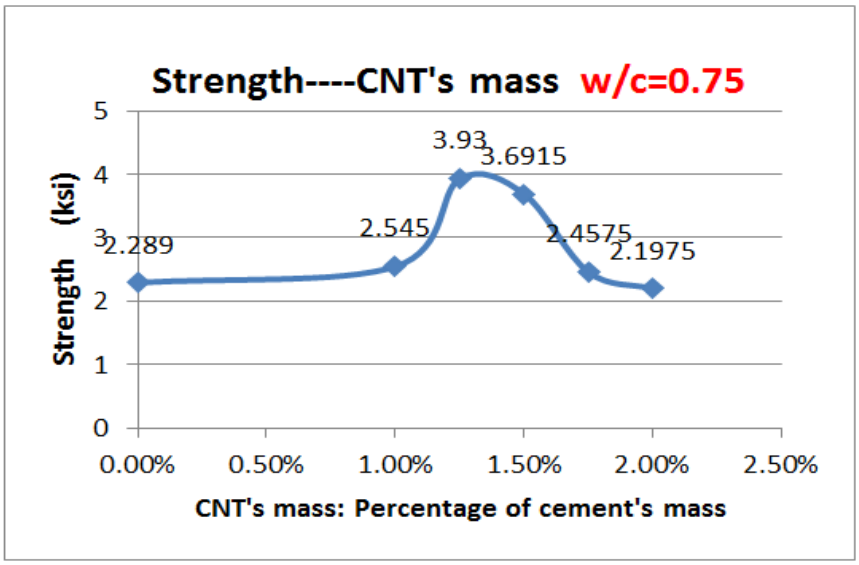

Fig. 58. Test data with w/c = 0.75 and different CNT contents

For w/c = 0.4, different amounts of superplastcizer were added into the concrete mixtures in order to improve the workability of concrete. With the addition of superplasticizer, the contents of the CNT used ranged from 0% to 1.75%. Fig. 59 shows the relation of dosage of superplasticizer against content of CNT. More samples were prepared with different w/c and contents of CNT to also conduct compressive strength tests. Fig.60 shows that the strength of CNT concrete follows the same trend compared with CNT mass, as in other w/c cases.

The peak strength is around 6.8 ksi with a 1.00% CNT's mass. It has increased about 108% from pure concrete with same w/c ratio.

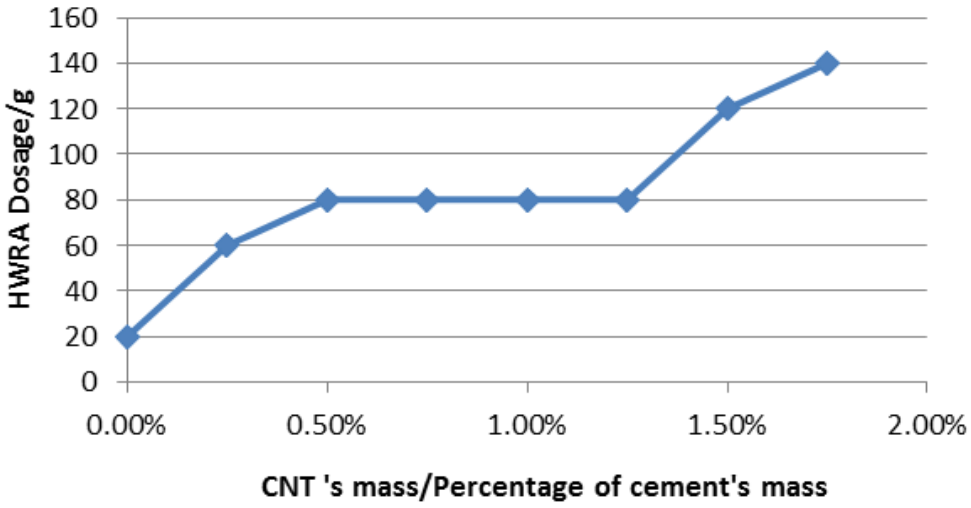

Fig. 59. Different CNT contents vs. dosage of HRWR

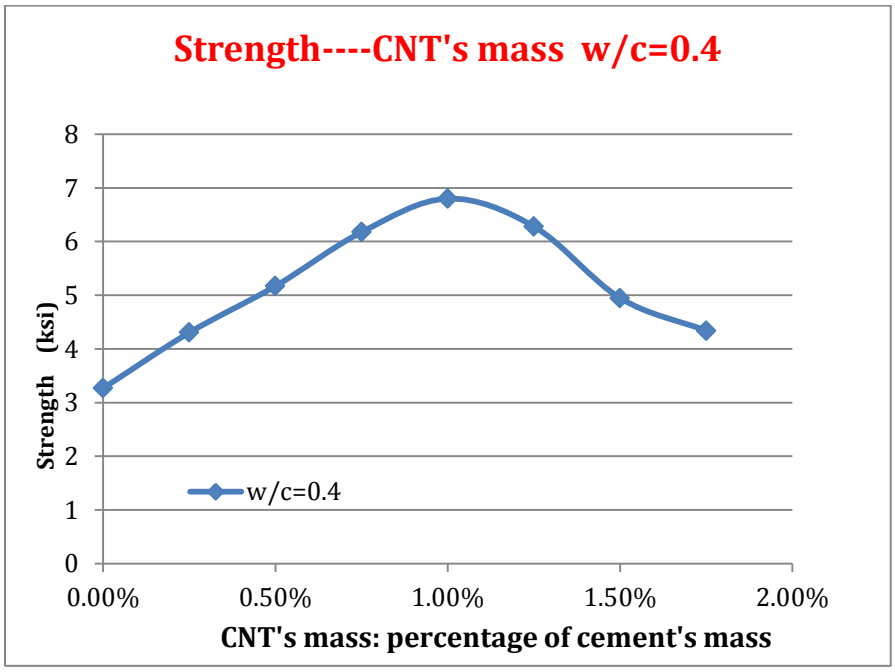

Fig. 60. Test data with w/c = 0.4 and different CNT contents

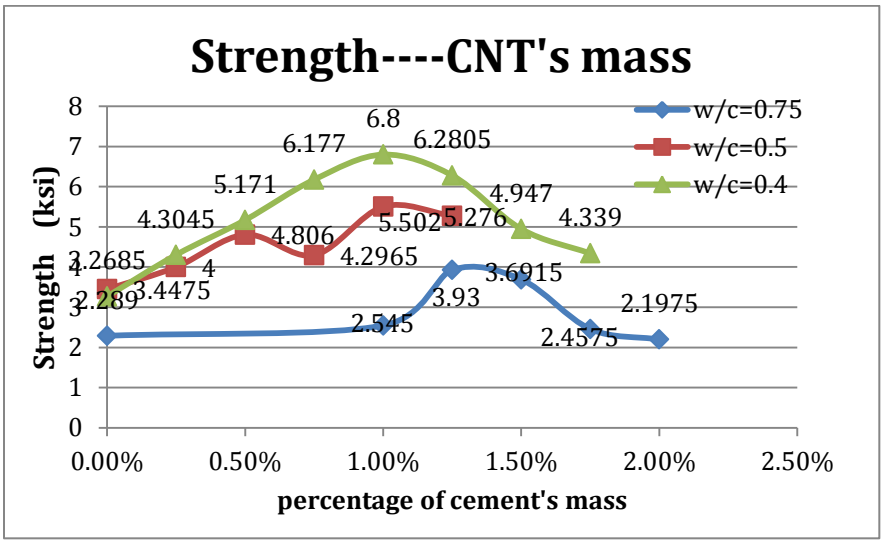

Fig. 61. Compressive strength of CNT concrete
with different w/c and CNT contents

Fig. 61 combines Fig. 57,Fig. 58 and Fig. 60 for the compressive strengths of concrete with different CNT contents and w/c = 0.5, 0.75 and 0.4. It is evident that the effect of CNT content on the compressive strength of concrete is different under different w/c. With a high w/c, part of the CNTs serves as a filler to fill the pores and reduce the total porosity. From there, the additional part of CNT can improve the strength of concrete. In this case, for w/c = 0.75, up to 1% of CNT served as the filler and the CNTs in addition to the 1% improved the compressive strength of concrete. The compressive strength of w/c = 0.4 can increase up to 108% compared to 59.5% of case w/c=0.5 and 71.7% of case w/c=0.75. At low w/c ratios, the CNT seems to disperse better with the help of superplasticizer. On the other hand, the more compact structure under low w/c ration can improve the function inside concrete.

Ultrasonic dispersion period

Five groups of samples of the same mixing design were made using the same ultrasonic dispersion method, but with different dispersion periods: 2 min., 6 min., 12 min., 18 min., and 24

min.). The test results are shown in Fig. 62. The compressive strength of CNT concrete increases first and then decreases after the dispersion period of about 12 min. This means that the optimum dispersion period is about 12 min. The dispersion period has a strong effect on the workability, and therefore on the strength of concrete as well. Fig. 63 shows the appearance of the concrete cylinders with the same mix design, but has different dispersion periods. The color of concrete varies gradually from light grey to dark grey with increasing dispersion period. More importantly, the surface of concrete cylinders varies from smooth to rough with high porosity.

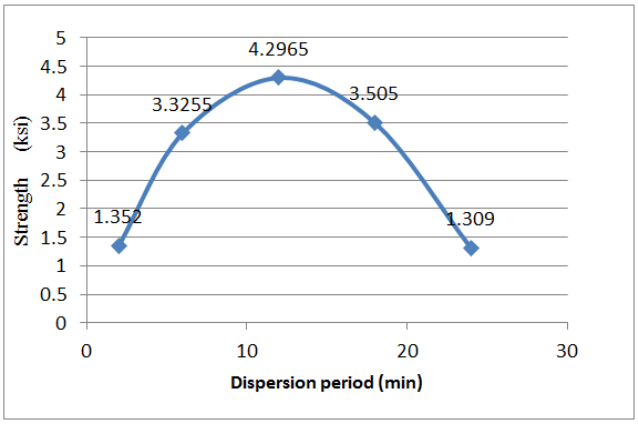

Fig. 62. Compressive strength vs. Ultrasonic dispersion period

Fig. 63. Surface smoothness variation with increasing CNT dispersion period (CNT content = 0.75% of weight of cement)

The ascending part of the curve shown in Fig. 62 can be explained due to the minimum time limit for the CNTs to be dispersed well in water. For the CNTs used in the present study, this time is about 12 minutes. It is difficult, however, to explain the descending part of the curve in Fig. 62. It appears that when CNTs are over-dispersed, the hydrophobic property of CNTs can be changed dramatically and the workability of concrete can be reduced rapidly with increasing dispersion time. Even this explained the cause of the strength reduction it is still surprising that the variation in hydrophobic property of such a small amount of CNTs (0.75% of cement) can cause such a large drop in the compressive strength. Apparently, the exact degradation mechanism was not understood well, and more systematic tests should be conducted in a follow-up project.

Different combination of chemicals

Under different treatments of chemicals, the CNT aqueous solutions were mixed with different dispersion periods. For example, when the CNT was treated by SOD Polycrylate, the electric resistance of solution is 19.8 ohm after 3 minutes, 6 ohm after 6 minutes, and 6.4 ohms after 9 minutes. We considered that the variation of resistance between 6 min. and 9 min. was small enough, and the dispersion was stopped at 9 min. This time is considered the optimum dispersion time in terms of the electric resistance measurement. Next, the concrete specimens were prepared using the optimum dispersion time and the compressive strength of concrete specimens was tested. The best effort was made to capture the minimum resistance. Since resistance is reciprocal to the conductivity, in addition to the fact that the CNT is conductible, the smaller the resistance, the better the dispersion of CNT will be. It should be mentioned that in the study for the effect of dispersion period (discussed in the above section), regardless of the measured electric resistance, the designed dispersion periods were used.

Table 6 lists the test results for different chemically-treated CNT concretes. Some of them show positive results, such as Sodium polyacrylate, silane, and methlculluose. Others, such as Propanol+Ethanol, show poor results. Dodecyl Sodium Sulfate (DSS) resulted in the lowest compressive strength in all three dispersion periods.

Table 6. Compressive Strengths of chemical treated CNT concrete specimens

CNT Mass	Chemical Treatment	Concrete Strength
0.75% of cement	0.75% of cement Gum Arabic, UP 9 MINS	2.944
0.75% of cement	snowpowder, UP 3MINS	3.5795
0.75% of cement	PROPANOL+ETHANOL,UP 12MINS	2.497
0.75% of cement	Silane, UP 12MINS	4.217
0.75% of cement	Methylculluose, UP 9 MINS	4.7735
0.75% of cement	DSS, UP 9 MINS	1.1135
0.75% of cement	DSS, UP 3 MINS	0.984
0.75% of cement	DSS, UP 2 MINS	0.843

The CNT concretes treated with snowpowder, silane and methycullose are the three most promising chemical combinations. The strengths of the three concretes are higher than that of the control sample. The surface smoothness of cylinders of the three concrete is also good. DSS resulted in the most dispersed CNT aqueous solution, in terms of the resistance measurement. The concrete samples also had a smooth surface. The strength of DSS-treated CNT concrete turned out to be the lowest, however, which might be caused by the air-entraining effect in the concrete.

Bandyopadhyaya et al. (2002) were able to disperse up to 15 wt% (by weight of water) CNTs into an aqueous solution containing gum arabic and mixing for 20 minutes with an ultrasonic mixer. The same approach was used in the present study to make CNT concrete, but the resulting strength of the concrete was only 1.74 ksi. This indicated that the processing method developed for CNT cement paste or mortar cannot be directly used for CNT concrete.

Mixing sequence

For the test results shown above, all concrete samples were prepared with the same mixing approach in which CNTs were mixed in 300 ml water (the ultimate processing volume of the ultrasonic device) first, and the rest of the water (without CNTs) was added following the general casting process of concrete. This may be called the first mixing sequence in this study. The second mixing sequence used in the present study differs from the first mixing sequence in that a certain amount of Portland cement was added in the CNT aqueous solution and mixed with CNTs first, and followed then by the general casting process of concrete. The purpose of the second mix sequence was to study if there is any interaction between CNTs and Portland cement during the dispersion process. When the Portland cement and CNTs are mixed and dispersed in water together, the Portland cement particles react with water and the products of hydration reactions may have a positive or negative impact on the dispersion of CNTs.

Table 7 shows the test result using the second mixing sequence. As shown in the table, the test results of the second sequence are not as good as the first one except the one with silica fume as the additive. When silica fume was added in the concrete, however, it was not clear whether the strength improvement was due to the CNTs or due to the silica fume, because silica fume alone can increase the strength of concrete.

Table 7. Compressive Strengths of CNT concrete made by the second mixing sequence

Second Approach Combinations	Ave Strength (ksi)
add (30g cement++water +CNT)+Gum Arabic	2.7365
add (50g cement++water +CNT)+Methlyculluose	2.895
add (40g cement++water +CNT)+SOD	1.2725
add (40g cement++water +CNT)	3.097
add (40g cement++water +CNT)	2.897
add (50g cement++water +CNT)+Silica Fume	3.4525
add (50g cement+water +CNT)+Silica Fume+Gum Arabic	3.103
add (50g cement++water +CNT)+Silica Fume+Methylcullose	4.0095

Due to the limited processing volume of ultrasonicator, only 300 ml of water can be used for CNT dispersion at a time. When the amount of the water needed for a concrete mix was more than 300 ml, the water (and the CNTs) had to be processed with several batches in the first two mixing sequences. As the third mixing sequence, all water needed for a concrete mix was used for CNT dispersion in one batch. In this approach, the time of dispersion was longer when the amount of water was more than 300 ml. For the third mixing sequence, only one group of samples was made, and the compressive strength test result was 3.276 ksi for a CNT content of 1% of the weight of the cement.

Comparison of Chemicals under different w/c

The three optimal chemicals were also used for making concrete under the w/c ratio of 0.4. The result shows with the decrease of the w/c, the strength of chemical treated CNT concrete become smaller than the ones at higher w/c values. Compared to the pure concrete, all the three chemical treated concrete at w/c of 0.75 show increases in strength, but all three chemical treated did not show increases for w/c equal to 0.4. This suggests that methycullose and silane would help for concrete strength at high w/c values At low w/c ratios, however, chemicals' hydrophilcity might have negative effect for the incorporation of CNT. Among these chemicals, Sodium polyacrylate-treated CNT concrete seems to a similar strength to the pure CNT concrete. Tests durability will determine whether it is worth putting this chemical into concrete.

Table 8. Effect of Chemicals under different w/c values

Chemicals	w/c=0.75	w/c=0.4
Methyculluose	4.774	3.855
Silane	4.217	4.226
Sodium polyacrylate	3.58	6.15
Pure CNT Concrete	2.545	6.281

DURABILITY OF CONCRETE

Based on the test results for compressive strength, three optimum mixes were selected and CNT concrete samples were prepared for two durability tests. The three optimum mixes used the same w/c = 0.4 and the same CNT content of 1.25% wt., but with different chemicals: Methylculluose, Sodium polyacrylate, and Silane. They were processed by the ultrasonic dispersion method. Two durability tests will be conducted on the CNT concrete samples: ponding test and freeze/thaw test. The ponding test will last for 15 days, and the freeze/thaw test will last for one month.

Ponding test for chloride permeability of CNT concrete

The electric resistance of CNTs is lower than that of concrete, and therefore, CNT concrete is more conductive than regular concrete. As a result, the rapid chloride permeability test method described in ASTM C1202 is not appropriate for testing the chloride permeability of CNT concrete. In the present study, the ponding test (ASTM C1543) was used. Instead of 90 days of ponding, 15 days of ponding was used. Then, concrete samples were drilled and concrete powders at different depths was collected for testing chloride concentration profile. The concentration profiles was then be used to determine the chloride permeability of the CNT concretes.

The process is as follows. The concrete will be clamped and sealed by Epoxy, sodium chloride solution above the concrete surface was kept at a depth of 2 in all the time. (Fig. 64).

Fig. 64. Concrete Specimen with NaCl Solution on top

Fig. 65. Drilling holes at different depth

After fifteen days, the NaCl solution will be disposed, but concrete will be drilled at different depths: 0.25in, 0.5in, 0.75in, 1in, 1.25in, 1.5in. (Fig. 65). Those different powders will be mixed with 10 ml Chloride Solution in separate tubes for 24 hours. (Fig. 66).

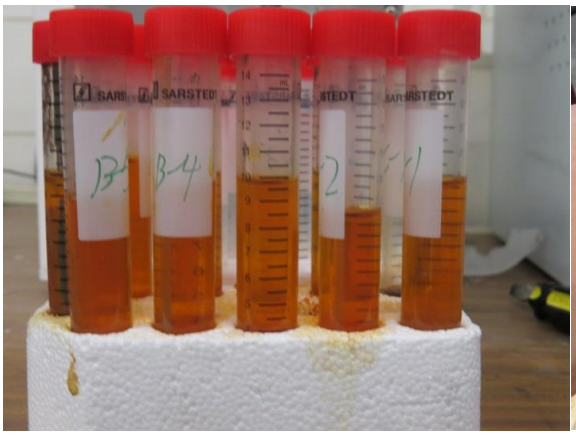

Fig. 66. Mixing Concrete Powder with Cl2 Solution

Fig. 67. Testing concentration of Cl

After 24 hours, German Instrument was used to test the concentration of Cl . The data of voltage was obtained from the machine. When the voltage of mixing solution is higher than 120 mv, the concentration of Cl can be neglected. The higher the voltage, the lower [Cl] will be. The [Cl] versus depth curve for all the three samples was based on the German Curve. The

result shows Sodium polyacrylate has the lowest value of [Cl] at the depth of 0.25in, which was much higher than [Cl] at all other depth. If the 90 days test had been completed, it is predicted that the [Cl] at other depths will increase with time. This would occur because the deepest areas will become more penetrated by [Cl]. The Sodium polyacrylate-CNT concrete is quite compacted, which means that it will not allow much [Cl] deep into concrete. Thus, it seems the best among the three optimal mixing choices.

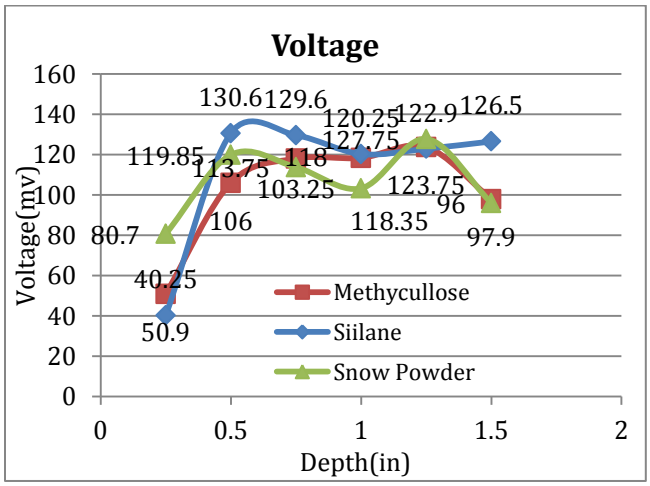

Fig. 68. Voltage Result of Concrete

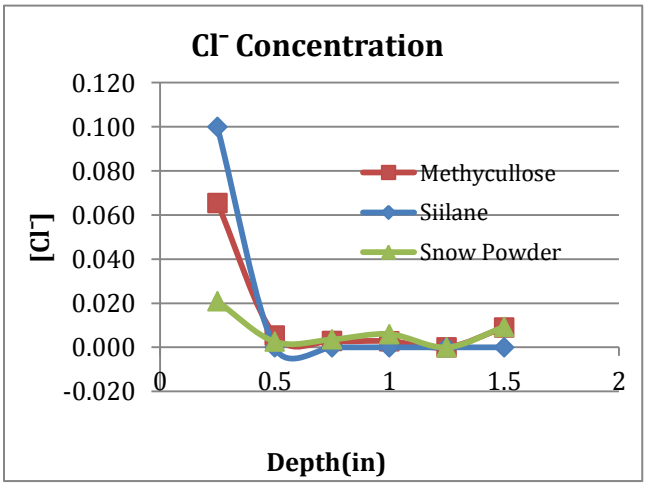

Fig. 69. [Cl⁻] at different depth of concrete

Freeze/thaw test of CNT concrete

The freeze/thaw test was based on ASTM C666. Three different parameters will be measured in interval of every 30 cycles: length change, weight loss and pulse velocity change.

As in the other experiments, 3 x 3 x 6 in specimens were used for the freeze thaw test. The specimens were surrounded by water of 1/16 in deep. For each cycle, the temperature of the center of concrete was lowered from 4 ℃ to -18 ℃, then raised from -18 ℃ to 4 ℃ again. A difference of 3 ℃ is allowed in this test. In our case, the running time per cycle is about two and a half hours, which is in the reasonable range (2hr to 5 hr) according the ASTM C666.

There are two possibilities to test the relative dynamic elastic modulus: ultrasonic impulse method and resonance method. It is better to adopt both of them to get a more precise result, however, only the first method was taken in this case. The transmit time was tested at the beginning. After that, the impulse time will be tested every 30 cycles. The weight and length change were measured every 30 cycles, too. The formula for the dynamic modulus is as follows, $t_{S,0}$ is the initial transmit time, while $t_{S,n}$ is the transmit time after n cycles.

$$RDM_{UPPT,n} = \left(\frac{t_{S,0}}{t_{S,n}}\right)^2$$

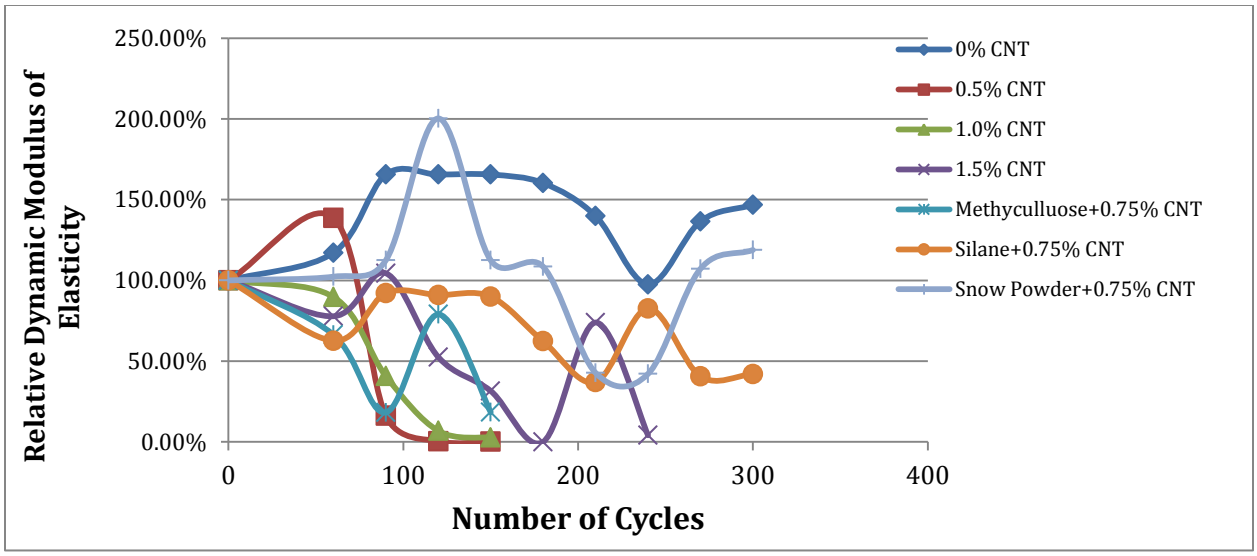

Fig. 70. RDM of different concrete mix

The result of dynamic modulus is as above in Fig. 70. Several specimens appeared to be broken after 150 cycles. The concrete with pure CNT(0.5%, 1.0%) and CNT concrete treated with methylcellulose had some scaling and even collapsed only after 150 cycles. The elasticity has decreased greatly. Pure concrete without CNT, CNT treated with Silane and CNT treated with Sodium polyacrylate remain undamaged after 300 cycles.

According to the ASTM C666 standard, concrete that fails to last all the 300 cycles has poor durability. Comparing those CNT concrete without treatment, treated with Methylcellulose, Silane, Sodium polyacrylate in Fig. 71, the surface of the 0.5% CNT, 1.0% CNT, 1.5% CNT, and Methylcellulose treated concrete already collapsed and the aggregates and sands can be easily seen. The Silane and Sodium polyacrylate-treated concrete, however seem to have the ability to stay sound. They are the only samples undamaged besides the pure concrete. In particular, the Sodium polyacrylate treated concrete has a smooth surface, and resisted the breaking of the concrete positively.

In all of experiments, a temperature gradient exists between the surface and center of concrete. This will make the strain of concrete vary at different depths. Thus, stretch and

shrinkage will occur at different depth of concrete, which will extend to the network of cracks. The rate of freeze-thaw damage is related therefore to the rate of internal drainage and the rate of external water update. In these experiments, the water/cement ratio of 0.4 leads to a low porosity. This in turn produces a dense pore structure. The addition of CNT also causes the concrete to have a dense pore structure. The internal drainage will occur much faster than water uptake, which will lead to an overall shrinkage of the specimen. The combined effect of these two issues produce a condition of poor freeze thaw durability for the CNT concrete at this condition,, compared to the high DRM of pure concrete after three hundred cycles. Once the scaling happens on the surface of the concrete, the dynamic modulus will decrease, but the water uptake rate will increase. This therefore will increase the rate of deterioration. Finally, the freezing and thawing will generate a network of microcracks.

It is worth mentioning that after 300 cycles, the pure concrete has a slightly higher DRM than the Sodium polyacrylate-treated CNT concrete, and a much higher value than the silane-treated CNT concrete. Silane-treated CNT concrete has some small defects, and pieces that fell of the surface. By comparison, Sodium polyacrylate-treated concrete is very sound. Given its high compressive strength, it should be considered one of most promising mixing option.

It should also be noted that the calculation of relative dynamic modulus of elasticity is based on the assumption that the shape, weight and length of concrete specimen will not change after several cycles. The dynamic modulus of concrete with 1.5% CNT is less than that of concrete with 0.5% or 1.0% CNT after 150 cycles. It can be seen from the Fig.70 that case with 0.5% or 1.0% CNT is worth than that with 1.5% CNT. Percentage of length change and weight were also plotted (Fig. 74 & Fig. 75), from which no large changes were observed. The dynamic modulus is still the best way to tell the distribution of cracks. In addition to these observations,

the durability factor (DF) can be calculated using the formulas DF=PN/M. P is the relative dynamic modulus after N cycles, N is the number of cycle after when the concrete is not allowed or necessary to continue the test, and M is the specified number of cycles (300 in this case). The durability factor of pure concrete and CNT concrete treated with Sodium polyacrylate are the outmost among all the CNT concrete. The durability factor of CNT concrete treated with silane also seems fair. All other mixes did not produce good results.

Fig .71 CNT concrete after 300 cycles of freezing and thawing
(From left to right: 0% CNT, 0.5% CNT, 1.0% CNT, 1.5% CNT, Methycelluose+CNT, Silane+CNT, Sodium polyacrylate+CNT)

Table 9. Durability factor of each concrete mix

	P	N	M	DF
0% CNT	146.81%	300	300	1.468111
0.5% CNT	0.17%	150	300	0.000846
1.0% CNT	2.68%	150	300	0.013388
1.5% CNT	4.09%	240	300	0.032731
Methylcelluose+0.75% CNT	18.32%	150	300	0.091613
Silane+0.75% CNT	41.87%	300	300	0.418685
Sodium polyacrylate+0.75% CNT	118.82%	300	300	1.188235

It is interesting to consider why the three different chemicals all have the function to disperse the CNT well: they produced a good result for compressive strength at a water/cement 0.75, but had a big difference in their contributions to the durability. More in-depth studies between the chemicals is necessary for any of them to be considered for industrial use. This section describes the qualities of the chemicals used for this study.

Silane is silicon analogue of methane. While the chemical equation of methane is CH_4, the chemical equation of Silane is SiH_4. The polarity of Si-H, however, is higher than that of C-H, so it is more like ionic bond. Silane also has the coupling effect to make the fibers stable.

Methylcellulose is an ether, and D.D.L Chung (1996) found that the addition of methylcellulose will lead to the thermal stability, which will affect the CTE of concretein an unstable , thus leading to a lot of freeze thaw damage. Chung (1997) also found that Methylcellulose will decrease the thermal conductivity of the concrete, which means there will be a larger temperature gradient between the surface and center of concrete.

Sodium polyacrylate is a synthetic polymer composed of one repeating formula, linked together in a long flexible chain. The most important property of laboratory size Sodium Polyacrylate is that it can absorb water 100 times its original weight, which will make the product almost like an artificial snow. Sodium polyacrylate is a polymer (a long chain molecule) with ionic groups (negative charges with accompanying positively charged sodium ions) all along its length. It is these ionic groups that allow it to absorb a huge amount of water. The water molecules cluster around the negative and positive charges and become attached to the polymer chain. More than that, the hydrogen bonds can be found in pores or holes within the polymer structure such that whole water droplets can be held inside the polymer.

The modification methods of silane, sodium polyacrylate and methylcellulose is different. Methylcellulose belongs to covalent surface modification (chemically), which means it will increase the wettability of CNT or reduce their tendency to agglomerate. Sodium polyacrylate and silane both belong to the non-covalent surface modification, however,, which means the hydrophobic part of the molecules will be attached to the side walls of MWCNT. The hydrophilic part therefore will increase the solubility of the treated CNT. The following figure shows how the non-covalent modification works. The following figure shows microscopically how the sodium polyacrylate and silane help CNT disperse in water. They all have the same hydrophobic part: $[H]^-$. The hydrophilic part of silane is $[Si]^{4+}$, and that of sodim polyacrylate is $[Na]^+$. For applications in concrete mixing, sodium polyarylate is better because it has a long chain, and the hydrogen molecules will be absorbed to side walls of MWCNT. The high Van der Walls Force, make it easier for the long chain polymer to attach to the side wall rather than the single molecule of silane. Compartively, however, the sodium ion is easier to dissolve in the water than the silicon molecule, which also has a high polarity compared to hydrogen molecule. These reasons make the sodium polyacrylate a better chemical additive in CNT concrete.

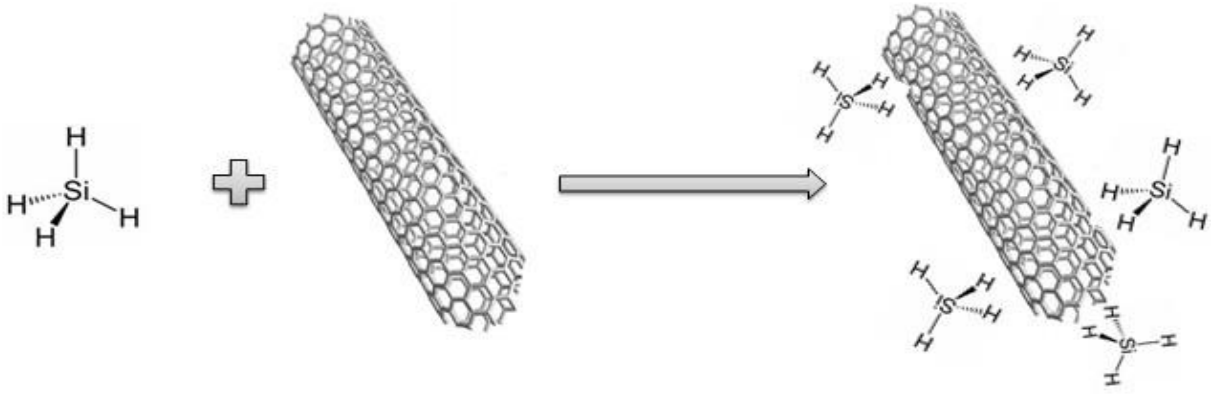

Fig. 72. Silane helps with dispersion of MWCNT

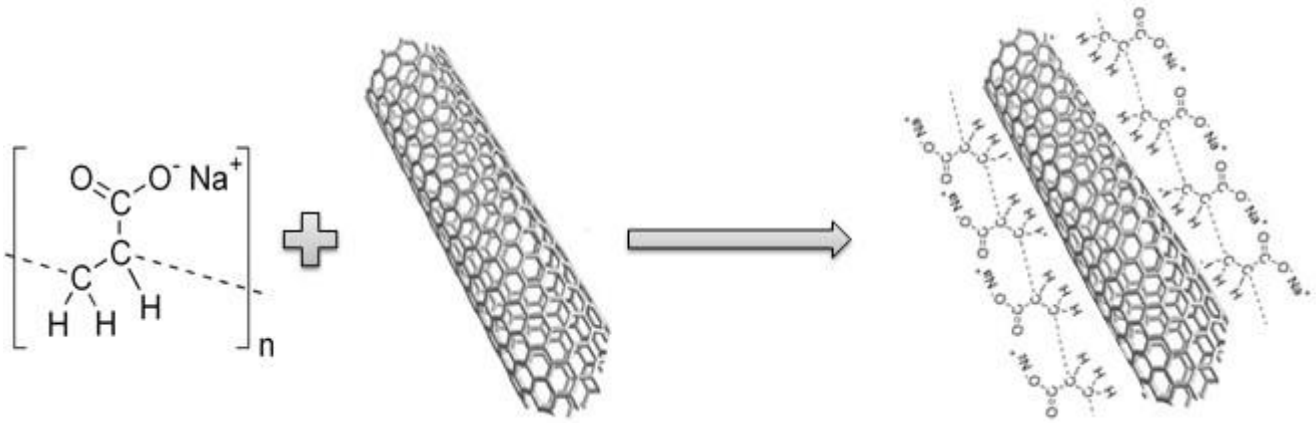

Fig. 73. Sodium Polyacrylate helps with dispersion of MWCNT

From the result of these experiments, it seems the non-covalent modification method is better than the covalent modification method for improving both the compressive strength and durability of CNT concrete.

Finally, the length change and weight change of concrete after the 300 cycles were also show on the next page.

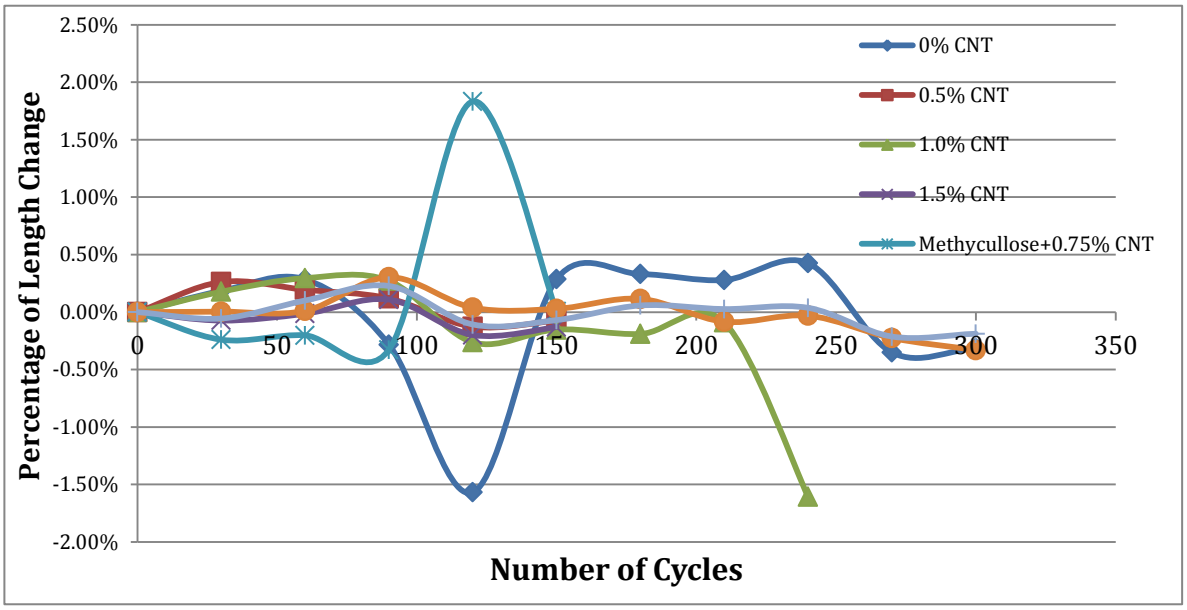

Fig. 74. Length Change vs. Cycles

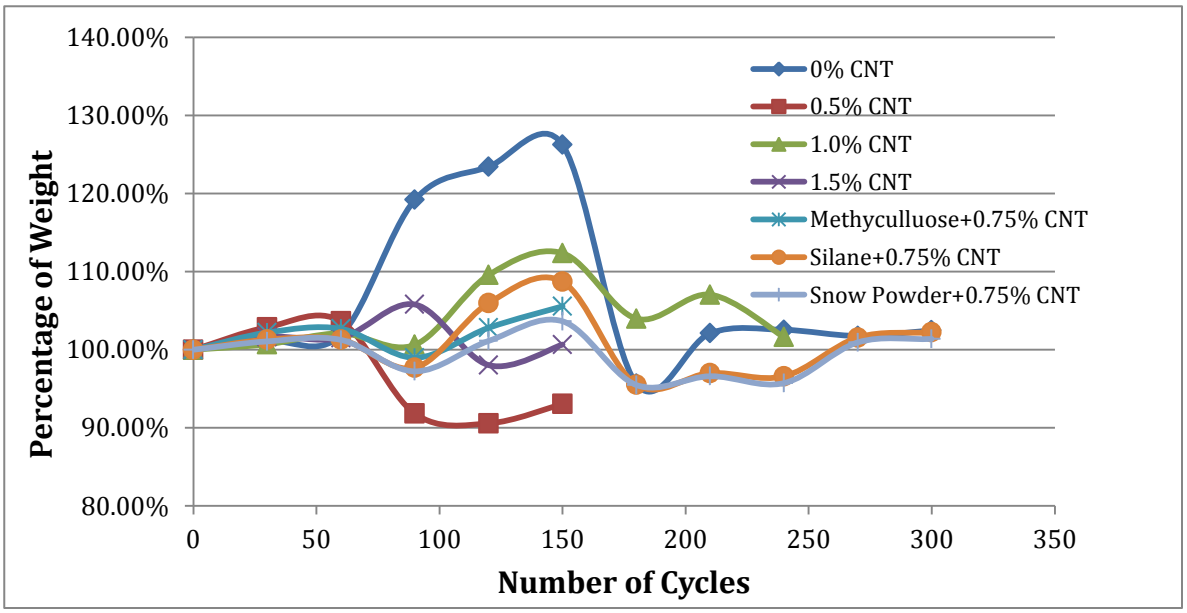

Fig. 75. Weight Change vs. Cycles

SUMMARY AND CONCLUSIONS

Summary

- Two steps were taken in the project. The first one was the dispersion of CNTs in water, and the second one was the compressive strength and durability properties of CNT concrete.
- In the first step, three dispersion methods were studied: ball mixing, magnetic mixing, and ultrasonic mixing. 10 different chemicals were used with the three dispersion methods. The test results showed that the ultrasonic mixing method was the most effective one among the three dispersion methods; and seven chemicals out of the 10 had potential to improve properties of CNT concrete.
- In the second step, five parameters were studied in terms of compressive strength of CNT concrete, which are
  - CNT contents: 0%, 0.25%, 0.5%, 0.75%, 1%, 1.5%, 1.75%, and 2% (depending on w/c)
  - Water/cement ratios: 0.75, 0.5, and 0.4
  - Ultrasonic dispersion periods: 2 min., 6 min., 12 min., 18 min., and 24 min.
  - Seven chemical agents
  - Three mixing sequences: CNT dispersed in the fixed amount of water (300 ml); CNT dispersed with cement and water at the same time, and CNT dispersed in the total amount water (could be more than 300 ml)
- Three CNT processing methods were selected for testing durability properties of CNT concrete and the concrete samples were prepared.

Conclusions

- The strength of CNT concrete can increase with greater CNT content. The strength enhancement is significant, and could be as high as 108%. With a high w/c (0.75 for example), however, the strength increases first and then decreases. There is an optimum CNT content depending on the w/c ratio. When w/c are 0.4 and 0.5, the optimum CNT content is 1% by weight of cement, when w/c is 0.75, the optimum CNT content is 1.25% by weight of cement.
- The strength enhancement comes from two mechanisms: CNTs as filler reducing the porosity and CNTs as fibers bridging the cracks. The first likely plays the major role in the present test of concrete cylinders.
- Electric resistance of CNT solution was used as an indicator for the effectiveness of CNT dispersion. It is a good indicator for CNT dispersion. The lower the electrical resistance, the more adequate the dispersion will be.
- A well dispersed CNT solution may not lead to high strength CNT concrete. The test results showed that over-dispersed CNT solution reduces workability of CNT concrete and results in poor strength. It seems that the hydrophobic property of CNTs can be changed dramatically and the workability of concrete can be reduced rapidly with increasing dispersion time. Despite these findings, the exact causal mechanism is not understood well.
- Among all chemicals used in the project, Methylculluose, Sodium polyacrylate, and Silane are effective dispersion agent for the CNTs. Among them, Sodium polyacrylate-treated CNT concrete has a higher freeze thaw durability, higher compressive strength and lower chloride permeability. These results are promising for future use in commercial CNT concrete mixes.

- For the three mixing sequences used in the project, the first mixing sequence reached a strength of 5.502 ksi; the second, 4.225 ksi, and the third, 3.276 ksi. The first mixing sequence should be used to make high strength concrete. In the first mixing sequence, CNTs are dispersed in the fixed amount of water within the capacity of the ultrasonicator.
- Long time dispersion of pure CNT in water would not be advantageous, but it is conclusive as to how the dispersion time will affect the sodium polyacrylate treated CNT concrete.

REFERENCES

Cwirzen, A., Habermehl-Cwirzen, K., and Penttala, V. (2008). "Surface decoration of carbon nanotubes and mechanical properties of cement/carbon nanotube composites", *Advances in Cement Research*, 20(2), 65-73.

Cwirzen, A., Habermehl-Cwirzen, K., Nasibulin, A., Kaupinen, E., and Penttala, V. (2009) "SEM/AFM studies of cementitious binder modified by MWCNT and nano-sized Fe needles", *Material Characterisization*, 60(7), 735-740.

Franklin Colins (2012) "The influence of admixtures on the dispersion, workability and strength of carbon nanotube OPC paste mixtures", *Cement & Concrete Composites*, (34), 201-207.

Florence, S., & Konstantin, S. (2010) "Nanotechnology in concrete – A review", *Construction and Building Material*, 24(11), 2060-2071

Gopalakrishan, K., Birgisson, B., Taylor, P., and Attoh-Okine, N.O. (2011) "Multfunctional and Smart Carbon Nanotube Reinforced Cement-Based Materials", *Nanotechnology in Civil Infrastructure – A Paradigm Shift, Springer*, 1(3), 1-47.

Hunashyal, A.M., Tippa, S.V., Quadri, S.S., and Banapurmath, N.R. (2011) "Experimental Investigation on Effect of Carbon Nanotubes and Carbon Fibres on the Behavior of Plain Cement Mortar Composite Round Bars under Direct Tension", *Nanotechnology*, 1-6.

Kay, W., & Loh K.J. (2010) "Nanoengineering Ultra-High-Performance Concrete with Multiwalled Carbon Nanotubes", *Transportation Research Record*, (2142), 119-126.

Konsta-Gdoutos, M.S., Metaxa, Z.S., and Shah, S.P. (2010) "Multi-scale mechanical and fracture characteristics and early age strain capacity of high performance carbon nanotube/cement nanocomposites", *Cement Concrete Composites*, 32(2), 110-115.

C, L., & Bassem, A. (2009) "Characterization of the uncertainties in the constitutive behavior of carbon nanotube/cement", *Science and technology of Advanced Materials*, 10(4), 1-13.

C, L., & Bassem, A. (2010) "Finite element analysis of carbon nanotube/cement composite with degraded bond strength", *Computational Materials Science*, (47), 994-1004.

Li, G.Y., Wang, P.M., and Zhao, X. (2006) "Pressure-sensitive properties and microstructure of carbon nanotube reinforced cement composites", *Cement and Concrete Composites*, (29), 377-382.

Li, G.Y., Wang, P.M., and Zhao, X. (2004) "Mechanical Behavior and microstructure of cement composites incorporating surface-treated multi-walled carbon nanotubes", *Carbon*, 43(6), 1239-1245.

Makar, J.M., Margeson, J., and Luh, J. (2005) "Carbon nanotube/cement composites – early results and potential applications", *Proceedings of 3rd international conference on construction material: performance, innovation and structural implication*. Vancouver, BC. August 22-24, 2005, 1-10.

Mann, S. (2006) "Nanotechnology and Construction", Nanoforum Report http://www.nanoforum.org (May 30, 2008).

Konsta-Gdoutos, M.S., Metaxa, Z.S., and Shah S.P. (2010) "highly dispersed carbon nanotube reinforced cement based materials", Cement and Concrete Research, (40),1052-1059.

Metaxa, Z.S., Konsta-Gdoutos, M.S., Shah, S.P. (2010) "Carbon nanofiber-reinforced cement based materials", Journal of Transportation Research Record, 2(2142), 114–118.

Mukhopadhyay, A.K. (2011) "Next-Generation Nano-based Concrete construction products: A Review", *Nanotechnology in Civil Infrastructure – A Paradigm Shift, Springer*, 1(3), 207-223.

Musso, S., Tulliani, J-M., Ferro, G., and Tagliaferro, A. (2009) "Influence of carbon nanotubes structure on the mechanical behavior of cement composites", *Composites Science and Technology*, (69), 1985-1990.

Naaman, A.E., Namur, G.G., Alwan, J.M., and Najm, H.S. (1991) "Fiber Pullout and Bond Slip .2. Experimental Validation", *Journal of Structural Engineering*, 117(9), 2791-2800.

Nochaiya, T., and Chaipinch, A. (2010) "Behavior of multi-walled carbon nanotubes on the porosity and microstructure of cement-based materials", *Applied Surface Science*, 257, 1941-1945.

Rajdip Bandyopadhayaya (2001) "Stabilization of individual carbon nanotubes in aqueous solutions", *Nano Letters*, 1(2), 25-28.

Raki, L., Beaudoin, J., Alizadeh, R., Makar, J., and Sato, T. (2010) "Cement and Concrete Nanoscience and Nanotechnology", *Materials*, 3(1), 918-942.

Sanchez, F., and Ince, C. (2009) "Microstructure and macroscopic properties of hybrid carbon nanofiber/silica fume composites", *Composites Science and Technology*, (69), 1310-1318.

Sanchez, F. (2009) "Carbon nanofiber/cement composites: challenges and promises as structural materials", Composite Science Technology, 69(11-12), 1985-1990.

Shah, S.P., Konsta-Gdoutos, M.S., Metaxa, Z.S., and Mondal, P. (2009) "Nanoscale Modification of cementitious materials", *Nanotechnology in Construction*, 3(2), 125-130.

Steyn, W.J. (2011) "Application of Nanotechnology in Road Pavement Engineering", *Nanotechnology in Civil Infrastructure – A Paradigm Shift, Springer*, 1(3), 49-83.

Tyson, B. S.M. ASCE, Rashid, K., Yazdanbakhsh, A., and Grasley, Z. (2011) "Carbon Nanotubes and Carbon Nanofibers for Enhancing the Mechanical Properties of Nanocomposite Cementitious Materials", *Journal of Materials in Civil Engineering*, 23(7), 1028-1035.

Xie, X.H., Mai, Y.W., Zhou, X.P. (2005) "Dispersion and alignment of carbon nanotubes in polymer matrix: a review", *Material Science Engineering*, 49(4), 89-112.

Fu, X., & Chung D.D.L. (1996) "Effect of methylcellulose admixture on the mechanical properties of cement." *Cement and Concrete Research*, 26(4), 535-538.

Fu, X., & Chung D.D.L. (1997) "Effects of silica fume, latex, methylcellulose, and carbon fibers on the thermal conductivity and specific heat of cement paste," *Cement and Concrete Research*, 27(12), 1799-1804.

CHAPTER 4: CONCLUSION

CONTRIBUTIONS

- The thermal strain of concrete under low temperatures was studied. The effects of air-entraining agent, water/cement ratio, and degree of saturation on the strain behavior was tested systematically.
- Optimal dosage of air-entraining agent in order to minimize dilation of concrete under cooling were found depending on the humidity of the environment..
- A low water/cement ratio will help control the deformation of concrete specimen under continuous cooling.
- An elastic model combing the pore size distribution of concrete and self-consistent model was established and was capable of capturing the trend of concrete under continuous cooling.
- Carbon Nanotubes was found to increase the compressive strength of concrete by up to108%.
- The optimum CNT content varies between 1% to 1.25%.
- 12 minutes of ultrasonication was found to be an optimal time to obtain the best dispersion and to get a highest compressive strength.
- Sodium Polyacrylate treated CNTs can be used in concrete, which was found to be the best option that can both increase the strength and not lose the durability.

SUGGESTIONS FOR FUTURE WORK

- More concrete specimens under different degrees of saturation should be tested. The optimal dosage of air-entraining agent can be determined .
- A theoretical model should be developed for partially saturated concrete, which is common under actual service condition. .
- Mechanical method without the help of ultrasonicator needs to be found in order to have a wide spread use of CNT concrete in construction industry.
- Better chemicals need to be identified to increase both strength and durability of CNT concrete.

BIBLIOGRAPHY

Atahanm, H.N., Oktar, O.N. and Tasdemir, M.A. (2009). "Effects of water–cement ratio and curing time on the critical pore width of hardened cement paste." *Construction and Building Materials*, (23), 1196–1200.

Bazant, Z.P., Chern, J.C., Rosenberg, A.M., and Gaidis, J.M. (1988). "Mathematical Model for Freeze-Thaw Durability of Concrete." *J AMER CERAM SOC* , 71(9), 776-783.

Barrett, E.P., Joyner L.G., and Halenda, P.P. (1951). "The Determination of Pore Volume and Area Distributions in Porous Substances. I. Computations from Nitrogen Isotherms." *J. Am. Chem. Soc.*, 73(1), 373-380.

Chen X., & Wu, S. (2013). "Influence of water-to-cement ratio and curing period on pore structure of cement mortar," Construction and Building Materials, (38), 804–812.

Chatterji, S. (2003). "Freezing of air-entrained cement-based materials and specific actions of air-entraining agents." *Cement & Concrete Composites*, (25), 759-765.

Chatterji, S. (1999). "Aspects of the freezing process in a porous material‐water system: Part 2. Freezing and the properties of water and ice." *Cement and Concrete Research*, (29), 781–784,

Cwirzen, A., Habermehl-Cwirzen, K., and Penttala, V. (2008). "Surface decoration of carbon nanotubes and mechanical properties of cement/carbon nanotube composites", *Advances in Cement Research*, 20(2), 65-73.

Cwirzen, A., Habermehl-Cwirzen, K., Nasibulin, A., Kaupinen, E., and Penttala, V. (2009) "SEM/AFM studies of cementitious binder modified by MWCNT and nano-sized Fe needles", *Material Characterisization*, 60(7), 735-740.

Franklin Colins (2012) "The influence of admixtures on the dispersion, workability and strength of carbon nanotube OPC paste mixtures", *Cement & Concrete Composites*, (34), 201-207.

Florence, S., & Konstantin, S. (2010) "Nanotechnology in concrete – A review", *Construction and Building Material*, 24(11), 2060-2071

Fagerlund, G. (1997). "On the Service Life of Concrete Exposed to Frost Action." *Freeze thaw Resistance of Concrete*, 23-41.

Fu, X., & Chung D.D.L. (1996) "Effect of methylcellulose admixture on the mechanical properties of cement." *Cement and Concrete Research*, 26(4), 535-538.

Fu, X., & Chung D.D.L. (1997) "Effects of silica fume, latex, methylcellulose, and carbon fibers on the thermal conductivity and specific heat of cement paste," *Cement and Concrete Research*, 27(12), 1799-1804.

Gopalakrishan, K., Birgisson, B., Taylor, P., and Attoh-Okine, N.O. (2011) "Multfunctional and Smart Carbon Nanotube Reinforced Cement-Based Materials", *Nanotechnology in Civil Infrastructure – A Paradigm Shift, Springer*, 1(3), 1-47.

Hunashyal, A.M., Tippa, S.V., Quadri, S.S., and Banapurmath, N.R. (2011) "Experimental Investigation on Effect of Carbon Nanotubes and Carbon Fibres on the Behavior of Plain Cement Mortar Composite Round Bars under Direct Tension", *Nanotechnology*, 1-6.

Helmuth, R.A. (1961). "Dimensional changes of hardened Portland cement pastes caused by temperature changes." *Highway Research Board Proceedings*, (40), 315–336.

Konsta-Gdoutos, M.S., Metaxa, Z.S., and Shah S.P. (2010) "highly dispersed carbon nanotube reinforced cement based materials", Cement and Concrete Research, (40),1052-1059.

Kay, W., & Loh K.J. (2010) "Nanoengineering Ultra-High-Performance Concrete with Multiwalled Carbon Nanotubes", *Transportation Research Record*, (2142), 119-126.

Konsta-Gdoutos, M.S., Metaxa, Z.S., and Shah, S.P. (2010) "Multi-scale mechanical and fracture characteristics and early age strain capacity of high performance carbon nanotube/cement nanocomposites", *Cement Concrete Composites*, 32(2), 110-115.

Larsson, L-E., & Purins, E. (1980). "Determination of the critical degree of saturation autoclaved lightweight aerated concrete by studying deformations in single-cycle freezing tests." *The International Journal of Lightweight Concrete, cement and concrete research*, 2(1), 33-41.

Metaxa, Z.S., Konsta-Gdoutos, M.S., Shah, S.P. (2010) "Carbon nanofiber-reinforced cement based materials", Journal of Transportation Research Record, 2(2142), 114–118.

Mukhopadhyay, A.K. (2011) "Next-Generation Nano-based Concrete construction products: A Review", *Nanotechnology in Civil Infrastructure – A Paradigm Shift, Springer*, 1(3), 207-223.

Musso, S., Tulliani, J-M., Ferro, G., and Tagliaferro, A. (2009) "Influence of carbon nanotubes structure on the mechanical behavior of cement composites", *Composites Science and Technology*, (69), 1985-1990.

Naaman, A.E., Namur, G.G., Alwan, J.M., and Najm, H.S. (1991) "Fiber Pullout and Bond Slip .2. Experimental Validation", *Journal of Structural Engineering*, 117(9), 2791-2800.

Nochaiya, T., and Chaipinch, A. (2010) "Behavior of multi-walled carbon nanotubes on the porosity and microstructure of cement-based materials", *Applied Surface Science*, 257, 1941-1945.

C, L., & Bassem, A. (2009) "Characterization of the uncertainties in the constitutive behavior of carbon nanotube/cement", *Science and technology of Advanced Materials*, 10(4), 1-13.

C, L., & Bassem, A. (2010) "Finite element analysis of carbon nanotube/cement composite with degraded bond strength", *Computational Materials Science*, (47), 994-1004.

Li, G.Y., Wang, P.M., and Zhao, X. (2006) "Pressure-sensitive properties and microstructure of carbon nanotube reinforced cement composites", *Cement and Concrete Composites*, (29), 377-382.

Li, G.Y., Wang, P.M., and Zhao, X. (2004) "Mechanical Behavior and microstructure of cement composites incorporating surface-treated multi-walled carbon nanotubes", *Carbon*, 43(6), 1239-1245.

Makar, J.M., Margeson, J., and Luh, J. (2005) "Carbon nanotube/cement composites – early results and potential applications", *Proceedings of 3rd international conference on construction material: performance, innovation and structural implication*. Vancouver, BC. August 22-24, 2005, 1-10.

Mann, S. (2006) "Nanotechnology and Construction", Nanoforum Report http://www.nanoforum.org (May 30, 2008).

Rajdip Bandyopadhayaya (2001) "Stabilization of individual carbon nanotubes in aqueous solutions", *Nano Letters*, 1(2), 25-28.

Raki, L., Beaudoin, J., Alizadeh, R., Makar, J., and Sato, T. (2010) "Cement and Concrete Nanoscience and Nanotechnology", *Materials*, 3(1), 918-942.

Sanchez, F., and Ince, C. (2009) "Microstructure and macroscopic properties of hybrid carbon nanofiber/silica fume composites", *Composites Science and Technology*, (69), 1310-1318.

Sanchez, F. (2009) "Carbon nanofiber/cement composites: challenges and promises as structural materials", Composite Science Technology, 69(11-12), 1985-1990.

Shah, S.P., Konsta-Gdoutos, M.S., Metaxa, Z.S., and Mondal, P. (2009) "Nanoscale Modification of cementitious materials", *Nanotechnology in Construction*, 3(2), 125-130.

Steyn, W.J. (2011) "Application of Nanotechnology in Road Pavement Engineering", *Nanotechnology in Civil Infrastructure – A Paradigm Shift, Springer*, 1(3), 49-83.

Setzer, M., Augberg, R., and Keck, H-J. (2002). "Frost Resistance of Concrete." Essen, Germany: RILEM Publications,

Sun, Z.H. & Scherer, G.W. (2010). "Effect of air voids on salt scaling and internal freezing." cement and concrete research, (40), 260-270.

Tyson, B. S.M. ASCE, Rashid, K., Yazdanbakhsh, A., and Grasley, Z. (2011) "Carbon Nanotubes and Carbon Nanofibers for Enhancing the Mechanical Properties of

Nanocomposite Cementitious Materials", *Journal of Materials in Civil Engineering*, 23(7), 1028-1035.

Xi, Y., & Jenning, H.M. (1997). "Shrinkage of cement paste and concrete modeled by a multiscale effective homogeneous theory," Materials and Structures, (30), 329-339.

Xie, X.H., Mai, Y.W., Zhou, X.P. (2005) "Dispersion and alignment of carbon nanotubes in polymer matrix: a review", *Material Science Engineering*, 49(4), 89-112.

Zhou, Z. & Mihashi, H. (2008). "Micromechanics Model to Describe Strain Behavior of Concrete in Freezing Process." *J. Mater. Civ. Eng.* 20, SPECIAL ISSUE: Durability and Service Life of Concrete Structures: Recent Advances, 46–53.

Zuber, B., Marchand, J., Delagrave, A., and Bournazel, J.P. (2000). "Ice formation mechanisms in normal and high-performance concrete mixtures," *Journal of Materials in Civil Engineering*, 12(1), 16-23,

Zuber, B. & Marchand, J. (2004)."Predicting the volume instability of hydrated cement systems upon freezing using poro-mechanics and local phase equilibria." Materials and structures/Concrete science and engineering, (37), 257-270.

APPENDIX

Appendix A. BET Test Result for III'-1

micromeritics®

Micromeritics Instrument Corp.

Gemini V2.00 Unit 1 Serial #: 5501 Page 1

Sample: III'-V Run 2
Operator: KZ OL
Submitter:
File: C:\GEMINI\DATA\001-153.SMP

Started: 4/29/2013 9:43:34AM
Completed: 4/29/2013 2:22:13PM
Report Time: 4/29/2013 3:05:48PM
Free Space Diff.: -0.3742 cm³
Free Space Type: Measured
Gemini Model: 2380

Analysis Adsorptive: N2
Equilibration Time: 5 s
Sat. Pressure: 636.560 mmHg
Sample Mass: 0.2485 g
Sample Density: 1.000 g/cm³

Isotherm Tabular Report

Relative Pressure (P/Po)	Absolute Pressure (mmHg)	Quantity Adsorbed (cm³/g STP)	Elapsed Time (h:min)	Saturation Pressure (mmHg)
0.050136674	31.915001	3.3743	00:43	636.559998
0.075185373	47.860001	3.6184	00:45	
0.100210508	63.790001	3.8159	00:48	
0.125314184	79.769997	3.9937	00:50	
0.150323619	95.690002	4.1536	00:53	
0.175395881	111.650002	4.3025	00:55	
0.200397453	127.565002	4.4536	00:58	
0.225501129	143.544998	4.5915	01:00	
0.250565541	159.500000	4.7404	01:02	
0.275582826	175.425003	4.8937	01:05	
0.300592249	191.345001	5.0425	01:07	
0.325601672	207.264999	5.1958	01:09	
0.350556106	223.149994	5.3446	01:12	
0.375699070	239.154999	5.5069	01:14	
0.400645665	255.035004	5.6778	01:16	
0.425796491	271.045013	5.8534	01:19	
0.450680236	286.885010	6.0397	01:21	
0.475823199	302.890015	6.2330	01:23	
0.500832598	318.809998	6.4504	01:26	
0.526077677	334.880005	6.6792	01:28	
0.550733652	350.575012	6.9162	01:30	
0.575578133	366.390015	7.1755	01:33	
0.600870290	382.489990	7.4730	01:35	
0.625738358	398.320007	7.7876	01:37	
0.650834195	414.295013	8.1557	01:40	
0.675725802	430.140015	8.5523	01:42	
0.700743063	446.065002	9.0420	01:46	
0.725901703	462.079987	9.5629	01:49	
0.750738369	477.890015	10.1763	01:53	
0.776006988	493.975006	10.8832	01:56	
0.801000710	509.885010	11.6761	02:01	
0.825625235	525.559998	12.5836	02:05	
0.851105994	541.780029	13.7047	02:10	
0.876154609	557.724976	15.0266	02:16	
0.900637803	573.309998	16.3766	02:22	
0.925600123	589.200012	18.2319	02:28	
0.950680188	605.164978	20.8309	02:37	
0.975579705	621.015015	26.2295	02:55	
0.998059907	635.325012	860.6244	04:38	

micromeritics®

Micromeritics Instrument Corp.

Gemini V2.00 Unit 1 Serial #: 5501 Page 2

Sample: III'-V Run 2
Operator: KZ OL
Submitter:
File: C:\GEMINI\DATA\001-153.SMP

Started: 4/29/2013 9:43:34AM
Completed: 4/29/2013 2:22:13PM
Report Time: 4/29/2013 3:05:48PM
Free Space Diff.: -0.3742 cm³
Free Space Type: Measured
Gemini Model: 2380

Analysis Adsorptive: N2
Equilibration Time: 5 s
Sat. Pressure: 636.560 mmHg
Sample Mass: 0.2485 g
Sample Density: 1.000 g/cm³

Isotherm Linear Plot

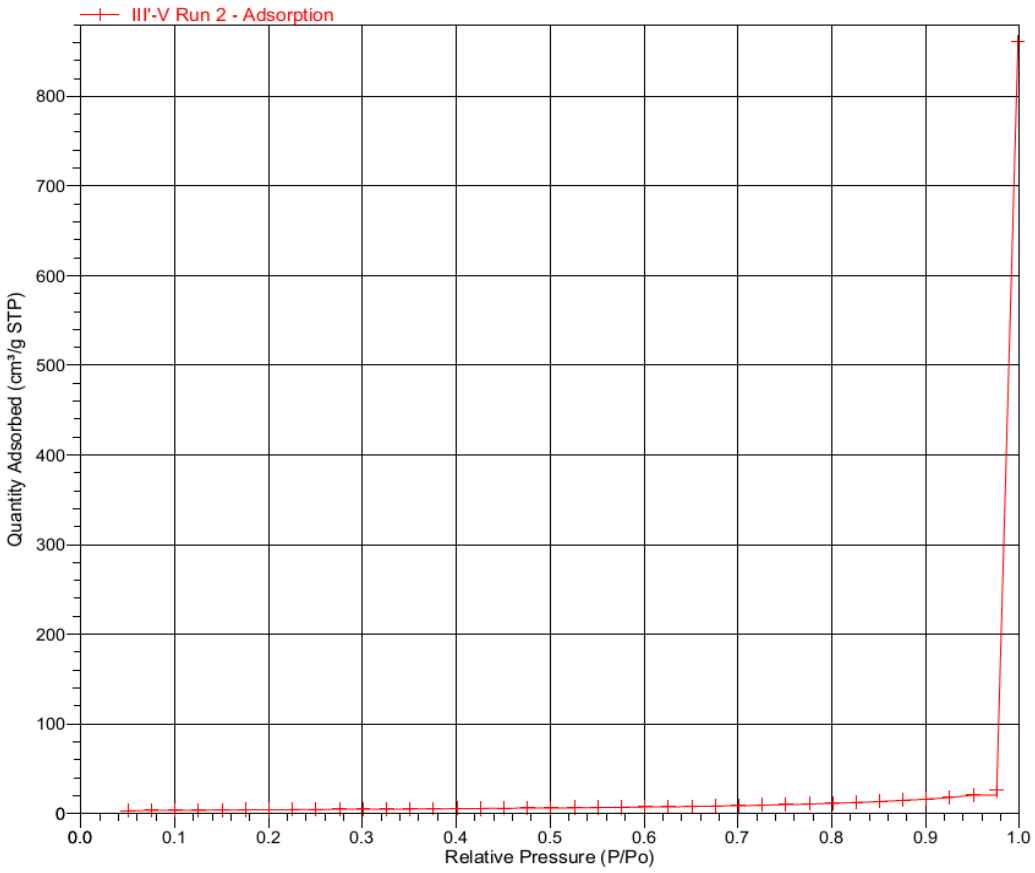

micromeritics®

Micromeritics Instrument Corp.

Gemini V2.00 Unit 1 Serial #: 5501 Page 3

Sample: III'-V Run 2
Operator: KZ OL
Submitter:
File: C:\GEMINI\DATA\001-153.SMP

Started: 4/29/2013 9:43:34AM
Completed: 4/29/2013 2:22:13PM
Report Time: 4/29/2013 3:05:48PM
Free Space Diff.: -0.3742 cm³
Free Space Type: Measured
Gemini Model: 2380

Analysis Adsorptive: N2
Equilibration Time: 5 s
Sat. Pressure: 636.560 mmHg
Sample Mass: 0.2485 g
Sample Density: 1.000 g/cm³

BET Surface Area Report

BET Surface Area: 6.8622 ± 1.3821 m²/g
Slope: 0.795081 ± 0.110434 g/cm³ STP
Y-Intercept: -0.160711 ± 0.064259 g/cm³ STP
C: -3.947268
Qm: 1.5764 cm³/g STP
Correlation Coefficient: 0.7682035
Molecular Cross-Sectional Area: 0.1620 nm²

Relative Pressure (P/Po)	Quantity Adsorbed (cm³/g STP)	1/[Q(Po/P - 1)]
0.050136674	3.3743	0.015643
0.075185373	3.6184	0.022468
0.100210508	3.8159	0.029186
0.125314184	3.9937	0.035874
0.150323619	4.1536	0.042594
0.175395881	4.3025	0.049437
0.200397453	4.4536	0.056274
0.225501129	4.5915	0.063413
0.250565541	4.7404	0.070530
0.275582826	4.8937	0.077737
0.300592249	5.0425	0.085231
0.325601672	5.1958	0.092922
0.350556106	5.3446	0.100996
0.375699070	5.5069	0.109280
0.400645665	5.6778	0.117733
0.425796491	5.8534	0.126687
0.450680236	6.0397	0.135841
0.475823199	6.2330	0.145638
0.500832598	6.4504	0.155546
0.526077677	6.6792	0.166194
0.550733652	6.9162	0.177244
0.575578133	7.1755	0.188997
0.600870290	7.4730	0.201453
0.625738358	7.7876	0.214690
0.650834195	8.1557	0.228548
0.675725802	8.5523	0.243655
0.700743063	9.0420	0.258970
0.725901703	9.5629	0.276938
0.750738369	10.1763	0.295967
0.776006988	10.8832	0.318327
0.801000710	11.6761	0.344733
0.825625235	12.5836	0.376265
0.851105994	13.7047	0.417097
0.876154609	15.0266	0.470803
0.900637803	16.3766	0.553483
0.925600123	18.2319	0.682371
0.950680188	20.8309	0.925348
0.975579705	26.2295	1.523077

micromeritics®

Micromeritics Instrument Corp.

Gemini V2.00 Unit 1 Serial #: 5501 Page 4

Sample: III'-V Run 2
Operator: KZ OL
Submitter:
File: C:\GEMINI\DATA\001-153.SMP

Started: 4/29/2013 9:43:34AM
Completed: 4/29/2013 2:22:13PM
Report Time: 4/29/2013 3:05:48PM
Free Space Diff.: -0.3742 cm³
Free Space Type: Measured
Gemini Model: 2380

Analysis Adsorptive: N2
Equilibration Time: 5 s
Sat. Pressure: 636.560 mmHg
Sample Mass: 0.2485 g
Sample Density: 1.000 g/cm³

BET Surface Area Plot

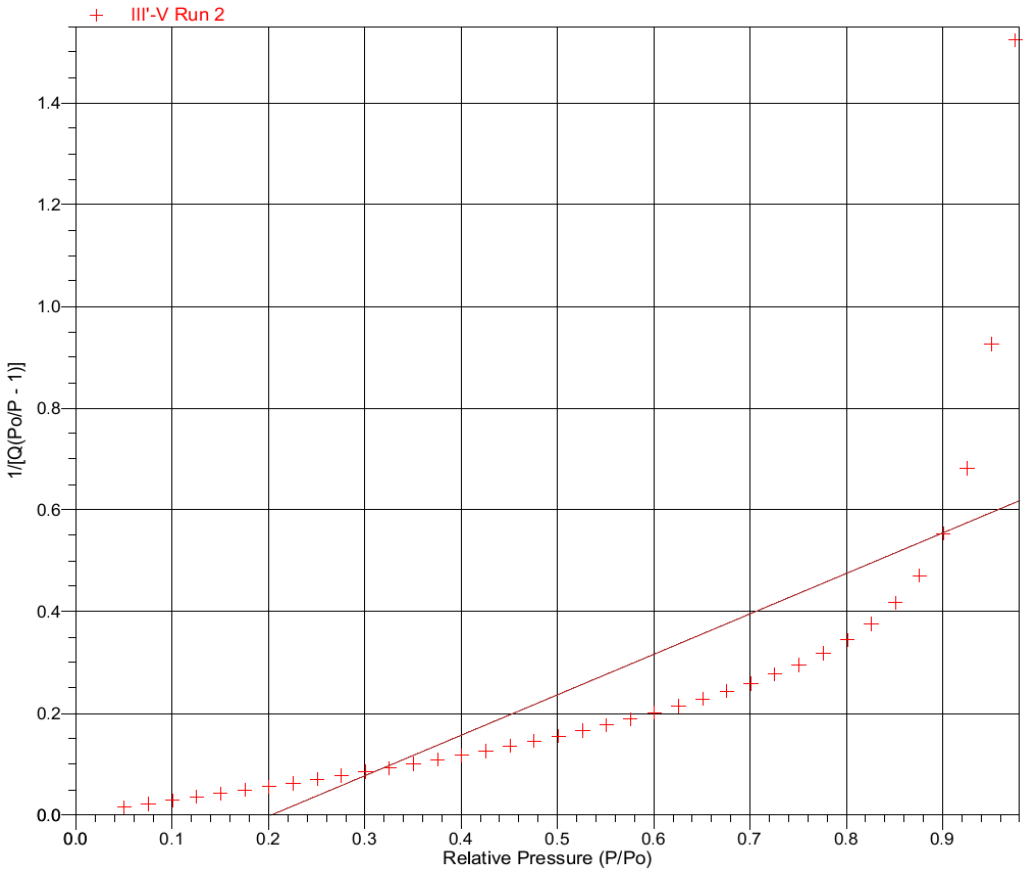

micromeritics®

Micromeritics Instrument Corp.

Gemini V2.00 | Unit 1 | Serial #: 5501 | Page 5

Sample: III'-V Run 2
Operator: KZ OL
Submitter:
File: C:\GEMINI\DATA\001-153.SMP

Started: 4/29/2013 9:43:34AM
Completed: 4/29/2013 2:22:13PM
Report Time: 4/29/2013 3:05:48PM
Free Space Diff.: -0.3742 cm³
Free Space Type: Measured
Gemini Model: 2380

Analysis Adsorptive: N2
Equilibration Time: 5 s
Sat. Pressure: 636.560 mmHg
Sample Mass: 0.2485 g
Sample Density: 1.000 g/cm³

BJH Adsorption Pore Distribution Report

Faas Correction
Halsey
t = 3.54 [-5 / ln(P/Po)] ^ 0.333

Diameter Range: 17.000 Å to 3000.000 Å
Adsorbate Property Factor: 9.53000 Å
Density Conversion Factor: 0.0015468
Fraction of Pores Open at Both Ends: 0.00

Pore Diameter Range (Å)	Average Diameter (Å)	Incremental Pore Volume (cm³/g)	Cumulative Pore Volume (cm³/g)	Incremental Pore Area (m²/g)	Cumulative Pore Area (m²/g)
811.5 - 408.6	486.7	0.009557	0.009557	0.786	0.786
408.6 - 274.0	314.5	0.004635	0.014192	0.590	1.375
274.0 - 206.8	230.6	0.003381	0.017573	0.586	1.962
206.8 - 167.0	182.4	0.002499	0.020072	0.548	2.510
167.0 - 139.5	150.6	0.002536	0.022608	0.674	3.183
139.5 - 119.5	127.8	0.002185	0.024793	0.684	3.867
119.5 - 104.9	111.2	0.001789	0.026582	0.644	4.511
104.9 - 93.3	98.4	0.001580	0.028163	0.643	5.154
93.3 - 83.9	88.0	0.001426	0.029588	0.648	5.801
83.9 - 76.2	79.6	0.001247	0.030835	0.626	6.427
76.2 - 69.7	72.7	0.001049	0.031884	0.577	7.005
69.7 - 64.2	66.7	0.001005	0.032889	0.603	7.607
64.2 - 59.5	61.6	0.000788	0.033676	0.511	8.119
59.5 - 55.3	57.2	0.000735	0.034411	0.514	8.632
55.3 - 51.6	53.3	0.000610	0.035021	0.458	9.090
51.6 - 48.3	49.8	0.000578	0.035599	0.464	9.554
48.3 - 45.4	46.7	0.000489	0.036088	0.418	9.972
45.4 - 42.8	44.0	0.000440	0.036528	0.400	10.372
42.8 - 40.3	41.4	0.000424	0.036951	0.409	10.781
40.3 - 38.1	39.1	0.000405	0.037356	0.414	11.195
38.1 - 36.0	37.0	0.000335	0.037691	0.362	11.557
36.0 - 34.1	35.0	0.000326	0.038017	0.373	11.930
34.1 - 32.4	33.2	0.000295	0.038312	0.355	12.285
32.4 - 30.7	31.5	0.000290	0.038603	0.368	12.654
30.7 - 29.2	29.9	0.000262	0.038865	0.351	13.004
29.2 - 27.7	28.4	0.000217	0.039082	0.306	13.311
27.7 - 26.3	27.0	0.000239	0.039321	0.355	13.666
26.3 - 25.0	25.6	0.000223	0.039544	0.348	14.014
25.0 - 23.7	24.3	0.000241	0.039785	0.398	14.411
23.7 - 22.5	23.0	0.000216	0.040002	0.376	14.787
22.5 - 21.3	21.8	0.000154	0.040156	0.283	15.070
21.3 - 20.1	20.6	0.000207	0.040363	0.402	15.472
20.1 - 18.9	19.4	0.000170	0.040533	0.350	15.821
18.9 - 17.7	18.3	0.000193	0.040726	0.423	16.245
17.7 - 16.5	17.1	0.000231	0.040957	0.540	16.785

micromeritics®

Micromeritics Instrument Corp.

Gemini V2.00 Unit 1 Serial #: 5501 Page 6

Sample: III'-V Run 2
Operator: KZ OL
Submitter:
File: C:\GEMINI\DATA\001-153.SMP

Started: 4/29/2013 9:43:34AM
Completed: 4/29/2013 2:22:13PM
Report Time: 4/29/2013 3:05:48PM
Free Space Diff.: -0.3742 cm³
Free Space Type: Measured
Gemini Model: 2380

Analysis Adsorptive: N2
Equilibration Time: 5 s
Sat. Pressure: 636.560 mmHg
Sample Mass: 0.2485 g
Sample Density: 1.000 g/cm³

BJH Adsorption Cumulative Pore Volume

Halsey : Faas Correction

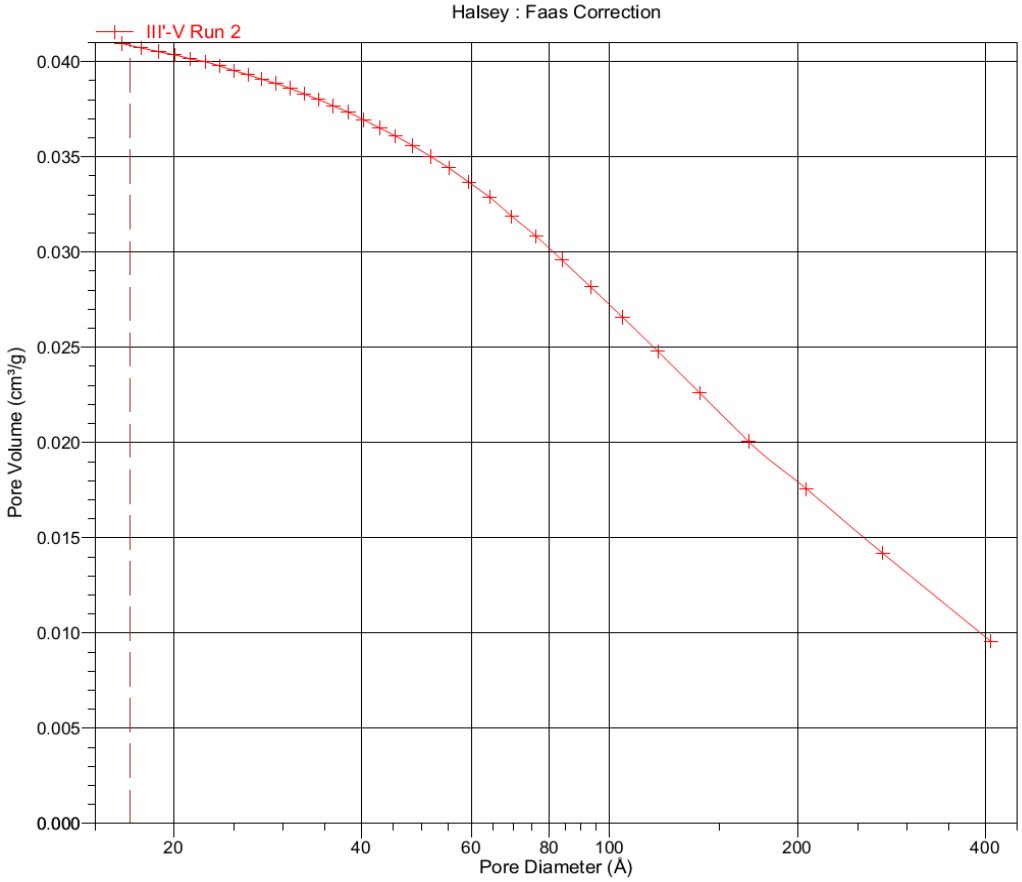

micromeritics®

Micromeritics Instrument Corp.

Gemini V2.00 Unit 1 Serial #: 5501 Page 7

Sample: III'-V Run 2
Operator: KZ OL
Submitter:
File: C:\GEMINI\DATA\001-153.SMP

Started: 4/29/2013 9:43:34AM
Completed: 4/29/2013 2:22:13PM
Report Time: 4/29/2013 3:05:48PM
Free Space Diff.: -0.3742 cm³
Free Space Type: Measured
Gemini Model: 2380

Analysis Adsorptive: N2
Equilibration Time: 5 s
Sat. Pressure: 636.560 mmHg
Sample Mass: 0.2485 g
Sample Density: 1.000 g/cm³

BJH Adsorption dV/dD Pore Volume

Halsey : Faas Correction

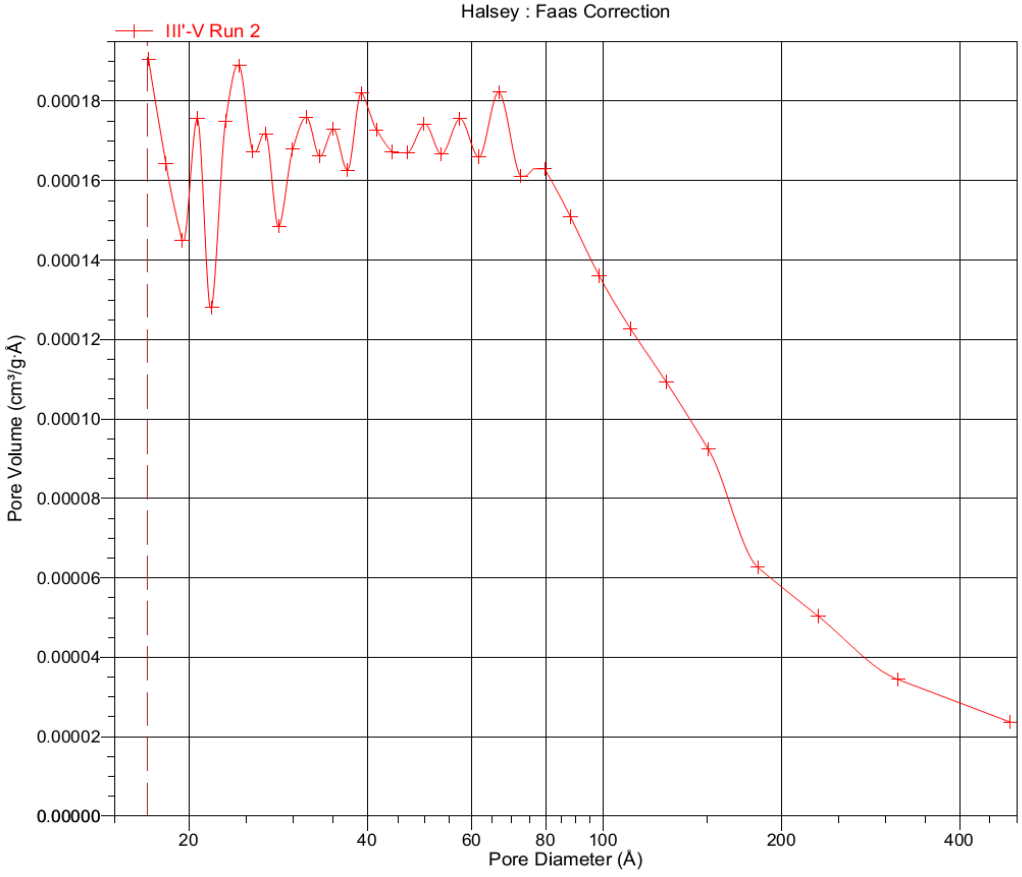

micromeritics®

Micromeritics Instrument Corp.

Gemini V2.00 Unit 1 Serial #: 5501 Page 8

Sample: III'-V Run 2
Operator: KZ OL
Submitter:
File: C:\GEMINI\DATA\001-153.SMP

Started: 4/29/2013 9:43:34AM
Completed: 4/29/2013 2:22:13PM
Report Time: 4/29/2013 3:05:48PM
Free Space Diff.: -0.3742 cm³
Free Space Type: Measured
Gemini Model: 2380

Analysis Adsorptive: N2
Equilibration Time: 5 s
Sat. Pressure: 636.560 mmHg
Sample Mass: 0.2485 g
Sample Density: 1.000 g/cm³

BJH Adsorption dV/dlog(D) Pore Volume

Halsey : Faas Correction

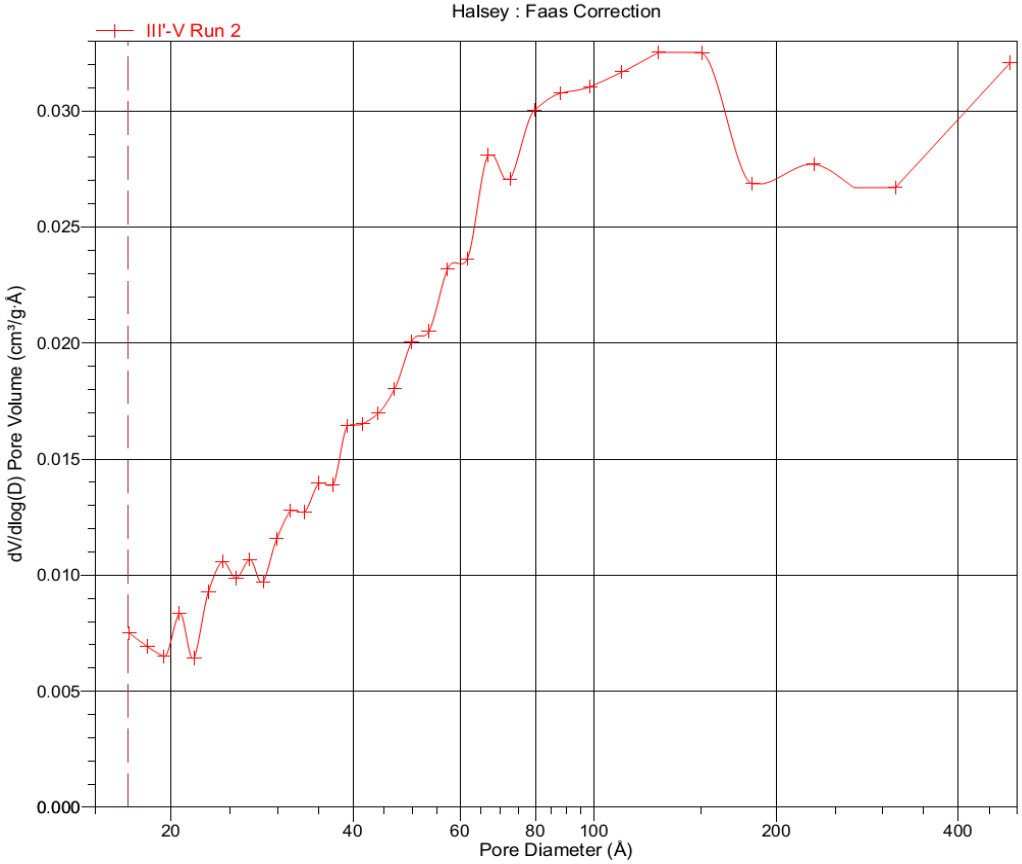

micromeritics®

Micromeritics Instrument Corp.

Gemini V2.00 Unit 1 Serial #: 5501 Page 9

Sample: III'-V Run 2
Operator: KZ OL
Submitter:
File: C:\GEMINI\DATA\001-153.SMP

Started: 4/29/2013 9:43:34AM
Completed: 4/29/2013 2:22:13PM
Report Time: 4/29/2013 3:05:48PM
Free Space Diff.: -0.3742 cm³
Free Space Type: Measured
Gemini Model: 2380

Analysis Adsorptive: N2
Equilibration Time: 5 s
Sat. Pressure: 636.560 mmHg
Sample Mass: 0.2485 g
Sample Density: 1.000 g/cm³

BJH Adsorption Cumulative Pore Area

Halsey : Faas Correction

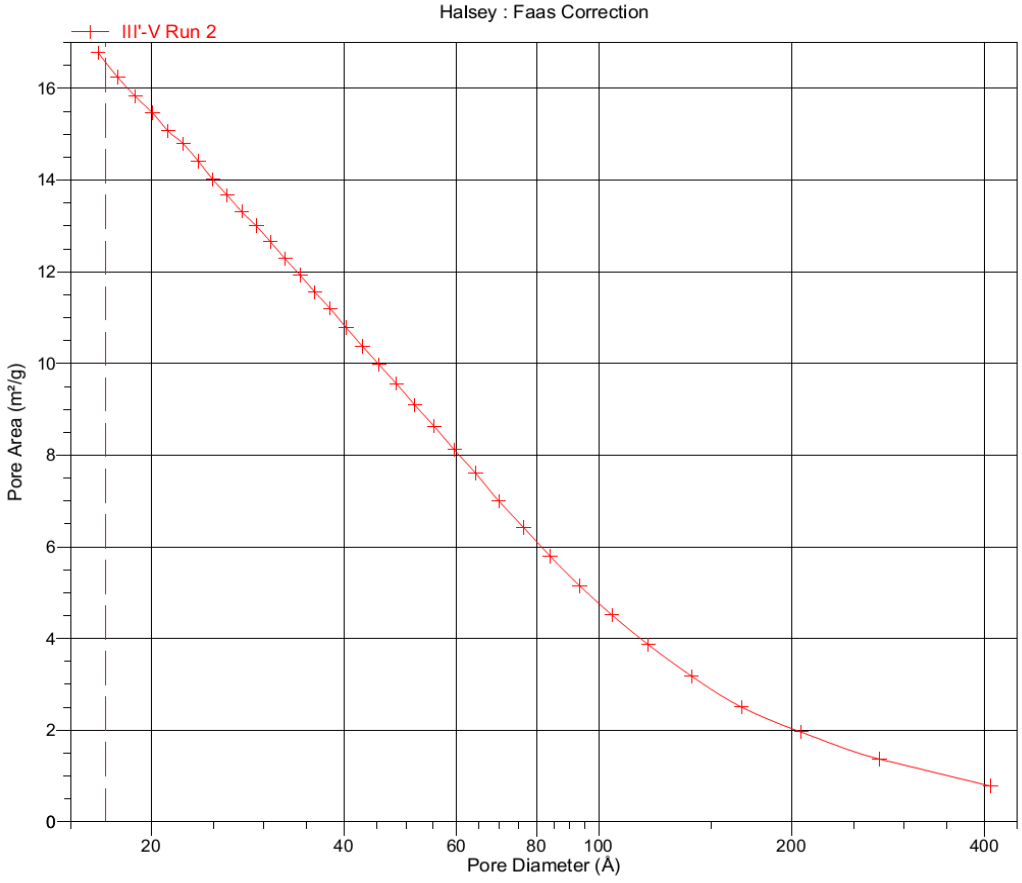

micromeritics®

Micromeritics Instrument Corp.

Gemini V2.00 Unit 1 Serial #: 5501 Page 10

Sample: III'-V Run 2
Operator: KZ OL
Submitter:
File: C:\GEMINI\DATA\001-153.SMP

Started: 4/29/2013 9:43:34AM
Completed: 4/29/2013 2:22:13PM
Report Time: 4/29/2013 3:05:48PM
Free Space Diff.: -0.3742 cm³
Free Space Type: Measured
Gemini Model: 2380

Analysis Adsorptive: N2
Equilibration Time: 5 s
Sat. Pressure: 636.560 mmHg
Sample Mass: 0.2485 g
Sample Density: 1.000 g/cm³

BJH Adsorption dA/dD Pore Area

Halsey : Faas Correction

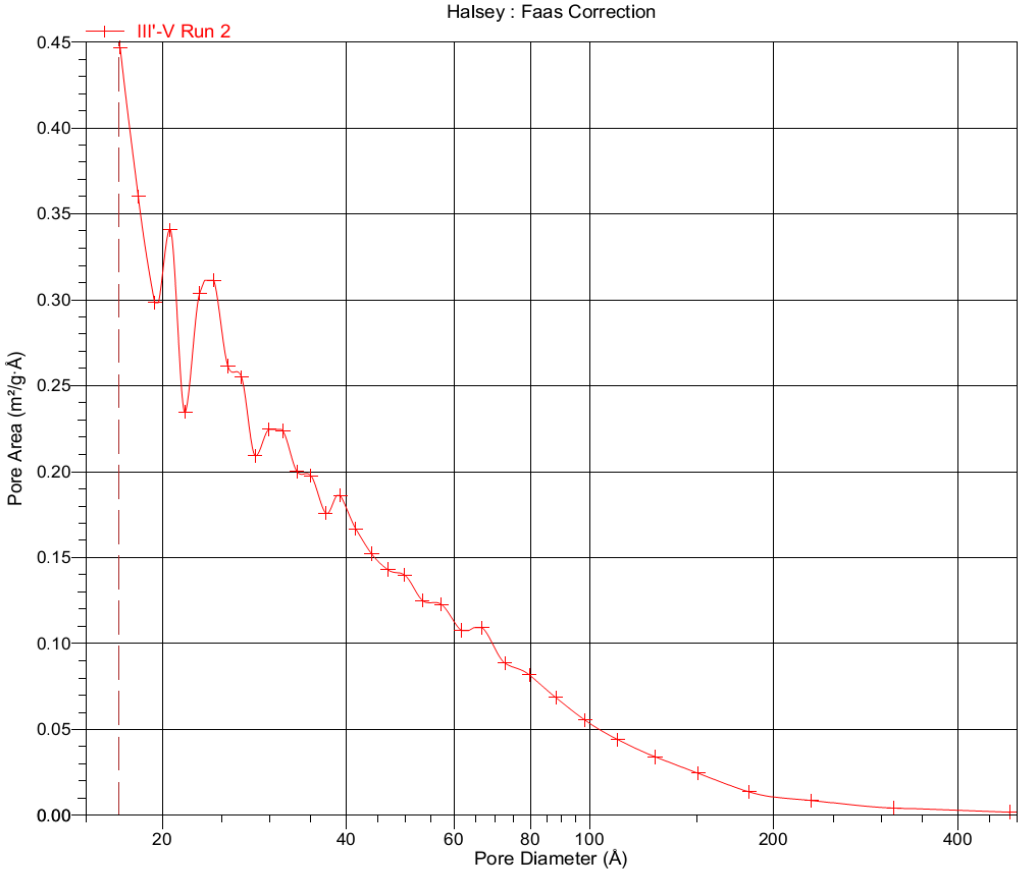

micromeritics®

Micromeritics Instrument Corp.

Gemini V2.00 Unit 1 Serial #: 5501 Page 11

Sample: III'-V Run 2
Operator: KZ OL
Submitter:
File: C:\GEMINI\DATA\001-153.SMP

Started: 4/29/2013 9:43:34AM
Completed: 4/29/2013 2:22:13PM
Report Time: 4/29/2013 3:05:48PM
Free Space Diff.: -0.3742 cm³
Free Space Type: Measured
Gemini Model: 2380

Analysis Adsorptive: N2
Equilibration Time: 5 s
Sat. Pressure: 636.560 mmHg
Sample Mass: 0.2485 g
Sample Density: 1.000 g/cm³

BJH Adsorption dA/dlog(D) Pore Area

Halsey : Faas Correction

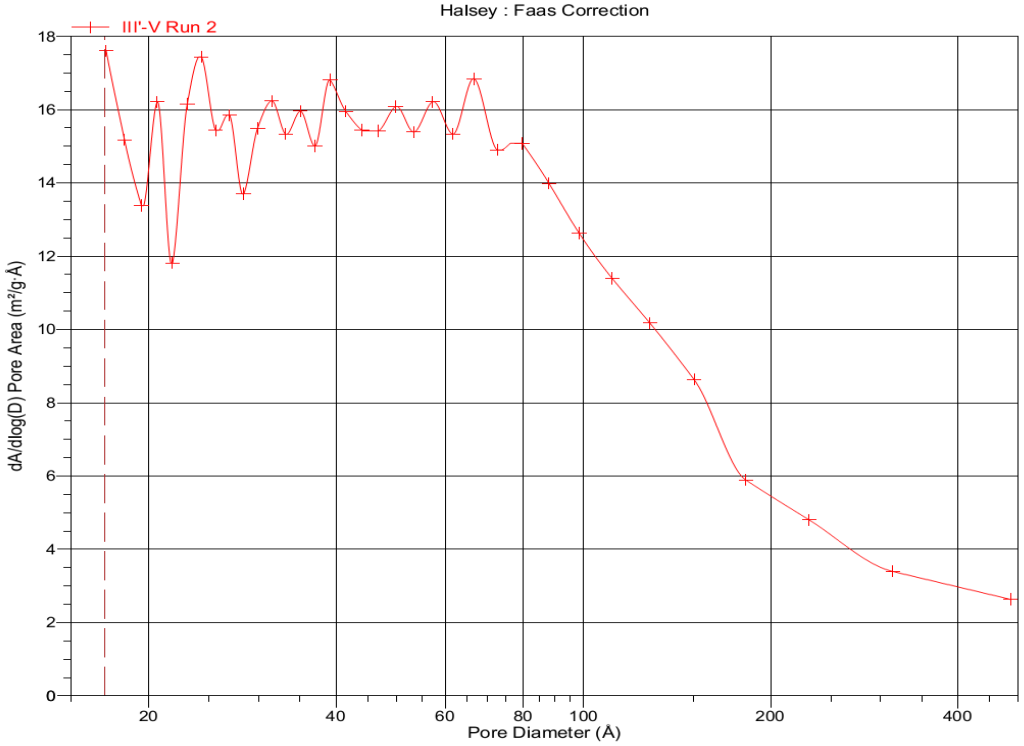

Appendix B. BET Test Result for IV'-1

micromeritics®

Micromeritics Instrument Corp.

Gemini V2.00 Unit 1 Serial #: 5501 Page 1

Sample: IV-1 Run 2
Operator: KZ OL
Submitter:
File: C:\GEMINI\DATA\001-160.SMP

Started: 5/1/2013 8:48:15AM
Completed: 5/1/2013 12:13:43PM
Report Time: 5/1/2013 12:28:31PM
Free Space Diff.: -0.4473 cm³
Free Space Type: Measured
Gemini Model: 2380

Analysis Adsorptive: N2
Equilibration Time: 5 s
Sat. Pressure: 643.815 mmHg
Sample Mass: 0.2819 g
Sample Density: 1.000 g/cm³

Isotherm Tabular Report

Relative Pressure (P/Po)	Absolute Pressure (mmHg)	Quantity Adsorbed (cm³/g STP)	Elapsed Time (h:min)	Saturation Pressure (mmHg)
0.050146393	32.285000	3.7744	00:38	643.815002
0.075106978	48.355000	4.0245	00:40	
0.100191821	64.504997	4.2319	00:43	
0.125222311	80.620003	4.4177	00:45	
0.150260552	96.739998	4.5860	00:48	
0.175275507	112.845001	4.7425	00:50	
0.200298224	128.955002	4.9010	00:52	
0.225460727	145.154999	5.0558	00:55	
0.250421325	161.225006	5.2084	00:57	
0.275568281	177.414993	5.3612	00:59	
0.300606545	193.535004	5.5236	01:02	
0.325567119	209.604996	5.6821	01:04	
0.350636432	225.744995	5.8504	01:06	
0.375643625	241.845001	6.0225	01:09	
0.400681866	257.964996	6.2006	01:11	
0.425642463	274.035004	6.3824	01:13	
0.450999098	290.359985	6.5609	01:17	
0.476394601	306.709991	6.7550	01:20	
0.501067853	322.595001	6.9696	01:22	
0.526176011	338.760010	7.2160	01:24	
0.551004549	354.744995	7.4601	01:27	
0.599690897	386.089996	7.9919	01:31	
0.602735237	388.049988	8.0369	01:33	
0.626259105	403.195007	8.2851	01:35	
0.650924583	419.075012	8.6441	01:38	
0.675644383	434.989990	9.0500	01:40	
0.700705945	451.125000	9.4895	01:43	
0.725705365	467.220001	10.0070	01:46	
0.750479581	483.170013	10.5748	01:48	
0.775704203	499.410004	11.4204	01:53	
0.800548337	515.405029	12.2615	01:58	
0.851789749	548.395020	13.3196	02:06	
0.853389538	549.424988	13.3198	02:08	
0.875756250	563.825012	15.3965	02:13	
0.900677979	579.869995	17.0786	02:19	
0.925421100	595.799988	18.9459	02:27	
0.951103997	612.335022	21.2807	02:38	
0.975559772	628.080017	24.1328	02:51	
1.004877200	646.955017	139.6800	03:24	

micromeritics®

Micromeritics Instrument Corp.

Gemini V2.00 Unit 1 Serial #: 5501 Page 2

Sample: IV-1 Run 2
Operator: KZ OL
Submitter:
File: C:\GEMINI\DATA\001-160.SMP

Started: 5/1/2013 8:48:15AM
Completed: 5/1/2013 12:13:43PM
Report Time: 5/1/2013 12:28:31PM
Free Space Diff.: -0.4473 cm³
Free Space Type: Measured
Gemini Model: 2380

Analysis Adsorptive: N2
Equilibration Time: 5 s
Sat. Pressure: 643.815 mmHg
Sample Mass: 0.2819 g
Sample Density: 1.000 g/cm³

Isotherm Linear Plot

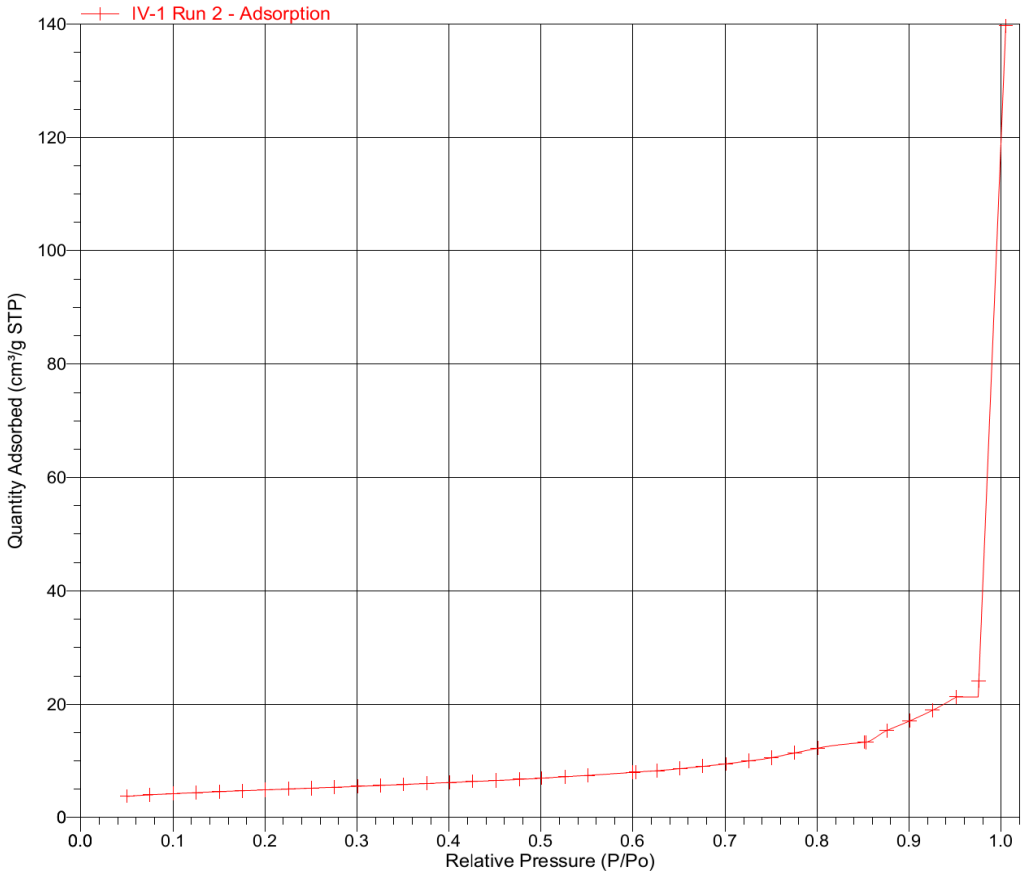

micromeritics®

Micromeritics Instrument Corp.

Gemini V2.00 | Unit 1 | Serial #: 5501 | Page 3

Sample: IV-1 Run 2
Operator: KZ OL
Submitter:
File: C:\GEMINI\DATA\001-160.SMP

Started: 5/1/2013 8:48:15AM
Completed: 5/1/2013 12:13:43PM
Report Time: 5/1/2013 12:28:31PM
Free Space Diff.: -0.4473 cm³
Free Space Type: Measured
Gemini Model: 2380

Analysis Adsorptive: N2
Equilibration Time: 5 s
Sat. Pressure: 643.815 mmHg
Sample Mass: 0.2819 g
Sample Density: 1.000 g/cm³

BET Surface Area Report

BET Surface Area: 6.8431 ± 1.5153 m²/g
Slope: 0.808966 ± 0.121656 g/cm³ STP
Y-Intercept: -0.172822 ± 0.071004 g/cm³ STP
C: -3.680921
Qm: 1.5720 cm³/g STP
Correlation Coefficient: 0.7424405
Molecular Cross-Sectional Area: 0.1620 nm²

Relative Pressure (P/Po)	Quantity Adsorbed (cm³/g STP)	1/[Q(Po/P - 1)]
0.050146393	3.7744	0.013987
0.075106978	4.0245	0.020178
0.100191821	4.2319	0.026312
0.125222311	4.4177	0.032403
0.150260552	4.5860	0.038559
0.175275507	4.7425	0.044813
0.200298224	4.9010	0.051105
0.225460727	5.0558	0.057575
0.250421325	5.2084	0.064143
0.275568281	5.3612	0.070953
0.300606545	5.5236	0.077813
0.325567119	5.6821	0.084956
0.350636432	5.8504	0.092296
0.375643625	6.0225	0.099900
0.400681866	6.2006	0.107823
0.425642463	6.3824	0.116112
0.450999098	6.5609	0.125211
0.476394601	6.7550	0.134691
0.501067853	6.9696	0.144094
0.526176011	7.2160	0.153892
0.551004549	7.4601	0.164501
0.599690897	7.9919	0.187449
0.602735237	8.0369	0.188780
0.626259105	8.2851	0.202248
0.650924583	8.6441	0.215721
0.675644383	9.0500	0.230170
0.700705945	9.4895	0.246715
0.725705365	10.0070	0.264388
0.750479581	10.5748	0.284419
0.775704203	11.4204	0.302827
0.800548337	12.2615	0.327345
0.851789749	13.3196	0.431483
0.853389538	13.3198	0.437004
0.875756250	15.3965	0.457812
0.900677979	17.0786	0.530971
0.925421100	18.9459	0.654951
0.951103997	21.2807	0.914048
0.975559772	24.1328	1.654019

micromeritics®

Micromeritics Instrument Corp.

Gemini V2.00 | Unit 1 | Serial #: 5501 | Page 4

Sample: IV-1 Run 2
Operator: KZ OL
Submitter:
File: C:\GEMINI\DATA\001-160.SMP

Started: 5/1/2013 8:48:15AM
Completed: 5/1/2013 12:13:43PM
Report Time: 5/1/2013 12:28:31PM
Free Space Diff.: -0.4473 cm³
Free Space Type: Measured
Gemini Model: 2380

Analysis Adsorptive: N2
Equilibration Time: 5 s
Sat. Pressure: 643.815 mmHg
Sample Mass: 0.2819 g
Sample Density: 1.000 g/cm³

BET Surface Area Plot

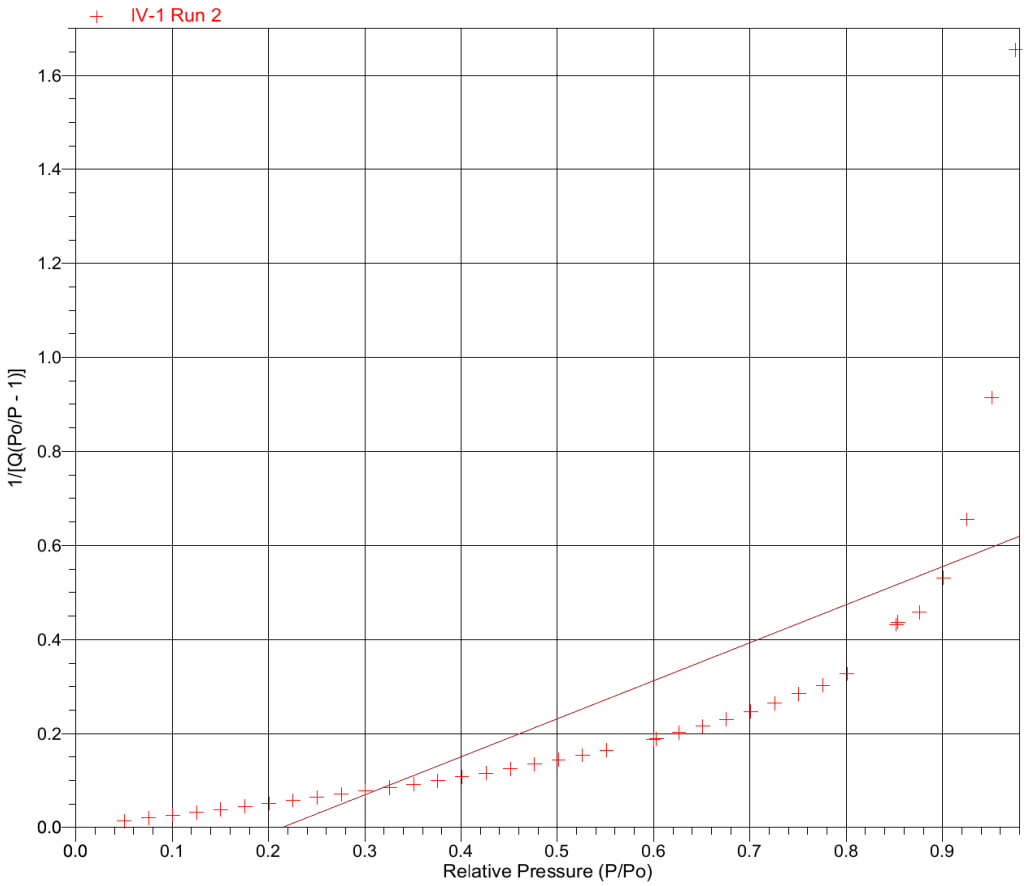

micromeritics®

Micromeritics Instrument Corp.

Gemini V2.00 Unit 1 Serial #: 5501 Page 5

Sample: IV-1 Run 2
Operator: KZ OL
Submitter:
File: C:\GEMINI\DATA\001-160.SMP

Started: 5/1/2013 8:48:15AM
Completed: 5/1/2013 12:13:43PM
Report Time: 5/1/2013 12:28:31PM
Free Space Diff.: -0.4473 cm³
Free Space Type: Measured
Gemini Model: 2380

Analysis Adsorptive: N2
Equilibration Time: 5 s
Sat. Pressure: 643.815 mmHg
Sample Mass: 0.2819 g
Sample Density: 1.000 g/cm³

BJH Adsorption Pore Distribution Report

Faas Correction
Halsey
t = 3.54 [-5 / ln(P/Po)] ^ 0.333

Diameter Range: 17.000 Å to 3000.000 Å
Adsorbate Property Factor: 9.53000 Å
Density Conversion Factor: 0.0015468
Fraction of Pores Open at Both Ends: 0.00

Pore Diameter Range (Å)	Average Diameter (Å)	Incremental Pore Volume (cm³/g)	Cumulative Pore Volume (cm³/g)	Incremental Pore Area (m²/g)	Cumulative Pore Area (m²/g)
811.0 - 412.2	490.7	0.005049	0.005049	0.412	0.412
412.2 - 273.5	314.5	0.004236	0.009284	0.539	0.950
273.5 - 207.1	230.7	0.003479	0.012763	0.603	1.554
207.1 - 166.6	182.1	0.003222	0.015986	0.708	2.261
166.6 - 141.8	152.0	0.004170	0.020156	1.097	3.358
141.8 - 104.9	117.1	0.001846	0.022002	0.631	3.989
104.9 - 93.4	98.4	0.001734	0.023737	0.705	4.694
93.4 - 84.0	88.2	0.001795	0.025531	0.814	5.508
84.0 - 76.4	79.8	0.001157	0.026689	0.580	6.088
76.4 - 70.0	72.9	0.001065	0.027754	0.585	6.673
70.0 - 64.4	66.9	0.000894	0.028648	0.534	7.207
64.4 - 59.7	61.9	0.000838	0.029486	0.542	7.749
59.7 - 55.6	57.5	0.000735	0.030220	0.511	8.260
55.6 - 52.1	53.7	0.000451	0.030672	0.336	8.596
52.1 - 51.7	51.9	0.000098	0.030770	0.076	8.672
51.7 - 45.7	48.2	0.001056	0.031826	0.876	9.547
45.7 - 43.0	44.2	0.000480	0.032305	0.434	9.981
43.0 - 40.6	41.7	0.000501	0.032807	0.481	10.462
40.6 - 38.4	39.4	0.000416	0.033222	0.422	10.884
38.4 - 36.3	37.3	0.000350	0.033573	0.376	11.260
36.3 - 34.4	35.3	0.000308	0.033880	0.349	11.610
34.4 - 32.6	33.4	0.000337	0.034217	0.403	12.013
32.6 - 30.9	31.7	0.000331	0.034548	0.418	12.430
30.9 - 29.4	30.1	0.000317	0.034865	0.421	12.851
29.4 - 27.9	28.6	0.000307	0.035172	0.429	13.280
27.9 - 26.5	27.2	0.000272	0.035444	0.400	13.680
26.5 - 25.2	25.8	0.000290	0.035735	0.450	14.130
25.2 - 23.9	24.5	0.000245	0.035979	0.399	14.530
23.9 - 22.7	23.3	0.000243	0.036222	0.418	14.947
22.7 - 21.5	22.0	0.000241	0.036463	0.437	15.385
21.5 - 20.3	20.8	0.000247	0.036711	0.475	15.860
20.3 - 19.1	19.7	0.000212	0.036923	0.431	16.291
19.1 - 18.0	18.5	0.000237	0.037160	0.513	16.803
18.0 - 16.7	17.3	0.000276	0.037436	0.638	17.441

micromeritics®

Micromeritics Instrument Corp.

Gemini V2.00 Unit 1 Serial #: 5501 Page 6

Sample: IV-1 Run 2
Operator: KZ OL
Submitter:
File: C:\GEMINI\DATA\001-160.SMP

Started: 5/1/2013 8:48:15AM
Completed: 5/1/2013 12:13:43PM
Report Time: 5/1/2013 12:28:31PM
Free Space Diff.: -0.4473 cm³
Free Space Type: Measured
Gemini Model: 2380

Analysis Adsorptive: N2
Equilibration Time: 5 s
Sat. Pressure: 643.815 mmHg
Sample Mass: 0.2819 g
Sample Density: 1.000 g/cm³

BJH Adsorption Cumulative Pore Volume

Halsey : Faas Correction

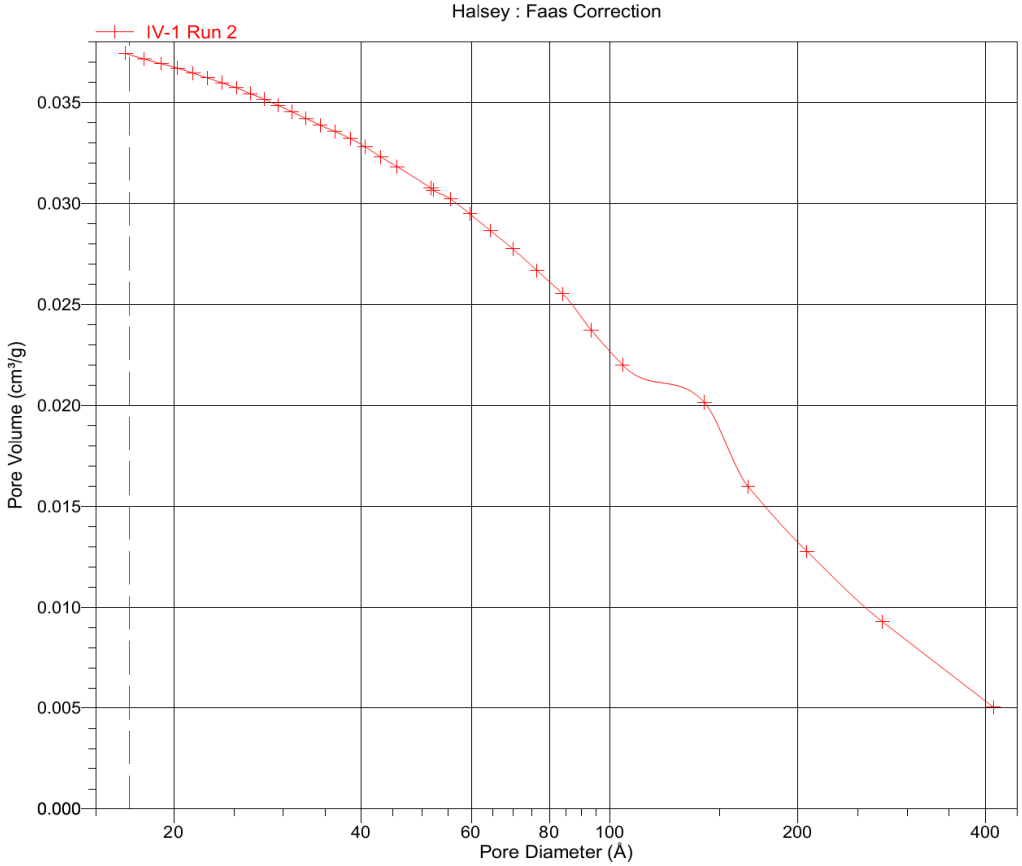

micromeritics®

Micromeritics Instrument Corp.

Gemini V2.00 Unit 1 Serial #: 5501 Page 7

Sample: IV-1 Run 2
Operator: KZ OL
Submitter:
File: C:\GEMINI\DATA\001-160.SMP

Started: 5/1/2013 8:48:15AM
Completed: 5/1/2013 12:13:43PM
Report Time: 5/1/2013 12:28:31PM
Free Space Diff.: -0.4473 cm³
Free Space Type: Measured
Gemini Model: 2380

Analysis Adsorptive: N2
Equilibration Time: 5 s
Sat. Pressure: 643.815 mmHg
Sample Mass: 0.2819 g
Sample Density: 1.000 g/cm³

BJH Adsorption dV/dD Pore Volume

Halsey : Faas Correction

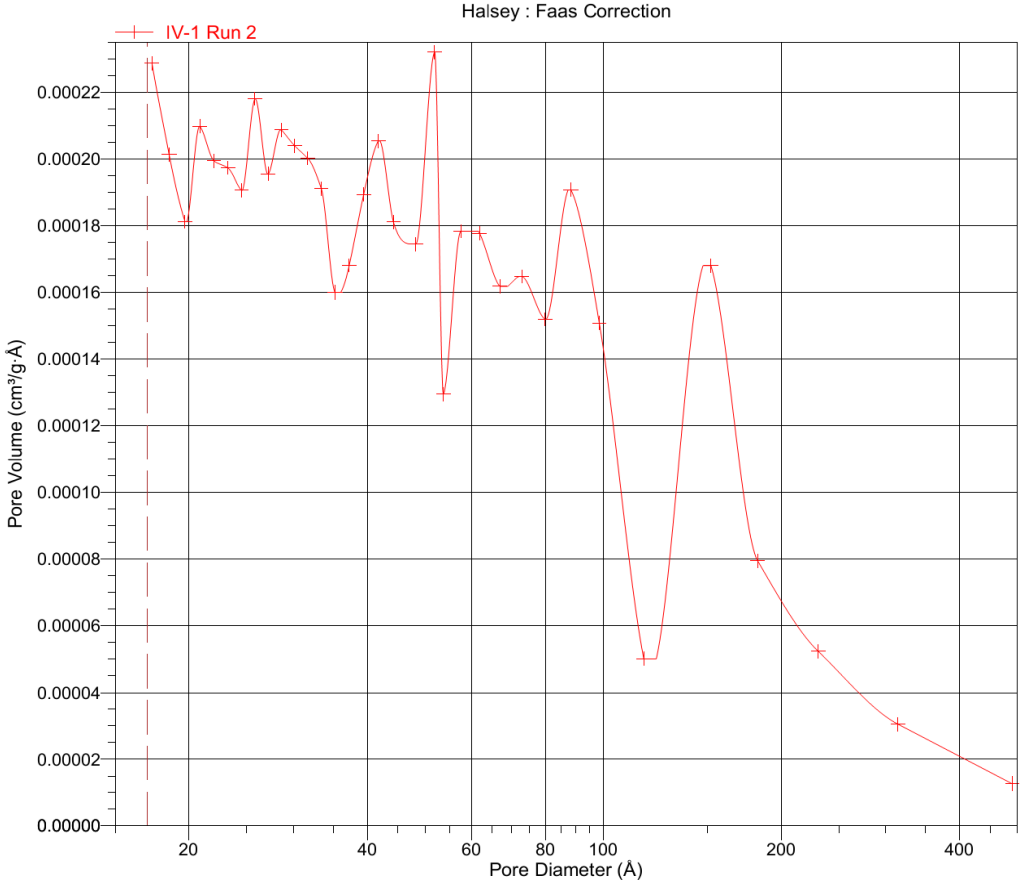

micromeritics®

Micromeritics Instrument Corp.

Gemini V2.00 Unit 1 Serial #: 5501 Page 8

Sample: IV-1 Run 2
Operator: KZ OL
Submitter:
File: C:\GEMINI\DATA\001-160.SMP

Started: 5/1/2013 8:48:15AM
Completed: 5/1/2013 12:13:43PM
Report Time: 5/1/2013 12:28:31PM
Free Space Diff.: -0.4473 cm³
Free Space Type: Measured
Gemini Model: 2380

Analysis Adsorptive: N2
Equilibration Time: 5 s
Sat. Pressure: 643.815 mmHg
Sample Mass: 0.2819 g
Sample Density: 1.000 g/cm³

BJH Adsorption dV/dlog(D) Pore Volume

Halsey : Faas Correction

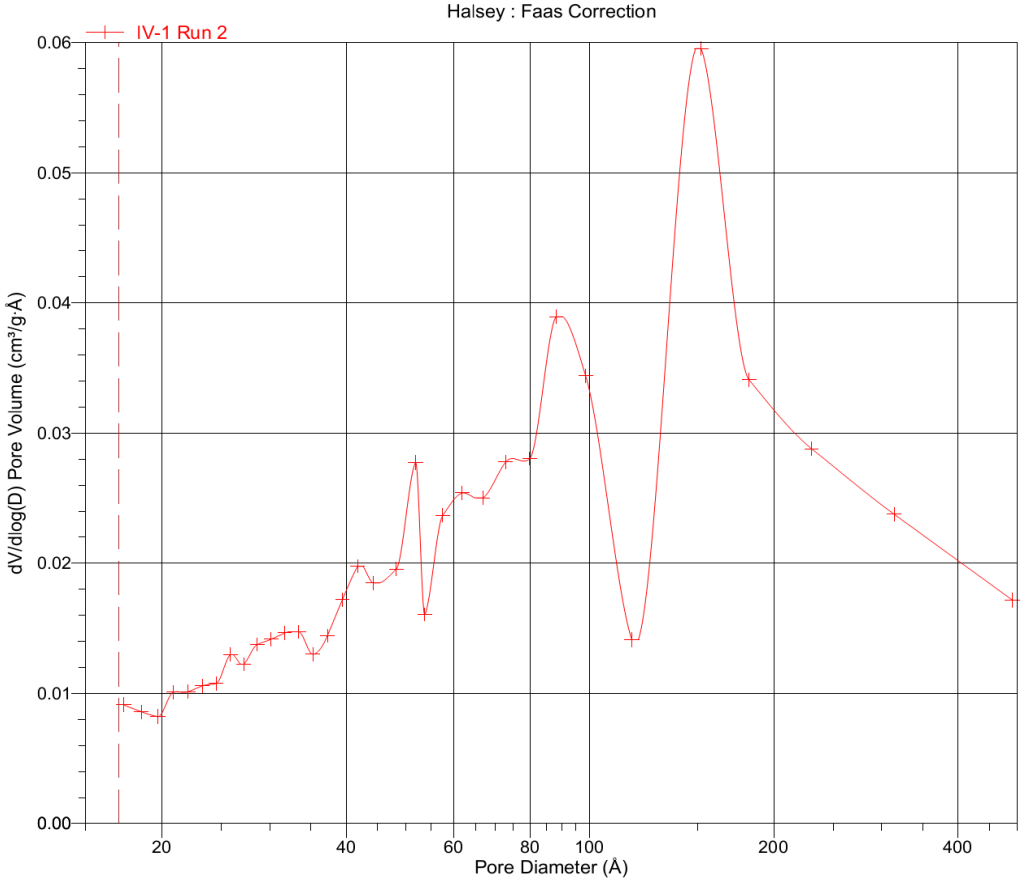

micromeritics®

Micromeritics Instrument Corp.

Gemini V2.00 Unit 1 Serial #: 5501 Page 9

Sample: IV-1 Run 2
Operator: KZ OL
Submitter:
File: C:\GEMINI\DATA\001-160.SMP

Started: 5/1/2013 8:48:15AM
Completed: 5/1/2013 12:13:43PM
Report Time: 5/1/2013 12:28:31PM
Free Space Diff.: -0.4473 cm³
Free Space Type: Measured
Gemini Model: 2380

Analysis Adsorptive: N2
Equilibration Time: 5 s
Sat. Pressure: 643.815 mmHg
Sample Mass: 0.2819 g
Sample Density: 1.000 g/cm³

BJH Adsorption Cumulative Pore Area

Halsey : Faas Correction

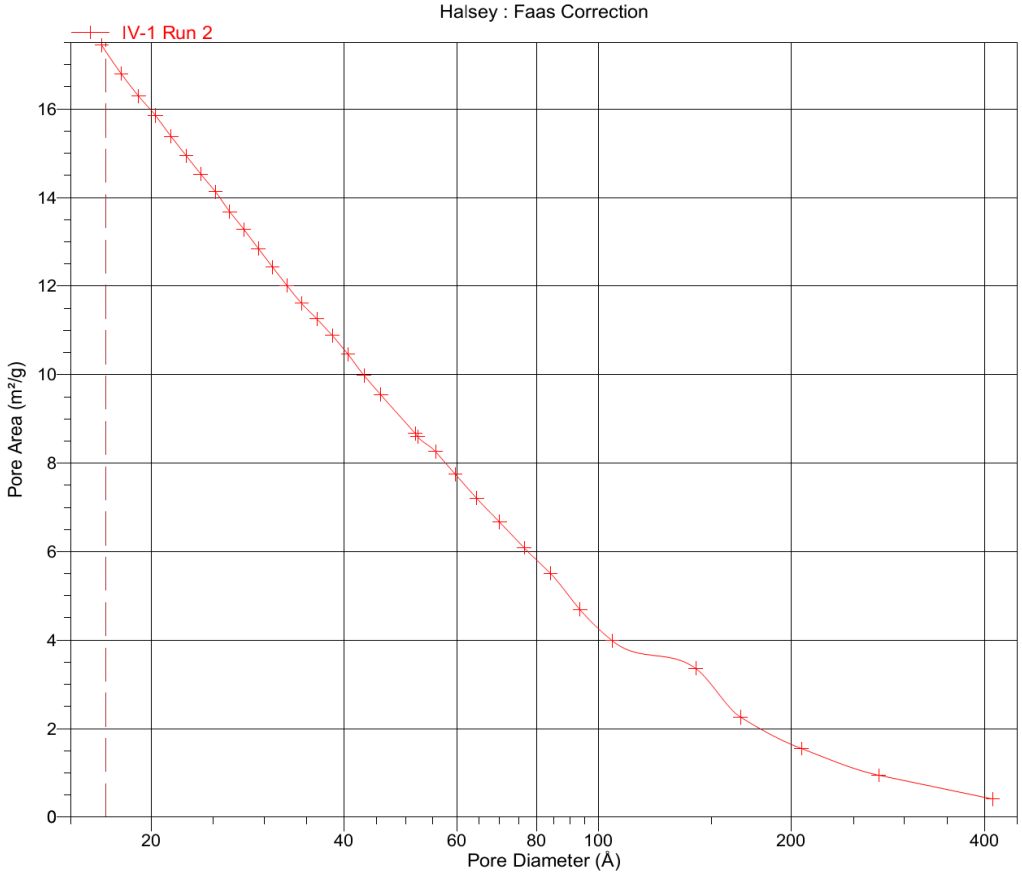

Appendix C. Resistance of CNT solution after adding chemicals

10/2/12	*Substance*	*Electrical Resistance(Ω)*	*Comments*
8-3	Methyl Cellylulose+ Gum Arabic	370K	No CNT
8-3	Methyl Cellylulose+ Gum Arabic+1/3 CNT	100K	
8-3	Methyl Cellylulose+ Gum Arabic+1/3 CNT	60.6K	EP
1	Nitric Acid	5.3K/4.6k	Only Nitric
1-3	Nitric Acid+Gum Arabic+1/3 CNT	3.56K/5.23K/3.17K	
10/3/12	*Substance*	*Electrical Resistance(Ω)*	*Comments*
1-3	Nitric Acid+Gum Arabic+1/3 CNT	5.79k	non-stable
		3.53k	after stirring
		4.03k	semi stable
	150 g cement+ 150 ml water	51.5K	
1-3	150 g cement+ 150 ml water+50ml 1-3	57.5k	
1-3	150 g cement+ 150 ml water+100ml 1-3	52.3	
10/4/12	*Substance*	*Electrical Resistance(Ω)*	*Comments*
1-8	Water+Nitric+Methycl Cellulose+CNT	9.1K	no stirring
		6.4K	stirring
		3.14K	EP
		1200	level 2
		800	level 4
		530	level full
		1.84K	5mins after EP
	Nitric	7.1K	Before EP
		0.9K	After EP
		2.24K	Keep for 10 mins
10/5/12	*Substance*	*Electrical Resistance(Ω)*	*Comments*
3	Gum Arabic	32.3K	EP
		42.4K	after EP
3-9	Silica Fume+Gum Arabic	37.5K	EP
3-9	Silica Fume+Gum Arabic+CNT	27K	EP
10/9/12	*Substance*	*Electrical Resistance(Ω)*	*Comments*
6	Ethanol	137.8K	
6-9	Ethanol+Silica Fume	107.8K	
		92K	EP
6-9	Ethanol+Silica Fume+CNT	87.5k	EP
6-9	Ethanol+5*Silica Fume+CNT	76.5K	EP
	Dodecyl Sodium	48.8K	
		31.3K	EP
10-9	Dodecyl Sodium+CNT+3*silica fume	35.7K	EP
10-9	Dodecyl Sodium+CNT+4*silica fume	28.6K	EP

Appendix.D Mix design of First batch of concrete (10.16.12-11.14.12 Done)

CNT (g)	water	cement	sand	Aggregates		Process	Method
I-1	2	0.1399	0.3082	0.661	0.805	Add superplasticizer	By hand
I-2	2	0.1399	0.3082	0.661	0.805	Add superplasticizer	By hand
	3	0.1399	0.3082	0.661	0.805	Add superplasticizer	By hand
I-4	4.5	0.1399	0.3082	0.661	0.805	Add superplasticizer	By hand
I-5	3	0.1399	0.3082	0.661	0.805	Add superplasticizer	By hand
I-6	3	0.1399	0.3082	0.661	0.805	Add snow powder +superplasticizer	
I-7	3	0.1399	0.3082	0.661	0.805	Add superplasticizer	Ball mixing
I-8	4.5	0.1399	0.3082	0.661	0.805		Ball mixing
I-9	3	0.15	0.3082	0.661	0.805	Add part of CNT and water mixing first	Ball mixing
I-10	3	0.15	0.3082	0.661	0.805	Mix CNT and cement together with little water first	Ball mixing
11	4.5	0.15	0.3082	0.661	0.805	Mix CNT and cement together with little water first	Ball mixing

Appendix E. Mix design of concrete for second batch
(Cast:11.07.12~11.16 , Test:1.10.13)

	CNT(g)	water(kg)	cement(kg)	sand(kg)	Aggregates(kg)	Chemicals	Method
C'-1	0.25%	0.121	0.242	0.575	0.700		Sonication: 12mins
C'-2	0.25%	0.121	0.242	0.575	0.700		Sonication: 12mins
C'-3	0.25%	0.121	0.242	0.575	0.700		Sonication: 12mins
C'-4	0.5%	0.121	0.242	0.575	0.700		Sonication: 12mins
C'-5	0.5%	0.121	0.242	0.575	0.700		Sonication: 12mins
C'-6	0.5%	0.121	0.242	0.575	0.700		Sonication: 12mins
C'-7	0.75%	0.121	0.242	0.575	0.700		Sonication: 12mins
C'-8	0.75%	0.121	0.242	0.575	0.700		Sonication: 12mins
C'-9	0.75%	0.121	0.242	0.575	0.700		Sonication: 12mins
C'-10	1%	0.121	0.242	0.575	0.700		Sonication: 12mins
C'-11	1%	0.121	0.242	0.575	0.700		Sonication: 12mins
C'-12	1%	0.121	0.242	0.575	0.700		Sonication: 12mins
C'-13	1.25%	0.121	0.242	0.575	0.700		Sonication: 12mins
C'-14	1.25%	0.121	0.242	0.575	0.700		Sonication: 12mins
C'-15	1.25%	0.121	0.242	0.575	0.700		Sonication: 12mins
C'-16	0.5%	0.121	0.242	0.575	0.700	+Gum Arabic	Sonication: 9mins
C'-17	0.5%	0.121	0.242	0.575	0.700	+Gum Arabic	Sonication: 9mins
C'-18	0.5%	0.121	0.242	0.575	0.700	+Gum Arabic	Sonication: 9mins
C'-19	0.75%	0.121	0.242	0.575	0.700	+Gum Arabic	Sonication: 9mins
C'-20	0.75%	0.121	0.242	0.575	0.700	+Gum Arabic	Sonication: 9mins
C'-21	0.75%	0.121	0.242	0.575	0.700	+Gum Arabic	Sonication: 9mins

Pictures of third batch concrete specimens under curing

Pictures of third batch concrete specimens under curing (cont.)

	CNT(g)	w(kg)	cement (kg)	sand(kg)	Agg (kg)	Process	Method	Dat1	Dat2
D-1	0%	0.4	0.99825	2.37188	2.8875	Ultrasonic Machine for 12mins	20g HWRA	3/18/2013	4/15/2013
D-2	0%	0.4	0.99825	2.37188	2.8875	Ultrasonic Machine for 12mins	20g HWRA	3/18/2013	4/15/2013
D-3	0%	0.4	0.99825	2.37188	2.8875	Ultrasonic Machine for 12mins	20g HWRA	3/18/2013	4/15/2013
D-4	0.25%	0.4	0.99825	2.37188	2.8875	Ultrasonic Machine for 12mins	60g HWRA	3/18/2013	4/15/2013
D-5	0.25%	0.4	0.99825	2.37188	2.8875	Ultrasonic Machine for 12mins	60g HWRA	3/18/2013	4/15/2013
D-6	0.25%	0.4	0.99825	2.37188	2.8875	Ultrasonic Machine for 12mins	60g HWRA	3/18/2013	4/15/2013
D-7	0.50%	0.4	0.99825	2.37188	2.8875	Ultrasonic Machine for 12mins	80g HWRA	3/19/2013	4/16/2013
D-8	0.50%	0.4	0.99825	2.37188	2.8875	Ultrasonic Machine for 12mins	80g HWRA	3/19/2013	4/16/2013
D-9	0.50%	0.4	0.99825	2.37188	2.8875	Ultrasonic Machine for 12mins	80g HWRA	3/19/2013	4/16/2013
D-10	0.75%	0.4	0.99825	2.37188	2.8875	Ultrasonic Machine for 12mins	80g HWRA	3/19/2013	4/16/2013
D-11	0.75%	0.4	0.99825	2.37188	2.8875	Ultrasonic Machine for 12mins	80g HWRA	3/19/2013	4/16/2013
D-12	0.75%	0.4	0.99825	2.37188	2.8875	Ultrasonic Machine for 12mins	80g HWRA	3/19/2013	4/16/2013
D-13	1.00%	0.4	0.99825	2.37188	2.8875	Ultrasonic Machine for 12mins	80g HWRA	3/19/2013	4/16/2013
D-14	1.00%	0.4	0.99825	2.37188	2.8875	Ultrasonic Machine for 12mins	80g HWRA	3/22/2013	4/19/2013
D-15	1.00%	0.4	0.99825	2.37188	2.8875	Ultrasonic Machine for 12mins	80g HWRA	3/22/2013	4/19/2013
D-16	1.25%	0.4	0.99825	2.37188	2.8875	Ultrasonic Machine for 12mins	80g HWRA	3/22/2013	4/19/2013
D-17	1.25%	0.4	0.99825	2.37188	2.8875	Ultrasonic Machine for 12mins	80g HWRA	3/22/2013	4/19/2013
D-18	1.25%	0.4	0.99825	2.37188	2.8875	Ultrasonic Machine for 12mins	80g HWRA	3/22/2013	4/19/2013
D-19	1.50%	0.4	0.99825	2.37188	2.8875	Ultrasonic Machine for 12mins	120g HWRA	3/22/2013	4/19/2013
D-20	1.50%	0.4	0.99825	2.37188	2.8875	Ultrasonic Machine for 12mins	120g HWRA	3/22/2013	4/19/2013
D-21	1.50%	0.4	0.99825	2.37188	2.8875	Ultrasonic Machine for 12mins	120g HWRA	3/22/2013	4/19/2013
D-22	1.75%	0.4	0.99825	2.37188	2.8875	Ultrasonic Machine for 12mins	140g HWRA	3/22/2013	4/19/2013
D-23	1.75%	0.4	0.99825	2.37188	2.8875	Ultrasonic Machine for 12mins	140g HWRA	3/22/2013	4/19/2013
D-24	1.75%	0.4	0.99825	2.37188	2.8875	Ultrasonic Machine for 12mins	140g HWRA	3/22/2013	4/19/2013